Université du Québec
à Rimouski

APPLICATION DE LA FABRICATION ADDITIVE AUX ACIERS INOXYDABLES EN MILIEU MARIN

Investigation des effets des paramètres de fabrication additive et de post-traitement thermiques sur les propriétés mécaniques et la résistance à la corrosion de l'acier inoxydable 17-4PH

Mémoire présenté

dans le cadre du programme de maîtrise en ingénierie

en vue de l'obtention du grade de maître ès sciences appliquées (M.Sc.A.)

PAR

© ANAS KERBOUT

FÉVRIER 2024

Composition du jury :

Abderrazak El Ouafi, président du jury, Université de Québec à Rimouski

Noureddine Barka, directeur de recherche, Université de Québec à Rimouski

Anwar Baiteche, examinateur externe, Compagnie Gentec

Dépôt initial le 19 décembre 2023 Dépôt final le 26 février 2024

REMERCIEMENTS

Pour commencer, j'aimerais exprimer ma sincère gratitude envers M. Noureddine Barka, mon directeur de recherche. Ses précieux conseils et son soutien ont été essentiels dans le développement de mon projet de recherche.

Je tiens également à remercier M. Hendra Hermawan, professeur à l'Université LAVAL, ainsi que l'ensemble du personnel du département de génie des mines, de la métallurgie et des matériaux à l'Université LAVAL. Plus particulièrement, je tiens à remercier Ayoub Tanji, Nathalie Moisan, Vicky Dodier et Olivera Ceperkovic, dont l'accueil et l'accompagnement ont grandement contribué au succès de mon projet.

Je tiens à remercier aussi le personnel du département de mathématiques, informatique et de génie de l'UQAR, tout particulièrement Charles-André Fraser, Suzie Loubert, Richard Lafrance et Dany Morin pour leur aide. De plus, je tiens à remercier sincèrement Asim Iltaf et Samuel Gagnon et tous les membres de l’équipe pour leur contribution à mon projet.

RÉSUMÉ

La fabrication additive représente une avancée technologique de la quatrième révolution industrielle, souvent appelée industrie 4.0, en raison des avantages qu'elle présente. L'acier inoxydable 17-4PH est un matériau qui se distingue par ses excellentes propriétés mécaniques et sa remarquable résistance à la corrosion. Cette combinaison en fait un matériau favori pour les applications soumises à de grandes contraintes mécaniques dans des milieux corrosifs, notamment en milieu marin. Cette étude vise à investiguer ce matériau et à trouver les paramètres de la fabrication additive et le post-traitement thermique qui permettent d'obtenir les meilleures performances mécaniques et électrochimiques. La première partie présente une revue de littérature axée sur l'étude des performances mécanique et électrochimiques des aciers inoxydables fabriqués par fabrication additive, dans le but d'identifier le matériau qui présente la meilleure combinaison des propriétés mécaniques et de résistance à la corrosion. La deuxième et la troisième partie de ce travail se concentrent sur l'analyse expérimentale des impacts des paramètres de la fabrication additive et du traitement thermique postérieur sur l'acier inoxydable 17-4PH. La deuxième partie concerne la microstructure et les propriétés mécaniques, tandis que la troisième se concentre sur les propriétés électrochimiques de ce matériau. Dans cette étude, les expériences ont été planifiées en se basant sur la méthode Taguchi et les résultats ont été analysés par l'analyse de la variance (ANOVA) dans le but de déterminer les paramètres significatifs. Les résultats de cette investigation permettent d'identifier la combinaison des paramètres qui donnent les meilleures propriétés mécaniques et électrochimiques du 17-4PH, ainsi que la prédiction des propriétés mécaniques et électrochimiques afin d'optimiser le processus de fabrication et de traitement thermique.

Mots clés : Fabrication additive, fusion sélective au laser, traitement thermique, corrosion, acier inoxydable, analyse de la variance, 17-4PH.

ABSTRACT

Additive manufacturing represents a technological advancement in the fourth industrial revolution, often referred to as Industry 4.0, due to the advantages it offers. Stainless steel 17-4PH is a material distinguished by its excellent mechanical properties and remarkable corrosion resistance. This combination makes it a favored material for applications subjected to high mechanical stresses in corrosive environments, particularly in marine settings. This study aims to investigate this material and find the additive manufacturing parameters and heat treatment that yield the best mechanical and electrochemical performance. The first part presents a literature review focused on the study of the mechanical and electrochemical performance of stainless steels manufactured through additive manufacturing, with the goal of identifying the material that exhibits the best combination of mechanical properties and corrosion resistance. The second and third parts involve experimental studies of the effect of additive manufacturing parameters and heat treatment on stainless steel 17-4PH. The second part deals with microstructure and mechanical properties, while the third part focuses on the electrochemical properties of this material. In this study, experiments were planned using the Taguchi method, and the results were analyzed through analysis of variance (ANOVA) to determine significant parameters. The results of this investigation identify the parameter combinations that yield the best mechanical and electrochemical properties of 17-4PH, as well as predict mechanical and electrochemical properties to optimize the manufacturing and heat treatment process.

Keywords: Additive manufacturing, selective laser melting, heat treatment, corrosion, stainless steel, analysis of variance, 17-4PH.

TABLE DES MATIÈRES

LISTE DES TABLEAUX

LISTE DES FIGURES

LISTE DES ABRÉVIATIONS, DES SIGLES ET DES ACRONYMES

A	Temps de vieillissement
Adj MS	Carré moyen ajusté
Adj SS	Somme des carrés ajustés
AM	Fabrication additive
ANOVA	Analyse de la variance
ASTM	American Society for Testing and Materials
BCC	Structure cubique centrée
CAD	Conception assistée par ordinateur
CPP	Polarisation potentiodynamique cyclique
DF	Degré de liberté
DED	Déposition à énergie dirigée
DMLS	Frittage laser direct de métal
EBM	Fusion par faisceau d'électrons
EIS	Spectroscopie d'impédance électrochimique
FCC	Structure cubique à faces centrées
HT	Traitement thermique
L-PBF	Fusion laser sur lit de poudre

CP	Potentiel en circuit ouvert
OM	Microscope optique
PBF	Fusion sur lit de poudre
PDP	Polarisation potentiodynamique
PH	Durcissement par précipitation
SCE	Électrode au calomel saturée
SEM	Microscope électronique à balayage
SLM	Fusion sélective au laser
SLS	Frittage sélectif par laser
SS	Acier inoxydable
T	Température de vieillissement
UTS	Résistance à la traction
YS	Limite d'élasticité

LISTE DES SYMBOLES

°C	Degré Celsius
C	Carbone
Cm	Centimètre
Cr	Chrome
Cu	Cuivre
E	Densité d'énergie
E_{corr}	Potentiel de corrosion
E_{oc}	Potentiel en circuit ouvert
F	Fréquence
Fe	Fer
gf	Gramme-force
H	Distance/espace d'hachurage
HRC	Dureté Rockwell
HV	Dureté Vickers
Hz	Hertz
I_{corr}	Courant de corrosion
Log	Logarithme

J	Joule
J/mm^3	Joule par millimètre au cube
K	Kelvin
kg	kilogramme
kgf	kilogramme force
kW	kilowatt
MΩ	MégaOhm
min	Minute
mm	Millimètre
mm/s	Millimètre par second
Mn	Manganèse
MPa	Mégapascal
Ni	Nickel
P	Phosphore
P	Puissance laser
pH	Potentiel hydrogène
R^2	Coefficient de détermination
R^2 (Adj)	Coefficient de détermination ajustée
R_p	Résistance à la polarisation
s	Seconde

S Soufre

Si Silicium

Sum of squares Somme des carrés séquentielle

T Épaisseur de couche

Ti Titane

V Vitesse de balayage

W Watt

wt. % Pourcentage de masse

µm Micromètre

Ω Ohm

INTRODUCTION GÉNÉRALE

1. GÉNÉRALITÉ

La fabrication additive, couramment connue sous le nom d'impression tridimensionnelle (3D), est une nouvelle technologie qui consiste à fabriquer des pièces, à partir d'un fichier de conception assistée par ordinateur en 3D, avec l'ajout de la matière couche par couche. Cette technique, et plus particulièrement la fusion sélective par laser, offre des multiples avantages, notamment des économies de temps et de coûts de production et d'assemblage, la fabrication des géométries complexes avec un nombre réduit de pièces ainsi que la réduction des déchets de la matière première. Ces technologies sont de plus en plus utilisées dans de nombreux domaine de haute technologie, notamment l'aérospatiale (22%), le biomédical (15%), l'automobile (6%) et le marché des machines-outils (20%) [1]. Cependant, cette technologie rencontre encore des contraintes et limitations qui entravent son déploiement dans des domaines exigeant une très haute précision à cause des coûts élevés. Toutefois, il est important de noter que le développement de cette technologie ouvrira la voie à son utilisation dans la production en série, ce qui pourrait entraîner la réduction des coûts.

La fabrication additive présente de nombreux avantages tels que ; La fabrication des structures complexes avec des formes à l'intérieur ou des structures en treillis impossibles à réaliser avec d'autres procédés de fabrication. De plus, elle réduit considérablement le gaspillage de matière et ne nécessite pas d'outillages spécialisés, tout en s'adaptant aux exigences de l'Industrie 4.0. Cependant, cette technologie présente des défauts, tels que la basse qualité de surface, les coûts élevés de fabrication, l'industrialisation limitée [1], la ségrégation des solutés, les contraintes résiduelles et la présence de porosité [2]. Yang et al. [3] ont souligné que la fusion sélective au laser est principalement limitée par les défauts internes. Zhang et al. [4] ont observé que la formation de défauts influe sur les propriétés

mécaniques, en particulier la résistance à la fatigue, des pièces fabriquées par fusion sélective au laser.

La fusion sélective au laser, une technologie de la fabrication additive, qui implique une série d'étapes, notamment le dépôt de poudre et le balayage au laser, réalisée à l'intérieur d'une enceinte à atmosphère contrôlée inerte pour éviter l'oxydation durant le processus [5]. Ce procédé est défini par un ensemble de paramètres tels que la puissance du laser, la vitesse de balayage, l'épaisseur de la couche, l'espace d'hachurage, la taille de la poudre, et la stratégie de balayage. L'optimisation de ces paramètres joue un rôle important dans l'amélioration des propriétés mécaniques, de la microstructure, de la résistance à la corrosion, de l'état de surface [6] et de la densité [7]. Kempen et al. [8] ont rapporté que l'augmentation de l'épaisseur de la couche et/ou de la vitesse de balayage conduit à une réduction de la densité, entraînant ainsi une baisse de la macrodureté de l'acier maraging 300. Larimian et al [9] ont étudié l'effet des paramètres sur la densification, la microstructure et les propriétés mécaniques de l'acier inoxydable 316L. Ils ont trouvé que les échantillons produits en utilisant une stratégie de balayage avec des hachures alternées et un seul passage de faisceau laser présentent les meilleures propriétés mécaniques, ainsi qu'une densification et une microstructure raffinée les plus élevées en raison de la vitesse de refroidissement maximale. Ettefagh et al. [6] ont montré que l'optimisation des paramètres de la fabrication additive permettra de résoudre certains défauts liés au processus, notamment l'évaporation, l'effet d'escalier et l'orientation des faces. Cela entraînera par la suite une amélioration de l'état de surface et une augmentation de la résistance à la corrosion.

Le post traitement thermique constitue une solution pour améliorer davantage les propriétés mécaniques et la résistance à la corrosion, ainsi qu'à recristalliser et homogénéiser la microstructure [10]. Stoudt et al. [11] ont montré que la résistance aux piqûres de l'acier inoxydable 17-4PH était améliorée après un traitement thermique. Nezhadfar et al. [12] ont illustré l'importance de la mise en solution sur la création d'une microstructure plus homogénéisée et l'augmentation de la résistance à la traction. Li et al. [13] ont aussi rapporté qu'une mise en solution pendant une heure, suivie d'un vieillissement, permettrait d'obtenir

une combinaison optimale de résistance et de ductilité. Garcia-Cabezon et al. [14] ont constaté qu'un post traitement thermique conduisait à une microstructure uniforme, avec une amélioration significative de la résistance à la corrosion.

L'application de la fabrication additive dans le maritime est encore limitée à la fabrication des prototypes et des pièces de rechange, l'installation d'une imprimante 3D à bord d'un navire a été réalisée par le groupe Lab-R.E.V [15] sur un voilier, et par la marine américaine sur l'USS Essex [16] dans le but de fabriquer les pièces de rechange nécessaire durant la navigation évitant ainsi le retour au port et économiser les coûts associés. Cependant, les applications maritimes sont confrontées à des défis, notamment les conditions environnementales extrêmes qui favorisent la corrosion. C'est pourquoi les aciers inoxydables sont privilégiés pour les environnements corrosifs, en particulier les aciers inoxydables durcis par précipitation, qui présentent une excellente résistance mécanique et une remarquable résistance à la corrosion. En effet, l'optimisation des paramètres de la fusion sélective au laser et le post-traitement thermique permettra d'avoir les meilleures performances.

2. PROBLÉMATIQUE

La fusion sélective au laser présente de nombreux paramètres qui influent sur la qualité des pièces imprimées, tels que les propriétés mécaniques, la résistance à la corrosion et à l'état de surface. L'optimisation de ces paramètres est essentielle pour réduire les effets indésirables du procédé et prévenir les défaillances. De plus, le post traitement thermique permettrait aussi une amélioration de ces propriétés. Ainsi, l'optimisation des paramètres de processus et le post-traitement thermique jouent un rôle important dans l'amélioration des caractéristiques des pièces imprimées.

L'acier inoxydable 17-4PH se démarque par ses excellentes propriétés mécaniques et sa forte résistance à la corrosion, ce qui en fait un choix privilégié pour les applications soumises à d'importantes contraintes mécaniques dans des environnements corrosifs, comme

en milieu marin. Néanmoins, il a été observé que l'utilisation de la fabrication additive et des traitements thermiques sur cet acier peut modifier ses propriétés mécaniques [12, 17-19] et électrochimiques [11, 20, 21]. Par exemple, Eskandari et al. [17] ont trouvé que le post traitement thermique a permis d'obtenir une meilleure combinaison de résistance ultime à la traction et d'allongement total par rapport à l'état initial, tels qu'imprimés. Hu et al. [18] ont étudié l'influence de paramètres de la fusion sélective au laser sur la densité, les défauts, la microdureté et l'influence du traitement thermique sur les propriétés mécaniques. Ils ont trouvé que la vitesse de balayage et l'épaisseur de la couche ont des effets significatifs sur la densité et les caractéristiques des pores des pièces fabriquées par fusion sélective au laser (SLM). Schaller et al. [20] ont rapporté que l'amélioration des techniques de la fabrication additive, en particulier la réduction de la porosité, entraîne une amélioration de la résistance à la corrosion. De même, Pan et al. [21] ont constaté qu'un post traitement thermique avait permis d'améliorer la résistance à la corrosion, avec une augmentation de la dureté passant de 330 à 438 $HV_{0.3}$. Cependant, il convient de souligner que l'étude visant à optimiser les paramètres de la fusion sélective au laser et du post-traitement thermique pour améliorer les performances mécaniques et électrochimiques des aciers inoxydables, notamment du 17-4PH, en utilisant une approche statistique, reste un domaine peu exploré.

3. OBJECTIFS

Le principal but de ce mémoire est de développer des modèles prédictifs pour prédire les propriétés mécaniques et électrochimiques de l'acier inoxydable 17-4PH fabriqué par fusion sélective laser et soumis à un post traitement thermique, à travers une analyse statistique après les tests expérimentaux. Cette étude se décompose en trois objectifs distincts. Le premier objectif est de réaliser une revue de littérature pour identifier le matériau le plus approprié pour les applications maritimes, en se concentrant sur l'impact des paramètres de fabrication additive et de traitement thermique sur plusieurs types d'aciers inoxydables. Le deuxième objectif consiste à mener une analyse expérimentale approfondie des paramètres de la fusion sélective au laser, tels que la puissance du laser, la vitesse de

balayage, ainsi que les conditions de vieillissement thermique, pour évaluer leur effet sur la microstructure, les propriétés mécaniques, et la dureté de l'acier 17-4PH. Enfin, le troisième objectif vise à étudier ces mêmes paramètres en relation avec les propriétés électrochimiques de l'acier, en particulier leur influence sur la résistance à la corrosion, afin d'optimiser l'usage de l'acier inoxydable 17-4PH dans des environnements exigeants tels que le milieu marin.

4. MÉTHODOLOGIE

Pour répondre au premier objectif, l'étude commence par l'exploration de la littérature dans le but d'investiguer le procédé de fabrication additive, en particulier la fusion sélective au laser, en explorant en détail les paramètres associés à ce processus, ainsi que les limitations et les éventuels défauts qui peuvent en découler. Ensuite, l'effet des paramètres de la fabrication additive et le post-traitement thermique sur la microstructure, les propriétés mécaniques et électrochimiques des aciers inoxydables (316L, 304L, 15-5PH, 17-4PH, and 420 SS) a été examiné.

Pour atteindre le deuxième objectif, une étude expérimentale est conduite sur les effets du processus de la fusion sélective au laser et le post-traitement thermique sur les propriétés mécaniques et électrochimiques de l'acier inoxydable 17-4PH. En premier lieu, la poudre atomisée au gaz de l'acier inoxydable 17-4PH a été fournie par EOS Inc (EOS GmbH Electro Optical Systems, Allemagne), les échantillons ont été imprimées sous atmosphère d'argon sur la machine EOS M290 équipée d'un laser à fibre d'ytterbium de 400 W, l'épaisseur des couches est de 40 μm, l'espace des hachures est de 100 μm, la puissance utilisée est comprise entre 170 et 220 W et d'une vitesse de balayage de 700 à 900 mm/s. La composition chimique de la poudre est reportée au Table 8 avec la spectroscopie de dispersion d'énergie des rayons X (EDS) en conjonction avec un microscope électronique à balayage (SEM) ainsi la morphologie de la poudre a été examinée avec le même microscope. Les échantillons destinés aux essais de traction ont été dimensionnés conformément à la norme ASTM-E8, et les échantillons destinés aux observations de microstructure et aux mesures de dureté ont été des

cubes de 15 x 15 x 20 mm. La planification d'expériences a été définis selon une table d'expériences Taguchi L9 (3^4) pour limiter le nombre d'expériences. Les pièces imprimées ont été traitées thermiquement, avant d'être découpées de la plaque, à 650°C pendant une heure suivie d'un refroidissement à l'air ambiant. Ensuite le traitement de mise en solution a été effectué à 1040 °C pendant 30 min suivi d'un refroidissement à l'air ambiant, puis ils ont subi un traitement par vieillissement à des températures situées entre 480 °C et 620 °C pour une à quatre heures. Les essais de traction ont été réalisés à l'aide d'une machine servo-hydraulique 810 MTS (Material Test System) d'une capacité de 100 kN à température ambiante avec une vitesse de traverse de 0,4 mm/min. La direction de chargement de chaque échantillon était verticale par rapport à la direction de construction et la valeur moyenne de trois essais de traction est rapportée dans les résultats pour des raisons de reproductibilité. Pour l'analyse de la microstructure, les échantillons ont été sectionnés, au milieu de coupons de forme rectangulaire, montés et polis, et enfin attaqué chimiquement avec le réactif de Fry à température ambiante pour révéler les microstructures. La microstructure a été étudiée au microscope électronique à balayage (SEM) Hitachi TM3000. La micro-dureté a été mesurée avec un testeur de micro-dureté Clemex. La charge appliquée était de 300 gf ($HV_{0,3}$) avec une durée de 10 s pour chaque indentation. La dureté moyenne et l'écart type ont été déterminés à partir de 20 points de mesure effectués par échantillon.

Pour atteindre le troisième objectif, une étude expérimentale électrochimique a été effectuée à l'Université Laval en réalisant trois méthodes électrochimiques : le potentiel à circuit ouvert (OCP), la polarisation potentiodynamique cyclique (CPP), et la spectroscopie d'impédance électrochimique (EIS), en utilisant un potentiostat (modèle 760E de CH Instruments, Austin, TX, États-Unis). Les tests de corrosion ont été réalisés dans une solution de chlorure de sodium (NaCl) à 3,5 % préparée avec de l'eau déionisée à 18,2 MΩ, maintenue à température ambiante, dans une cellule à trois électrodes comprenant l'échantillon en 17-4PH, l'électrode au calomel saturé (SCE), et la tige de graphite en tant qu'électrodes de travail, de référence, et de contre-électrode, respectivement. Avant chaque mesure électrochimique, la surface de l'échantillon a été polie, puis rincée et nettoyée avec de l'eau et de l'éthanol, et enfin séchée immédiatement. Tous les tests ont été répétés 3 fois pour garantir la fiabilité des

résultats, et les données ont été collectées et analysées à l'aide des logiciels CH Instruments et EC-Lab. Après les mesures électrochimiques, les surfaces corrodées ont été rincées, séchées à l'alcool, et examinées à l'aide de la microscopie optique LECO 300. Finalement, l'analyse de la variance ANOVA a été menées pour déterminer les paramètres significatifs.

5. ORGANISATION DU MÉMOIRE

Le mémoire est structuré en trois chapitres principaux en plus d'une introduction générale et une conclusion générale. Les chapitres sont sous formes d'articles, le premier est un article de revue de littérature, qui présente le processus de la fabrication additive, en mettant l'accent sur la fusion sélective au laser, et les problèmes et les limitations de cette technologie. Ensuite, le processus du post-traitement thermique, spécifiquement pour les aciers inoxydables durcis par précipitation. Le deuxième chapitre traite l'étude expérimentale des effets des paramètres du procédé de la fusion sélective au laser (puissance laser et vitesse de balayage) et le post-traitement thermique (température de vieillissement et durée de vieillissement) sur la microstructure et les propriétés mécaniques de l'acier inoxydable 17-4PH. Le troisième chapitre étudie les effets des mêmes paramètres mais cette fois-ci sur la résistance à la corrosion.

CHAPITRE 1
L'APPLICATION DE LA FABRICATION ADDITIVE AUX ACIERS INOXYDABLES POUR LES APPLICATIONS MARINES

Cet article a été soumis dans The International Journal of Advanced Manufacturing Technology portant le numéro de référence JAMT-D-24-00952

1.1 RESUME EN FRANÇAIS DU PREMIER ARTICLE

La fabrication additive suscite de plus en plus d'intérêt dans de nombreux domaines, notamment l'aérospatiale, l'automobile, les soins de santé et les industries marines. Cependant, dans l'industrie maritime, son utilisation se limite encore principalement à la production de prototypes ou de pièces de rechange pour des structures marines telles que les pipelines, les navires et les plates-formes offshore. La corrosion constitue une préoccupation majeure qui limite l'utilisation généralisée de la technologie de la fabrication additive dans l'environnement marin, car son impact sur les performances et la sécurité des structures marines reste à investiguer. Cet article de revue de littérature qui met en évidence l'effet du processus de la fabrication additive sur la résistance à la corrosion et les propriétés mécaniques des pièces en acier inoxydable destinées aux applications marines. Il examine les défauts les plus fréquemment rencontrés dans les produits de la fabrication additive, les solutions potentielles à ces défauts, et l'effet du traitement thermique sur les propriétés mécaniques et la résistance à la corrosion, par comparaison avec les pièces obtenues par des procédés de fabrication conventionnelle.

Mots clés : Fabrication Additive, Milieu marin, Corrosion, Acier inoxydable, Métaux, Traitement thermique.

Cet article, intitulé « *The application of additive manufacturing to stainless steels for marine applications* », a été soumis au journal *The International Journal of Advanced Manufacturing Technology*. En tant que premier auteur, j'ai contribué à l'essentiel de la recherche en effectuant une recherche bibliographique de la littérature pour explorer l'état actuel et les avancées de la technologie de fabrication additive. Le deuxième auteur de cet article est Noureddine Barka. Il est à l'origine de ce projet de recherche en proposant l'approche et la méthodologie pour aborder la problématique. Il a également contribué à l'amélioration de la rédaction pour la version finale. Le troisième auteur de l'article est Hendra Hermawan, qui a également contribué à la révision et la rédaction de l'article.

1.2 THE APPLICATION OF ADDITIVE MANUFACTURING TO STAINLESS STEELS FOR MARINE APPLICATIONS

The Application of Additive Manufacturing to Stainless Steels for Marine Applications

Anas Kerbout[1, a)], Noureddine Barka[1], Hendra Hermawan[2]

[1]Department of Mathematics, Computer Science and Engineering, Université du Québec à Rimouski, QC G5L 3A1, Canada

[2] Department of Mining, Metallurgical and Materials Engineering, Laval University, Quebec City, QC G1V 0A6, Canada

[a)] Corresponding author. E-mail address: Anas.Kerbout@uqar.ca

1.3 ABSTRACT

Additive manufacturing (AM) has been gaining attractions in many areas, including aerospace, automotive, healthcare, and marine industries. However, in the marine industry its use is still limited to the production of prototypes or spare parts of marine structures such as pipelines, ships, and offshore platforms. Corrosion is a major concern that hinders the widespread use of AM technology in the harsh marine environment due to its potential effects on the performance and safety of marine structures, which are yet to be thoroughly examined. This article aims to review the effect of AM process on the corrosion resistance and mechanical properties of the parts made of stainless steels for marine applications. It discusses the most frequent defects found in AM products and exploring potential solutions to these defects. Additionally, to investigating the effect of heat treatment on both mechanical properties and corrosion resistance in comparison with those of non-AM products to provide a comprehensive understanding of the challenges and opportunities that AM presents in the marine industry.

Keywords: Additive Manufacturing, Marine environment, Corrosion, Stainless Steel, Metals, Heat treatment.

1.4 INTRODUCTION

The maritime industry which covers shipping, ports, fishing, shipbuilding, and offshore, plays a critical role in worldwide trade and supply chains at many scales. Keeping the maritime assets and structures operating efficiently and safely in harsh environment is therefore primordial, not only for trade but also for environmental protection of the marine environment against threats related to possible failures of marine structures. These structures have multiple purposes including transportation, energy production, protection of coastal structures and offshore platforms. Offshore areas are located many kilometers from coastlines and extend into the open ocean, offering a wealth of resources and opportunities for a range of industries and activities. For example, oil and gas extraction and production, fishing, renewable energy production, and for scientific research on marine ecosystems and oceanography. These regions exhibit a variety of physical and chemical characteristics, such as strong ocean currents, waves, and winds, as well as high concentrations of salt, which can present problems for equipment and infrastructure. The ocean salinity is determined by the concentration of chloride (Cl^-) ions often approximated at a value equal to 3.5% NaCl [22] solution in water, with an average pH of 8.1 [23]. As the ocean temperature decreases, the concentration of dissolved salt decreases, causing a drop in solubility thus reducing the conductivity and increasing the electrolyte resistivity of seawater. The temperature decrease also facilitates the dissolution of oxygen, providing more dissolve oxygen readily available for corrosion reaction [24].

Corrosion has been a major problem for marine structures causing failure to critical equipment such as safety valves or fasteners leading to material lost, personnel injury and even death [25]. Corrosion resistant alloys such as stainless steels (SS) have been the reliable materials of choice to withstand the harsh conditions of the marine environment, with the 17-4 precipitation hardening (PH) as one of the most used SS given its excellent combination of mechanical properties (high tensile strength, fracture toughness, impact resistance) and high corrosion resistance up to 300°C [26-28]. Normally, parts made of 17-4PH are fabricated through traditional casting process followed by a heat treatment involving a solution

treatment at 1040°C for 30 minutes and an aging treatment at 480-760°C for one to four hours to form copper precipitates in the martensitic matrix [29]. Nowadays, the attractive additive manufacturing (AM) begins to gain attention of marine industries. The AM technology offers many benefits including lower inventory investment, transportation, safety stock, and overall supply chain costs [30], also higher asset availability in comparison to traditional manufacturing process. However, the widespread use of AM technology in marine industry is hindered over concern of corrosion that will likely affect the performance and safety of structures operating in the harsh marine environment. Therefore, this article aims at reviewing the effect of AM process on the corrosion resistance and mechanical properties of the parts made of SS for marine applications. It discusses the most frequent defects found in AM products and their potential solutions, and the effect of heat treatment on both mechanical properties and corrosion resistance in comparison with those non-AM products.

1.5 ADDITIVE MANUFACTURING OF STAINLESS STEELS

Commonly known as three-dimensional (3D) printing, AM involves digitally manufacturing of products by adding material layer by layer as predetermined by a 3D computer-aided design (CAD) file. The ASTM-F2792 standard defines AM technology to be the "process of joining materials to make objects from 3D model data, usually layer upon layer, as opposed to subtractive manufacturing methodologies" [31]. AM technology offers multiple benefits, including time and cost saving [32], on-demand product fabrication of various metals, freedom of design, creation of complex geometries with reduced part number [33, 34], material mass customization, and low material waste. It has been used in many high-tech areas [35] including aerospace, automotive, and healthcare. In marine industry, AM has been used to fabricate test prototypes and spare parts, where for a large vessel a missing part can create a costly problem due to the expenses related to vessel return, rent of the port, system downtime and shipping lost time. Installing a 3D printer onboard a vessel has been implemented by a group of individuals called Lab-R.E.V [15] on a sailboat, and by the US Navy on the USS Essex [16] to confirm the feasibility of printing spare parts during navigation, instead of returning to the port which could be thousands of miles away [16].

1.5.1 AM processes and parameters

The ASTM F2792 committee categorized AM processes into seven groups (Figure 1) [31, 36]. A binder jetting process selectively deposits liquid bonding agent to join powder materials, while a directed energy deposition uses a focused thermal energy to fuse materials by melting as deposited. A powder bed fusion process uses thermal energy to selectively fuse regions of a powder bed. A material extrusion process selectively dispenses material through a nozzle or orifice, almost like a material jetting process where droplets of build material are selectively deposited. The sheet lamination process uses sheets of material to be bonded to form an object, while a vat photopolymerization uses liquid photopolymer in a vat that is selectively cured by light-activated polymerization.

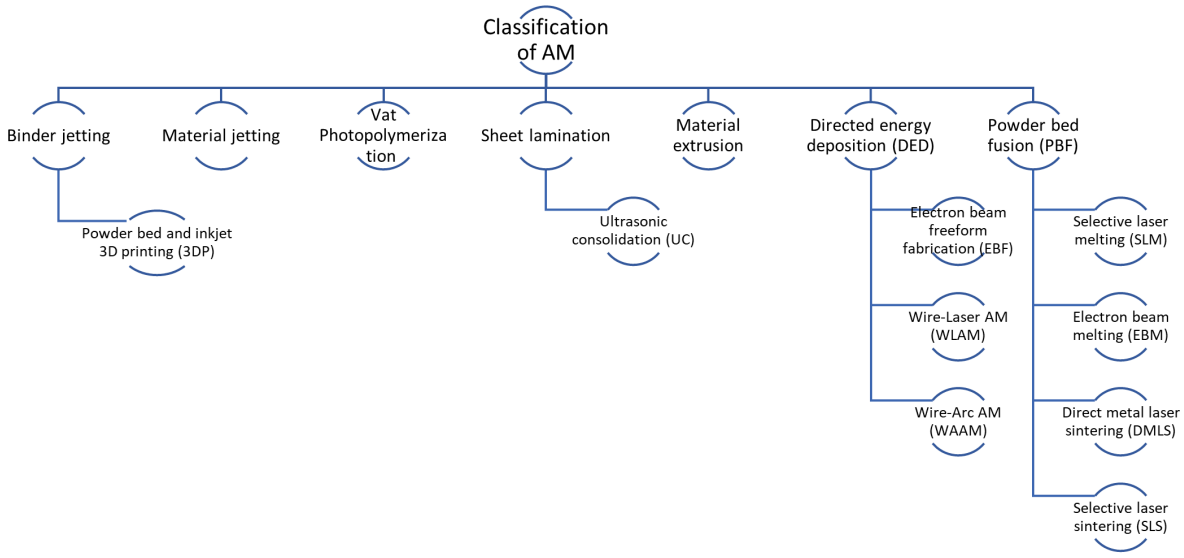

Figure 1: Classification of AM technologies.

1.5.1.1 Selective Laser Melting

One of most used powder bed fusion processes is selective laser melting (SLM) that uses a high-energy laser beam as a source of energy to melt a layer of deposited metal powder particles and fuse it against a previously melted layer in a typically inert atmosphere (argon (Ar) or nitrogen (N)) in order to protect the metal powder from oxidation [37]. SLM has been

employed in fabricating tools from SS for injection molding with complex cooling channel as shown in Figure 2 [38] that allows cooling liquid to absorb the heat from the mold [39].

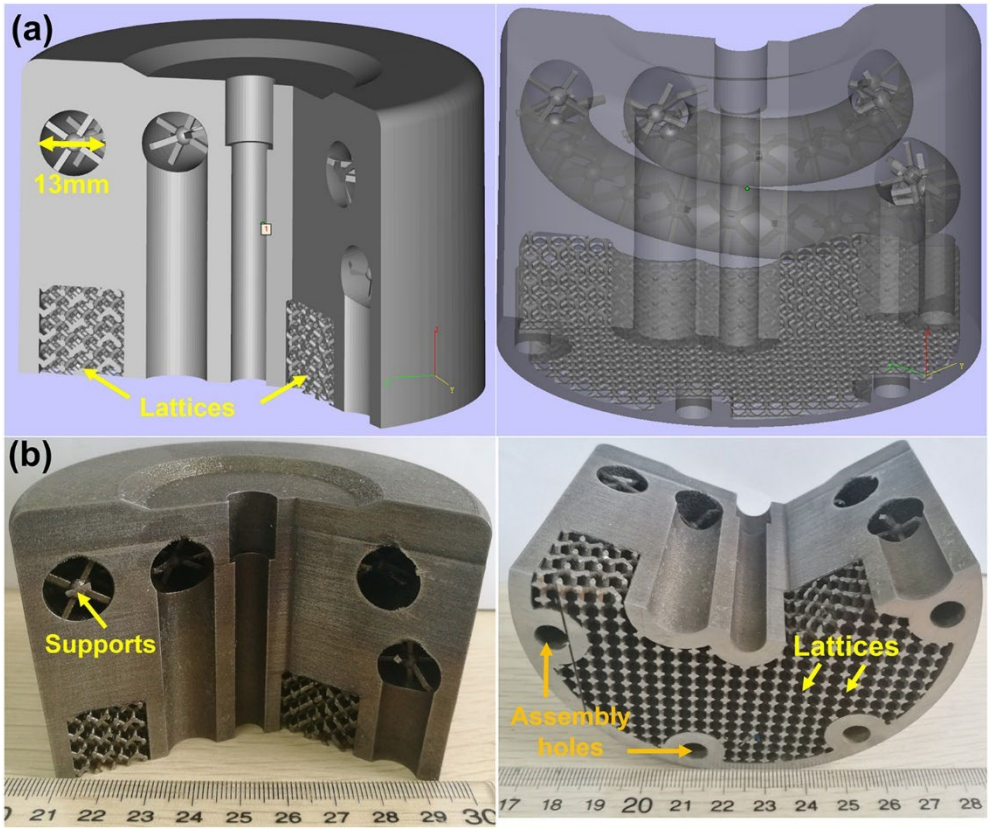

Figure 2: The injection mold with conformal cooling channel: (a) CAD model, (b) L-PBF parts (reprinted with permission from Ref. [19]).

1.5.1.2 **SLM parameters**

The literature shows that the value of the process parameters such as laser power, scanning speed, powder size, scanning strategy, hatch spacing, layer thickness, powder bed preheating process and build chamber atmosphere affects: Young's Modulus, ultimate tensile strength, yield tensile strength, hardness, density, microstructural and corrosion resistance. And will be different from one part to another by modifying the parameters [40, 41]. Energy density (E) is defined as the energy input (J) per unit volume (mm^3) and is calculated using equation (1) [42].

$$E = \frac{P}{h * V * t} \quad (1)$$

Where P is the laser power, it is the energy per second that the laser applies to the powder bed to heat up the material and melt it, V is the laser scanning speed that defines how fast the laser scanner moves while scanning, h is the hatch spacing, also known as diameter of the laser layer or distance between laser scan lines, it is defined as the distance between the central line of two neighboring paths scanned, and t is the layer thickness, it can be defined as the new layer height added to the powder bed (Figure 3).

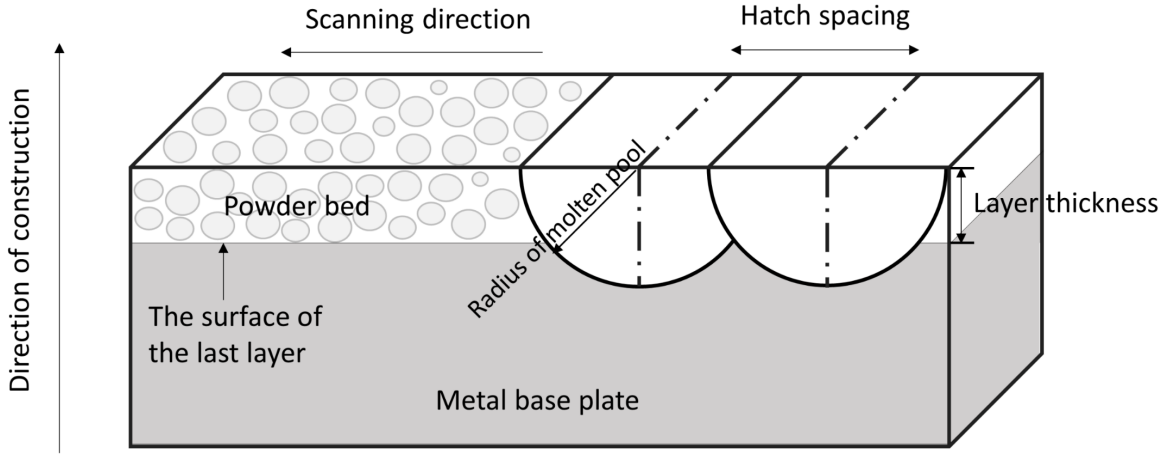

Figure 3: Schematic of SLM process parameters.

In general, among the SLM parameters powder characteristics; processing atmosphere, building orientation and laser scanning pattern (strategy). According to several studies, the atomizing gas and protective gas have an influence on the amounts of residual austenite and martensite present in the manufactured parts [43]. The metal powders are produced using water, gas or plasma atomization. The powder production methods affect chemical composition, particle morphology and particle size of powder [44]. The plasma atomized (PA) and gas atomized (GA) powders are commonly utilized in laser powder bed fusion (L-PBF) due to their chemical purity and near-spherical shape. On the other hand, the use of water atomized (WA) powder would be less expensive than other types [45]. Regardless of energy density the GA powder reveals a single martensitic phase, and the WA

powder involves dual martensitic and austenitic phase. However, after special heat treatment, the pair present fully martensitic structure [46]. Moreover, Pinkerton et al. [47] reported that water atomized powder had superior surface finish and deposition uniformity.

The processing atmosphere (argon or nitrogen) is necessary to prevent/minimize powder oxidation films during the L-PBF process at elevated temperature [10]. Since the wetting degree can be reduced by the oxidation films and contaminations [48]. Murr et al. [27] showed that by using an argon building chamber atmosphere, both 17-4PH SS powders; martensitic or austenitic, fabricated by SLM produced a martensitic product. While, by using a nitrogen processing atmosphere the product phase is identical to the antecedent powder phase. This unusual behavior happened due to the rapid cooling affected by nitrogen gas which has a 40% greater thermal conductivity in comparison to argon gas. Additionally, they reported that nitrogen building chamber atmosphere provides poor mechanical properties. Furthermore, Rafi et al. [49] reported that 17–4 PH SS L-PBF printed under argon gas promotes a martensitic structure with small proportion of retained austenite while a mixture of martensite and austenite phases was formed under nitrogen gas.

The build orientation of parts produced using SLM process can have a significant impact on their mechanical properties. Several studies have investigated the relationship between build orientation and mechanical properties such as strength, ductility, and fatigue resistance. Kai Guan et al. [50] have investigated the effects of building orientation on tensile properties of L-PBF 304 SS at the same laser power and scanning speed, the results showed that the vertical samples present an optimal strength and ductility ratio. Simonelli et al. [51] have reported that the ductility of SLM Ti–6Al–4V is dependent on the building orientation. Yadollahi et al. [52] have found that amount of retained austenite founded was 7% and 3% in horizontally and vertically orientated samples, respectively. Le Zai et al. [10] explained that the distance between layers is responsible for the austenite volume fraction difference between horizontally and vertically orientated samples. This is because horizontally built samples require more time to form, allowing for greater dissipation of heat energy into the surrounding environment. Consequently, the higher cooling rate observed in horizontally built samples is attributed to the larger initial temperature difference between the molten pool

and the previously solidified surface. This difference is due to the variation of thermal history during manufacturing. Therefore, rapid cooling has the same effect as quenching which provides a higher martensite proportion in horizontal specimens. In opposition, the vertically orientated samples present a slower cooling rate since there is less time between each layer melting and the next, which causes a quasi-annealing process and increased austenite content [52, 53]. Literature search shows that the scanning direction can influence the porosity and the microstructure, Kudzal et al. [54] have carried out a study on the effect of scanning strategy on the modification in porosity and percentage of retained austenite during melting. Rashid et al. [55] reported that samples printed with double scan strategy presents high density and hardness than samples printed with single scan. Fencheng et al. [56] have also carried out the effect of laser scanning path on microstructures and mechanical properties of Inconel 718. The Figure 4 below shows six different laser scanning strategies [54].

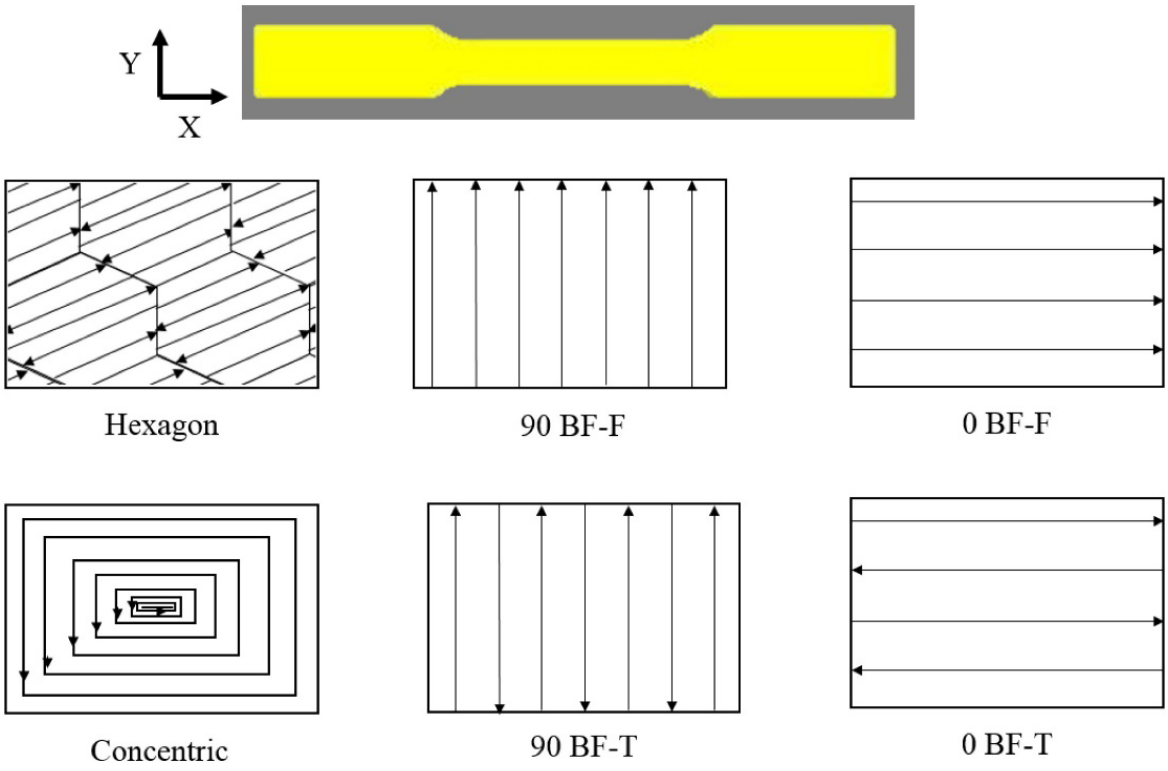

Figure 4: Schematic representation of different scanning strategies (reprinted with permission from Ref. [36]).

Wang et al. [57] indicated that high scanning speed and low laser power cause more manufacturing defects. Decreasing laser power and elevating the scanning rate resulted in a decrease in laser energy density, which made it difficult to melt the metal powder. Adeyemi et al. [58] reported that the microstructure of the 17-4PH at low laser power is finer due to rapid cooling while high laser power produced a coarser microstructure due to slow cooling. Also, the layer thickness has a significant effect on porosity [59], cracks, and manufacturing rate [41]. The literature shows that the lower the layer thickness is, the better mechanical properties of the 3D printed parts will be. But the cycle time will increase by reducing the layer thickness since the model needs more layers to be added. The SLM process can induce some defects such as pores, residual stress, poor surface roughness and cracks if the process conditions are not designed appropriately [60].

1.5.1.3 **Limitations and defects in SLM**

AM technology has been facing a lot of challenges that induce a wide range of material defects which affect the quality of fabricated parts, such as porosity creation, residual stress, deformation, low surface quality that could lead to long and expensive post-finishing operations [61, 62]. Other obstacles limited the wide adoption of this technology derive largely from economic reasons such the longtime of production which prevents the mass production [28, 30], powder cost, machine cost [63], or other reasons such reduced number of used AM materials or the difficulty to predict the mechanical properties of the manufactured part with certain levels of confidence from the input parameters [37]. Nevertheless, the cost of L-PBF process can be driven down further by improving the building rates [28].

High scan speeds create a localized heat source with a high temperature gradient, high cooling rate, which can reach 10^6 K/s in SLM [48], and Marangoni effect, the convective movement of the molten pool caused by a non-uniform distribution in the surface tension [64]. The Marangoni convection (Figure 5a) causes unpredictable particle movements around the melt pools, melt pool flow, pore formation, denudation zones [65], and residual stress

[66]. Which can affect the corrosion performance and the mechanical strength of parts [6]. The common defects are classified into porosity, residual stress and keyhole defects. Porosity is a frequent problem in the AM process, manifesting when the energy applied to the material is insufficient that leads to a small melt pool and insufficient melting. At the same time, excessive energy input causes the vaporization of metal which traps gas bubbles in the molten pool [67]. There are two types of pores that can be found in AM components: regular (spherical) pores, which form due to gas entrapment during powder production and/or in the melting pool; whereas, irregular (non-spherical) pores, which form due to the un-melted powder particles causes by improper processing parameters [6], non-spherical pores type are harmful if they are normal to the direction of loading since they have a significantly smaller cross-sectional area [53]. Multiple investigations have revealed that inadequate energy input can lead to the presence of unmelted powder regions. In particular, Akita et al. [32] have conducted research on specimens fabricated using SLM, and have discovered numerous microscopic defects (Figure 5b [32], Figure 5c [32]). Additionally, the specimens were found to have lower resistance to crack initiation compared to the CM specimen. One such effect is the formation of discontinuous tracks [68], which can lead to non-uniform deposition of material on the previous layers. This, in turn, can induce several physical defects such as porosity, which is more likely to occur at very high laser power and scan speed [69]. Additionally, balling can also result in delamination between layers [61], further compromising the structural integrity of the final product.

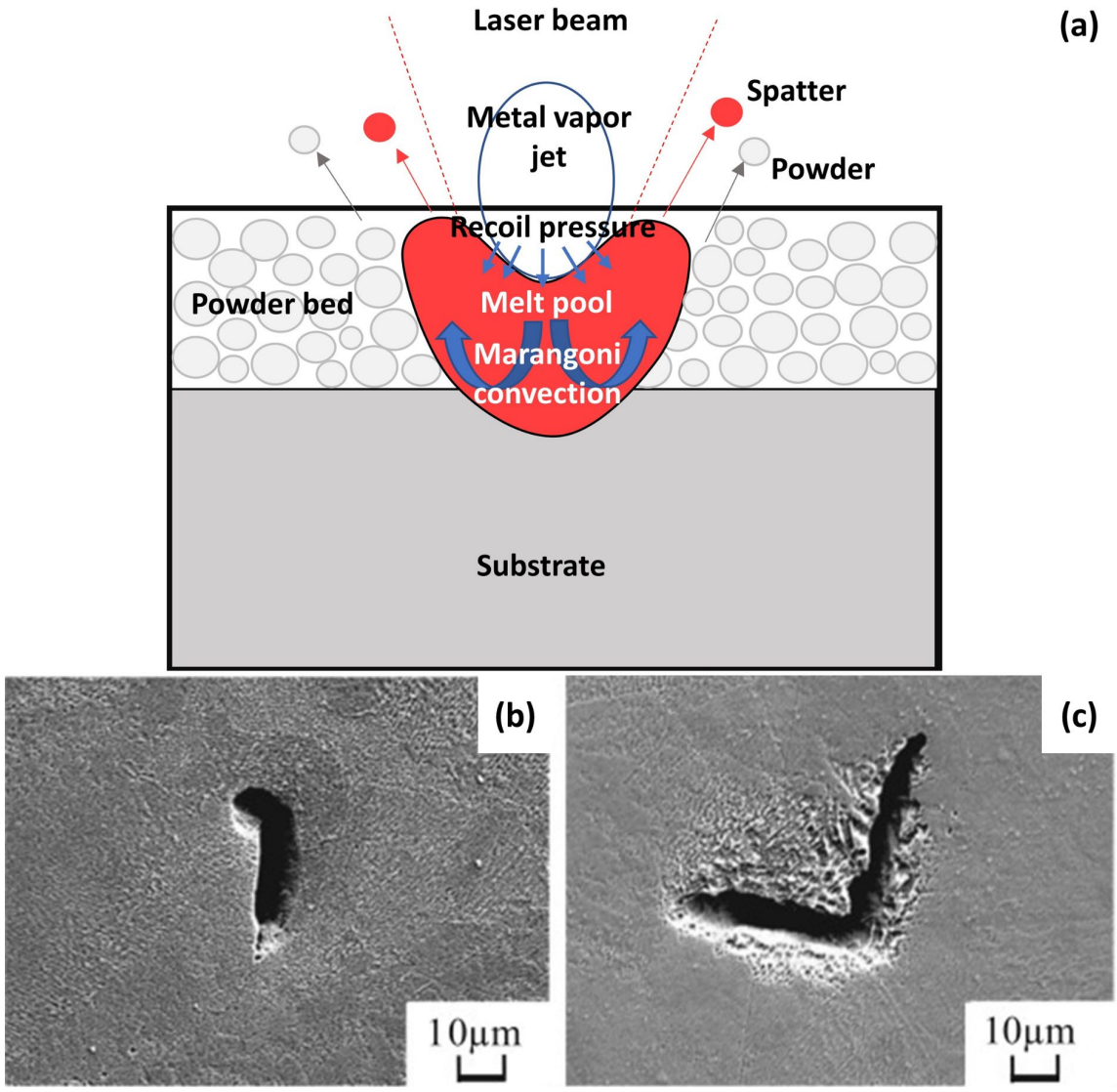

Figure 5: (a) Melting and solidification phenomenon by laser, Micrographs showing defects in SLM specimens: (b) cylindrical defects, (b) angular defects (reprinted with permission from Ref.[11]).

Residual stresses are internal stresses that exist within a material even when no external loads are applied, and they can develop as a result of the large thermal gradients that occur during the manufacturing or heating process [70]. They can affect corrosion performance [6], fatigue properties [63] and result in geometric distortion if they are higher than the yield strength of the material. In case of high residual stresses, cracking within the material can occur [67]. Simson et al. [71] have investigated the effect of residual stress on

samples made of 316L manufactured by SLM process and showed that the originating residual stresses depends on the selected process parameters. From previous work on reduction of residual stresses, it was found by Mercelis et al. [72] and by Bey Vrancken [73] that preheating substrate is one of the most effective methods to reduce residual stresses. Figure 6 [74] shows samples produced at different pre-heating temperatures, it indicates that the sample with low preheating contains spherical pores and lacks fusion defects in the lower part (Figure 6a). In contrast, the standard (Figure 6b) and high preheat (Figure 6c) samples only exhibit spherical pores. Also, Mercelis et al. [72] proved that pores relax the residual stresses since they don't contain internal stresses. Post-heat treatment was reported helpful in relieving the residual stress, it can decrease the crack growth rate and improves the fatigue life of the printed parts [75]. Furthermore, optimizing and controlling the process parameters, such laser power, scanning speed, layer thickness and scanning pattern, enables reduction of residual stresses. Oliveira et al. [67] found that implementation of scan strategies where a part is divided into smaller "islands" can reduce residual stress.

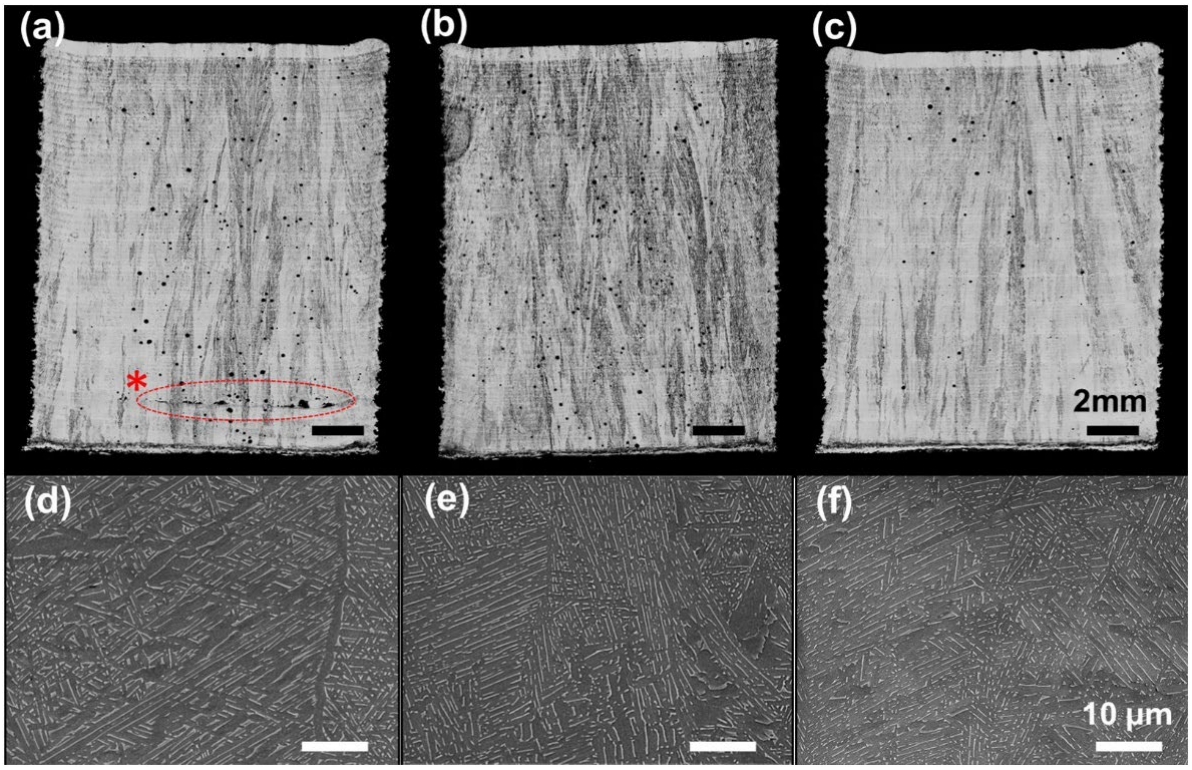

Figure 6: Micrographs of parts produced with (a) low, (b) standard, and (c) high preheating conditions in mm scale. SEM images of (d) low, (e) standard, and (f) high preheat sample at 2000× magnification (reprinted from Ref. [57] under the terms of the Creative.

Keyhole is another frequent defect during L-PBF of metals. It is a melt pool with a narrow and deep shape that is produced when a significant quantity of high energy is applied to a small area. The resulting melt pool shape makes the internal vapor bubbles escape during the brief cooling time before the materials solidify which leaves a keyhole inclusion inside the part. Kyogoku et al. [64] confirmed that the recoil momentum caused by the evaporation of metal exerts a pressure on the melt pool surface and creates keyhole. Oliveira et al. [67] found that when the energy density increases the melt pool transform from a conduction mode to a keyhole mode. Therefore, reducing laser power or increasing scanning speed are the most common ways to prevent keyhole porosity.

1.5.2 AM stainless steels

AM technology is specially applied to materials with high strength and poor machinability, like PH SS, maraging steels, tool steels, titanium, and nickel alloys. Examples of SS fabricated through AM process are 316L, 304L, 17-4PH, 15-5PH and 420 (Table 1) [32, 45].

Table 1: Material composition (wt%) of SS powders used in different AM processes

Powder	C	Mn	Si	Cr	Mo	Ni	Cu	S	N	P	Ref.
17-4PH	0.07	1.0	1.0	15.0-17.5	-	3.0-5.0	3.0-5.0	0.03	-	-	ASTM A564/A564M
15-5PH	0.07	1.0	1.0	14.0-15.5	-	3.5-5.5	2.5-4.5	0.03	-	-	ASTM A564/A564M
316L	0.03	2.0	0.75	16.0-18.0	2.0-3.0	10.0-14.0	-	0.03	0.1	0.045	ASTM A240/ A240M
304L	0.03	2.0	0.75	17.5-19.5	-	8.0-12.0	-	0.03	0.1	0.045	ASTM A240/ A240M
420	0.15 min	1	1	12.0-14.0	-	-	-	0.03	-	0.04	ASTM A276/ A276M

1.5.2.1 **PH Stainless Steels**

PH SS were developed in the 1940s, and since then they are used for a wide range of applications requiring the combination of excellent mechanical properties and high corrosion resistance [76]. They achieve high strength and high hardness due to precipitation of copper and niobium during aging at a range of temperature of 480°C to 760°C. Its low carbon content avoids their susceptibility to intergranular corrosion, but an improver heat treatment can cause chromium carbide precipitation leading to a loss of corrosion resistance [26, 77]. However, PH SS have a poor work and machine ability, rendering a difficult and long processing time to form through conventional manufacturing process [32]. The PH class can

be divided into three groups according to its microstructure: austenitic, semi-austenitic, and martensitic [78]. The first group is characterized by an austenitic structure at all temperatures, and an aging heat treatment produces a metallographically visible coherent precipitate formed from aluminum, titanium, or some other minor alloy addition. These alloys are not widely employed, since the strength remains lower than that for semi-austenitic or martensitic PH SS. The semi-austenitic PH alloys, such as 17-7PH and 15-7PH, have a much more complicated HT than the martensitic PH alloys. They are essentially austenitic at room temperature; but, at very low temperatures, martensite will develop. The martensitic PH SS contains low levels of carbon, and they have a primarily austenitic structure at annealing temperatures of approximately 1040°C to 1065°C. Once they cool to room temperature, austenite transforms to martensite. The heat treatment conditions referenced by a code according to ASTM A564/A564M standard specification are given in Table 2.

1.5.2.2 **Heat treatment of PH stainless steels**

The heat treatment sequence for PH SS takes place in three steps (Figure 7). First, solution treatment (known as Condition A) consists of heating the alloy to a relatively high temperature that allows any precipitates or alloying elements to go into a supersaturated solid solution. Temperatures used for solution treatment are typically between 982°C and 1066°C [26].

Second, quenching or cooling which can be done using air, oil or water. The cooling rate must be sufficiently rapid to create a supersaturated solid solution [26]. A faster cooling rate tends to produce a finer grain size which improve mechanical properties of materials [78]. Third, age hardening, in which the quenched alloy is heated to an intermediate temperature and held for a period of time. At these intermediate temperatures the supersaturated solid solution decomposes, and the alloying elements form small precipitate clusters. The precipitates prevent the movement of dislocations and as a result the metal resists deformation and acquire hardness [26]. A post-heat treatment is sometime required especially for PH SS to reduce AM defects and to improve the corrosion resistance, the

mechanical properties [10, 79] and the fatigue performance of the AM parts by reducing the residual stress and decreasing pores size and shape [12].

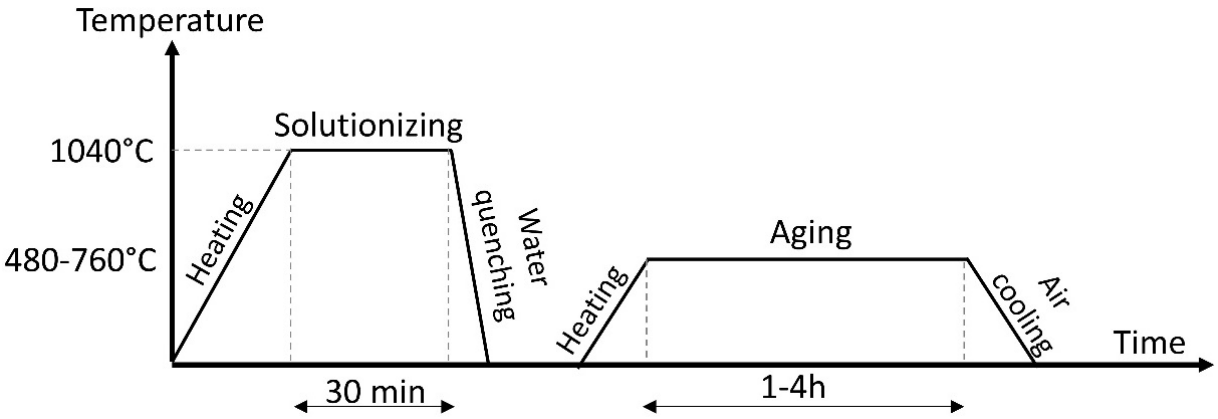

Figure 7: Schematic of the heat treatment solutionizing and aging conditions of 17-4PH SS.

Table 2: ASTM A564/A564M standard specification for 17-4PH SS aging treatments.

Condition	Temperature (°C)	Aging time (hours)	Cooling media
CA	1040	0.5	Air
H900	480	1	Air
H925	495	4	Air
H1025	550	4	Air
H1075	580	4	Air
H1100	595	4	Air
H1150	620	4	Air
H1150D	620+620	4 followed by 4	Air/Air

1.6 MECHANICAL PROPERTIES AND CORROSION OF AM STAINLESS STEELS

1.6.1 Mechanical properties of AM stainless steels

The mechanical properties of AB and heat-treated 17-4PH SS collected from the literature [12, 17-19, 27, 29, 32, 37, 43, 46, 49, 52, 53, 59, 79-84] are presented in the Supplementary Table 4, obtained using various laser power settings ranging from 48 W to 275 W, scanning speed ranging from 167 to 1550 mm/s, hatch spacing between 30 and 130

μm, and a layer thickness of 35±15 μm. The AB samples showed a yield strength (*YS*) of 676±246 MPa, an ultimate tensile strength (*UTS*) of 1033±105 MPa, a hardness of 308±27 HV, and an elongation of 16±8%. It was noted that the elongation was significantly lower (ranging from 2 to 6.56%) when the samples were built in the vertical (V) direction [37, 43, 52]. In contrast, Rafi et al. [49] reported a high elongation of 50% and mentioned that similar behavior has also been observed by Facchini et al. [85], suggesting that strain hardening resulting from the strain-induced transformation of retained austenite to martensite was responsible for this behavior. These results indicate that substantial amounts of retained austenite are present alongside the martensitic phase in the samples. The results show that H900 heat treatment after solution treatment (Cond A), led to a significant increase in yield strength, ultimate tensile strength, and hardness when compared to the other conditions.

The mechanical properties collected from the literature of AB 316L [86-97], 304L [98-106], 15-5PH [57, 107-113] and 420 [114-120] SS are presented in the Supplementary Table 5. The mechanical properties of the parts built in the vertical direction are notably reduced in the transverse samples compared to other orientations [86, 104, 105]. The strength of samples fabricated in the horizontal orientation was found to be higher than that of vertical samples. This phenomenon is attributed to dendrite and grain boundary orientation relative to the loading direction, overall grain size, and interinclusion spacing [121]. It can also be attributed to their higher proportion of "lack of melting" defects, as well as the extremely disadvantageous alignment of these defects in relation to the direction of tensile loading [92]. For the 316L, when laser power and scanning speed were decreased, the *YS*, *UTS* and elongation decreased from 450 to 400 MPa, 510 to 425 MPa, and 20 to 13.5% [97]. Similarly, Zeng confirmed that when the laser power was decreased the hardness decreased for 420 SS [119]. However, Wang et al. [95] reported that by decreasing laser power, the YS and UTS increased from 451 to 540 MPa and from 556 to 651 MPa, respectively, but the elongation decreased from 67 to 53%. Zhang et al. [101] confirmed that when scanning speed was decreased, the *YS* and *UTS* increased. Jiang et al. [120] reported low *YS* and *UTS* of SLM 420 SS in longitudinal orientation, it can be attributed to the higher quantity of martensite the

transverse specimens than does in the longitudinal specimens due to a faster cooling rate during the SLM process in the transverse direction.

The Figure 8 presents bar charts of the average values of *YS*, *UTS*, elongation to failure, and hardness for AB 17-4PH [12, 17-19, 27, 29, 32, 37, 43, 46, 49, 52, 53, 59, 79-84], 316L [86-97], 304L [98-106], 15-5PH [57, 107-113], and 420 [114-120] SS. It shows that AB 15-5 PH SS has a higher *YS* compared to other SS, and 420 exhibits higher *UTS* and hardness, while 304L demonstrates higher elongation.

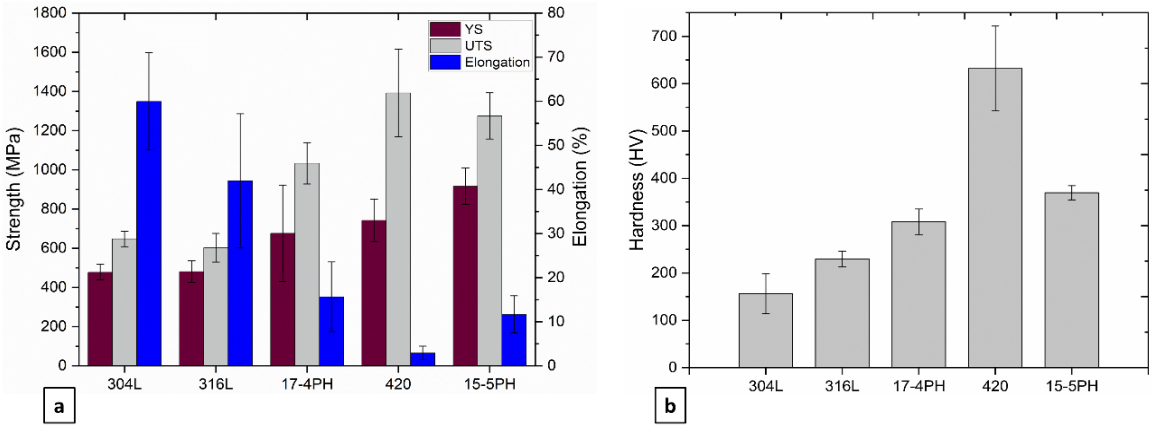

Figure 8: (a) bar charts of the average values of YS, UTS, elongation to failure, and (b) hardness of AB SS extracted from literature.

1.6.2 Corrosion of AM stainless steels

The marine assets are highly susceptible to corrosion due to the high concentrations of salt. This led to a significant rise in the expense of corrosion management in the United States in 2001, shockingly reaching over $600 billion, which is equivalent to approximately 5% of the country's Gross National Product [122]. SS are known for their high resistance to corrosion due to the presence of chromium (> ~ 10.5 wt%), which enables the formation of a protective surface layer of chromium oxide (Cr_2O_3) when the steel is exposed to corrosive media. The corrosion behavior of SS in marine environments has been widely investigated by researchers. Table 3 summarizes the reported studies [11, 21, 57, 91, 95, 99, 111, 112,

116, 123-139] on the corrosion of AM SS. It presents a comprehensive overview of the various environments and corrosion characterization techniques utilized in these studies, including details on the specific conditions under which the corrosion occurred. The most of these studies have focused on corrosion in a NaCl solution, which is known to be detrimental to the corrosion resistance of SS due to the presence of chloride ions.

Some studies [95, 123, 128, 133, 137] showed inferior corrosion resistance of SS produced through AM than non-AM parts, whereas others [124, 125, 127] showed superior properties. The instability in the corrosion behavior has been attributed to presence of residual stresses, microstructural defects, non-metallic inclusions (oxides, nitrides, and carbides), and chemical segregation that are inherent to the SLM process. Wang et al. [57] investigated the effects of manufacturing defects on mechanical behaviors and corrosion resistance of SLM 15-5PH SS with different process parameters, results show that the number of manufacturing defects increases when the laser power decreases and the scanning speed increases. However, the increase in the number of manufacturing defects causes the diminution of corrosion resistance. The manufacturing defects are present either at the interface or at the bottom of molten pool line. The presence of porosity in AM SS parts has been shown to significantly decrease the material's resistance to corrosion [123, 128, 133, 137]. Pores create regions of high stress concentration and act as preferential sites for the initiation of corrosion [123], especially pitting [6]. Pitting corrosion has been one of the most severe forms of attack, its initiation depends on the performance of the passive film in a high-chloride environment such seawater [140]. The risk that the passive film may break down increases with chloride concentration and the temperature [141]. The mechanism is fast because a damaged surface experiences successive deterioration within a short period of time [122]. Long et al. [142] investigated corrosion behavior and the pitting resistance of Cr15 supper martensitic SS in NaCl solutions and showed that a rise in Cl^- and a decrease of pH reduced the corrosion resistance. Schaller et al. [137] showed that surface roughness and porosity in the SLM 304 L SS decreased corrosion resistance with a decrease in pitting potentials. This form of corrosion affects the SS in the presence of water in a condensed state, and if the system operates in conditions involving a tensile stress, it is then rather typical to

observe pitting mixed with more severe stress corrosion phenomena [143]. The microstructural defects and residual stresses induced during the AM process can create regions of high stress concentration leading to stress corrosion cracking and other forms of degradation. Additionally, the presence of non-metallic inclusions and other types of defects can act as initiation sites for SCC, further compromising the material's integrity.

On the other hand, there exists another type of stress cracking called sulfide stress cracking (SSC). It is a specific type of corrosion that occurs in metals exposed to hydrogen sulfide (H_2S) environments. After several oil and gas system failures in Texas and Canada, SSC was initially discovered in the 1940s; the first focus was on wellhead and pipeline valves [144]. There were two opinions regarding the mechanism (stress-corrosion or hydrogen embrittlement (HE)). At that time, the SSC meant that certain systems would break when exposed under stress to H_2S-containing environments. In the addition to the toxicity of H_2S, in the presence of water it can break piping via SSC [145]. It is widely recognized that the steel's hardness creates internal stress, which is a significant factor impacting SSC susceptibility. However, the maximum allowable hardness for 17-4PH SS to resist SCC is HRC33, according to NACE MR0175/ISO 15156-1 standard [146]. For instance, one of the applications of 17-4PH is the pump impellers, where the high mechanical resistance is required even when hardness must be limited, to prevent destructive SSC in sour environments [143].

Heat treatment after AM process parameters can have a significant influence on the microstructure and corrosion behavior of precipitation-hardening SS. The heat treatment process results in the formation of a more protective passive film, which leads to improved corrosion and pitting resistance [21]. Stoudt confirmed that after homogenization, the AM samples could be more resistant to pitting than wrought SS17-4 in NaCl environment, and reported that homogenizing at 1150°C for 120 min followed by solutionizing at 1050°C for 30 min can eliminate the segregation and produce a uniform microstructure with a volume fraction of austenite of less than 0.1 [11]. Jiang et al. [147] showed that improper peak-aging treatment and phase segregation lead to increased hardness and susceptibility to high hydrogen embrittlement (HE) in 17-4PH SS, resulting in the failure of the valve stem

manufactured from this material and used in petrochemical pipeline. The increase in aging temperature and soaking time does not have a significant effect on various mechanical properties, but it does have a negative impact on corrosion properties. To ensure homogeneity in microstructure, it is advisable to perform solution annealing before aging. Corrosion was observed to be the least in samples subjected to the H900 aging heat treatment, while the highest corrosion levels were observed in the as-built SLM specimens. The reason for the higher corrosion rate at higher aging temperatures and longer soaking times is attributed to the formation of more $Cr_{23}C_6$ precipitates [111]. The presence of copper-rich precipitates (CRPs) is crucial for enhancing the material's strength. However, when the aging temperature surpasses 560°C, the structural changes and enlargement of CRPs can cause a swift decline in strength and hardness. Furthermore, the corrosion performance is also affected adversely [139].

However, it should also be noted that some studies have demonstrated that AM methods exhibit comparable or better corrosion resistance compared to non-AM techniques [124, 125, 127]. Ettefagh et al. [6] confirmed that process parameters can significantly influence the corrosion properties of AM parts. They also emphasized that with accurately defined printing process parameters, the corrosion resistance of AM SS components is superior to that of non-AM parts. Garcia-Cabezon et al. [124] studied the corrosion resistance of AM and non-AM parts by immersing them in a 0.1 M NaCl+0.5 M H_2SO_4 solution for 60 days. They found that AM parts exhibited considerably better corrosion resistance than the non-AM parts due to the absence of significant manufacturing defects, that contained a considerable amount of austenite produced by SLM, and a small number of non-metallic inclusions that formed due to the fast cooling and high solidification speed associated with the SLM process. However, it is important to note that some studies present contradictory results, and that only a limited number of studies have been conducted on corrosion investigation of AM 420 and 304L SS.

Table 3: Summary of reported studies on the corrosion of AM SS [11, 21, 57, 91, 95, 99, 111, 112, 116, 123-139].

Alloy	Ref.	AM technique	Environment (solution)	Corrosion Characterization	Corrosion as a Function of	Relevant properties	AM Alloy Corrosion Characteristics/findings
17-4PH	[123]	SLM	0.6 M NaCl	OCP, PDP	HT and porosity	E_{corr} and I_{corr}	Compared to wrought 17-4PH samples, the presence of porosity is a significant distinguishing characteristic that can affect passivity. It was observed that corrosion appeared to initiate at or near pores.
	[11]	DMLS	0.5 M NaCl	PDP	Build direction, HT	E_{pit}	The pitting potentials were found to be higher in the samples of AM parts than in samples of the alloy in non-AM parts. Compared to non-AM parts, the AM samples showed an increase in anodic pitting potentials. The additively manufactured and heat treated 17-4PH exhibit superior resistance to pitting as compared to the wrought alloy.

	[124]	SLM	0.1 M NaCl+0.5 M H_2SO_4	OCP, PDP, EIS	-	E_b, I_{corr}, E_{corr} and R_p	AM samples showed high corrosion resistance with a lower current density and a higher rupture potential than the non-AM samples independently of the build orientation.
	[21]	DED	3.5 wt.% NaCl	PDP, EIS	HT	E_{corr}, E_{pit}, I_{corr} and E_{prot}	The heat treatment process results in the formation of a more protective passive film, which leads to improved corrosion and pitting resistance.
	[125]	SLM	Solution with different pH in deaerated 3.0 wt.% NaCl solution.	PDP, OCP	HT re-austenitized =1050°C/1h +WQ	E_{pit}	The AB condition exhibited a higher pitting potential compared to the re-austenitized condition. And the general corrosion resistance of the re-austenitized SLM-made steel was significantly superior to that of the non-AM steel.
316L	[126]	SLM	simulated body fluid (SBF)	PDP, EIS	laser power	E_{pit}	As the laser power increased, the corrosion potential also increased, the highest corrosion resistance was observed in SLM 316L samples fabricated at 220 W.
	[127]	SLM-SPS	3 wt.% NaCl	OCP, EIS	AM techniques	E_{corr}, E_{pit}, I_{corr} and E_p	SLM samples showed superior corrosion resistance and passivation behavior compared with that of SPS and wrought samples due to

						the presence of pores on the surface of SPS samples.
[128]	SLM	0.1 M NaCl	OCP, PDP	laser power and scan speed	Porosity, E_{pit}, E_{corr}, E_{rep}, I_{corr}	E_{rep} decreased with increase in porosity.
[91]	SLM	3.5 wt.% NaCl	OCP, EIS, PDP	HT	E_{corr}, E_{pit}, I_{corr}	After heat treatment, the pitting potential decreased due to the presence of thin passive films on the enlarged pores following heat treatment
[129]	SLM	6.0 wt.% $FeCl_3$	PDP, weigh t loss	Powder morphology (coarse, raw, and fine)	E_{corr}, I_{corr}	Fine powder exhibited a higher corrosion potential and corrosion currents compared to other powder morphology
[130]	SLM	0.6 M NaCl	OCP, PDP	-	E_{pit}	The AB samples presented high pitting potential and wider passive window than wrought samples
[95]	SLM	0.6 M NaCl	OCP, PDP		Porosity, grain size, E_{pit}, E_{corr}, I_{corr}	The pitting potential is not significantly affected by grain size but highly sensitive to porosity level. By increasing the porosity level results in a significant decrease in the pitting potential and an increase in the passivation current density.
[131]	SLM	Ringer's solution	OCP, PDP	-	E_{corr}, I_{corr}	The substrate that underwent a 150 h thermal oxidation process at 700°C

						demonstrated improved corrosion behavior.
[132]	SLM	0.1 M HCl	PDP	-	E_{corr}, I_{corr}	Compared to wrought material, the SLM 316L alloy showed a decrease in passivity and an increase in anodic current density.
[133]	SLM	0.9 wt.% NaCl	OCP, PDP	Scan speed	Porosity, E_{corr}, E_{rep}, I_{corr} and E_b	The general corrosion behavior of the SLM samples is similar to wrought steel. However, the SLM steel exhibits a lower breakdown potential and increased susceptibility to pitting corrosion. A rise in porosity had no significant impact on the corrosion rate of SLM 316L, but the E_{rep} and E_b decreased
[134]	SLM	3.5 wt.% NaCl	OCP, PDP, EIS	HPT	E_{corr}, E_{pit}, I_{corr}, and corrosion rate	Compared to the AB samples, HPT (high-pressure torsion) processing can enhance the corrosion resistance.
[135]	SLM	3.5 wt.% NaCl	PDP	Scan speed	E_{corr}, I_{corr}, grain size and density	The sample scanned at 500 mm/s demonstrated the highest corrosion resistance, while the sample scanned at 800 mm/s exhibited the lowest density and corrosion resistance, with the surface being the roughest.

	[136]	SLM	Ringer's solution	PDP	Energy density	E_{corr}, E_b, E_{rep} and R_p	An optimal laser energy density of 600 mJ/mm^3 was identified.
304L	[99]	SLM	3.5% NaCl	OCP, EIS, PDP	HT	E_{corr}, E_{pit}, I_{corr}, and corrosion rate	Heat treatment improved the corrosion resistance.
	[137]	SLM	(0.01 ,0.1 ,0.6 ,1) M NaCl	OCP, PDP	Surface roughness and porosity	E_b and corrosion rate	Surface roughness and porosity decreased corrosion resistance and pitting potentials.
420	[116]	SLM	3.5 wt.% NaCl	PDP	HT	E_{corr}, E_{pit}, I_{corr} and E_b	An increase in the pitting potential was observed after the heat treatment.
	[138]	DED WAAM	3.5 wt.% NaCl	OCP, PDP, EIS	-	E_{corr}, E_{pit}, I_{corr}	The top section of the constructed wall demonstrated greater resistance to corrosion and lower susceptibility to pitting when compared to the lower layers.
15-5PH	[111]	SLM	3.56 wt.% NaCl	PDP	HT	Pit size, E_{pit}, E_{prot}	The pitting potential of AB SLM specimens is approximately six times greater than that of solution annealed specimens.
	[112]	SLM	0.1 M NaCl	EIS, PDP, OCP	HT	E_{corr}, E_{pit}, I_{corr} and I_p	Samples undergoing directly aging treatment exhibited a higher pitting potential and more stable passive film, but lower I_{corr} and I_p compared to those subjected to solution treatment followed by an aging treatment.

[139]	DED	3.5 wt.% NaCl	EIS, PDP, OCP	HT	E_{corr}, I_{corr}	The corrosion resistance of samples undergoes a significant decline once the aging temperature surpasses 560°C. E_{corr} of samples aged between 560°C to 650°C exhibits an increased susceptibility to pitting.
[57]	SLM	0.1 M NaCl	EIS, PDP, OCP	Laser power and scan speed	E_{pit}	As the number of manufacturing defects increases, the pitting potential decreases, and the passivation performance deteriorates. Most of the pitting is thought to originate from these manufacturing defects.

Potentiodynamic polarization (PDP), electrochemical impedance spectroscopy (EIS), linear resistance polarization (LPR), open circuit potential (OCP), pitting potential (E_{pit}), corrosion potential (E_{corr}), corrosion current density (I_{corr}), passivation potential (E_p), protection potential (E_{prot}), polarization resistance (R_p), repassivation potential (E_{rep}).

1.7 IMPROVING CORROSION RESISTANCE OF AM STAINLESS STEELS

To improve the corrosion resistance of AM SS, researchers are exploring various approaches, such as optimizing process parameters, using higher-quality feedstock, and implementing post-processing treatments to reduce porosity and enhance the corrosion resistance. By improving the corrosion resistance of AM parts, it may be possible to expand the potential industrial applications for these materials and extend their useful life in corrosive environments. It must be noted that literature sometimes presented contradictory results. Optimizing the processing parameters of additively manufactured SS has the potential to improve its corrosion behavior. By adjusting various processing parameters such as laser power, scan speed, and powder bed temperature, it is possible to achieve a more uniform microstructure with fewer defects, which can lead to better corrosion resistance.

Wang et al. [57] reported that controlling the processing parameters are the key to reducing manufacturing defects of SLM 15-5PH SS, specifically by utilizing low laser power, high scanning speed, and laser energy. Kong et al. [126] emphasized that samples produced using high laser power shows improved elongation and corrosion resistance for AM SS 316 L in simulated body fluid (SBF). Barile et al. [148] reported that samples produced using higher energy densities tended to exhibit better mechanical and corrosion properties than those made with lower energy densities.

To improve the corrosion resistance of AM-produced SS, various coating techniques can be used. One such technique is the application of thin films or coatings using chemical vapor deposition (CVD) or physical vapor deposition (PVD) methods. These techniques can deposit a wide range of materials, including metals, ceramics, and polymers, onto the surface of the SS substrate [149]. Another coating technique is electrochemical deposition (ECD) [150]. ECD can deposit various metals, such as nickel, copper, and chromium, onto the surface of the substrate in a controlled manner, resulting in a more uniform and dense coating compared to PVD or CVD methods. Furthermore, surface modification techniques such as shot peening, laser shock peening, and plasma electrolytic oxidation (PEO) can also be used to improve the corrosion resistance of AM-produced SS [151]. These techniques introduce compressive stresses on the surface of the substrate, which can improve the mechanical properties and the resistance to corrosion. Cruz et al. [152] showed that, in SLM 316 L, compressive stresses lead to improved pitting resistance but slowed down passive film growth. In addition to the techniques mentioned, thermal spray coatings, including high-velocity oxygen fuel and plasma spray coatings, can be applied to the surface of the substrate to provide an extra layer of protection against corrosion. These coatings can be made of various materials, such as ceramic, metallic, or composite materials, depending on the specific application. Moreover, surface treatments, such as passivation, can also be employed to enhance the corrosion resistance of AM-produced SS. Passivation involves the creation of a thin protective oxide film on the surface of the SS substrate, which can help to prevent further corrosion. Various methods can be employed to carry out the passivation process, such as chemical immersion, electropolishing, and ultrasonic cleaning. It is important to note

that the selection of the coating or surface treatment method should be based on the specific requirements of the application, including the type of corrosion, the environment, and the operating conditions. Proper surface preparation and cleaning are also critical to ensure the effectiveness of the coating or treatment. Taghavikish et al. [153] provided a comprehensive analysis and review of the different types of coatings and their effectiveness in preventing corrosion. They discussed various types of coatings including metallic, organic, and inorganic coatings. They also presented the importance of proper surface preparation before coating application, which includes cleaning, degreasing, and removing any rust or corrosion. Stojanovic et al. [154] conducted a study on the effect of polyester and epoxy-polyester based coatings in corrosive media and found that the surface texture of the coating plays a significant role in its adhesion and overall performance. They found that the epoxy–polyester powder coating demonstrated superior performance compared to the polyester coating. Ni-based alloys, including NiCrBSi, NiCrMo, NiCoCrAlY, and others, are commonly used as protective coatings in various industries. These alloys are recognized for their exceptional corrosion resistance, high-temperature strength, and wear resistance. Li et al. [155] used NiCoCrAlY coating with a nominal composition of Ni, Co (22.88%), Cr (17.96%), Al (11.82%), Y (0.9%) was fabricated on 17-4PH SS. NiCoCrAlY coatings are particularly well-suited for high-temperature applications, as they can form a protective oxide layer that helps to prevent further oxidation and corrosion.

It has been shown that grain refinement can improve the corrosion performance of AM SS. This helps to enhance the growth of the passive layer in acidic environments by reducing the diffusion path length for chromium to the surface, thus facilitating the formation of a protective and even layer of chromium oxide. Grain refinement has the potential to boost the growth of a passive film. This is likely because it reduces the distance that chromium needs to diffuse in order to form a surface film that is enriched with chromium [156]. Chen et al. [157] proposed a new approach for improving the mechanical properties and corrosion resistance of additively manufactured 15-5PH SS by combining layer-by-layer ultrasonic micro-forging treatment (UMT) with directed energy deposition (DED). The UMT process

played a crucial role in refining the grain structure and reducing the oxide inclusion content, which contributed to the material's enhanced corrosion resistance.

Some studies investigate the effect of heat treatment on the electrochemical properties of SS that was additively manufactured. Stoudt et al. [11] showed that the pitting resistance of the 17-4PH SS was improved after heat treatment, which involved homogenizing at 1150°C and subsequent solutionizing at 1050°C. This improvement can be attributed to the finer martensite lath structure present in the samples, which contained more homogeneously distributed NbC precipitates [158]. Recrystallization heat treatment can be employed to refine the grain structure. This process involves eliminating melt pool boundaries [159], sub-grain boundaries, and dislocations in order to achieve a uniform structure with a thicker passive film. After heat treatment, the proportion of oxides in the passive film of SLM 316L, particularly chromic oxide, was observed to increase [6, 160]. The shape of grains has an impact on the SCC behavior of AM SS, as elongated grains can induce anisotropic properties that affect the propagation of cracks [6]. Wang et al. [112] reported that the pitting potential of the 15-5PH SS samples subjected to the solution following by aging treatment was less compared to samples treated only with aging. Consequently, the samples subjected to aging treatment exhibited a higher pitting potential, a more stable passive film, and lower corrosion and passive current densities compared to those treated with solution and aging [158]. Ultimately, proper heat treatment can significantly increase the material's resistance to corrosion of additively manufactured SS. However, excessive heat treatment can lead to the formation of unwanted phases, which can adversely affect the material's corrosion performance.

1.8 CONCLUSIONS

This paper presents a review of previous research on SS parts manufactured through AM techniques. The main objective of the paper is to investigate the relationship between processing parameters, mechanical properties, and corrosion resistance of parts. By selecting appropriate printing parameters, it is possible to optimize the corrosion performance, density,

and mitigate AM defects such as porosity, residual stress, poor surface finish, balling phenomena, and keyhole defects. The paper emphasizes that a better understanding of the AM process can enhance the mechanical properties and corrosion resistance of parts while reducing the incidence of defects. Further development of the AM technology could lead to reduced production costs and increased efficiency in the AM process. Further advancements in AM technology are required to make it feasible for application in diverse areas, including marine environments, to replace CM methods for producing steel parts. Based on the comparison between 316L, 304L, 420, 17-4PH and 15-5PH SS, it can be concluded that each alloy is ideal for a specific application. For instance, 316L is highly corrosion-resistant, making it ideal for applications requiring excellent corrosion resistance and high strength. 17-4PH and 15-5PH offer high strength and corrosion resistance, but 17-4PH is more resistant to general and pitting corrosion due to its higher chromium content, making it a better option for applications requiring high strength and good corrosion resistance. In summary, the paper highlights the potential of AM techniques in the manufacturing of SS parts and emphasizes the need for further research and development in this field. The information presented in the paper can be useful to researchers, engineers, and manufacturers interested in utilizing AM techniques for the production of SS parts with improved mechanical properties, corrosion resistance, and reduced defects.

Future works will focus on investigating the mechanical and corrosion behaviors of 17-4PH SS manufactured by SLM process, through a systematic study of microstructural development, density, mechanical strength and corrosion resistance as a function of processing parameters and heat treatments.

Conflict of Interest

The authors declare that they have no conflict of interest.

Data Availability

Data will be made available on request.

SUPPLEMENTARY MATERIAL FOR: THE APPLICATION OF ADDITIVE MANUFACTURING TO STAINLESS STEELS FOR MARINE APPLICATIONS

Anas Kerbout[1, a)], Noureddine Barka[1], Hendra Hermawan[2]

[1]Department of Mathematics, Computer Science and Engineering, Université du Québec à Rimouski, QC G5L 3A1, Canada

[2] Department of Mining, Metallurgical and Materials Engineering, Laval University, Quebec City, QC G1V 0A6, Canada

[a)] Corresponding author. E-mail address: Anas.Kerbout@uqar.ca

Table 4: Processing parameters, heat treatment (HT) properties, and mechanical properties of 17-4PH produced by AM from previous studies [12, 17-19, 27, 29, 32, 37, 43, 46, 49, 52, 53, 59, 79-84].

Reference No.	Heat source		Processing parameters					HT properties	Mechanical properties				
	Machine Name	Gas atmosphere	P (W)	v (mm/s)	h (µm)	t (µm)	E (J/mm³)	HT Condition	YS (MPa)	UTS (MPa)	Elongation (%)		Hardness
											Percentage reduction in area RA%	True fracture strain or ductility ε_f	
[12]	EOS M290	Ar	220	755,5	100	40	72.8	**AB**	830	887	46	0.61	N/A
								AB [EOS]	861	924	N/A	N/A	N/A
								H900	1050	1117	16	0.17	N/A
								H1025	1072	1132	33	0.39	N/A
								CA-H900	1300	1375	15	0.16	N/A
								CA-H900 [EOS]	1235	1336	N/A	N/A	N/A
								CA-H1150	895	948	39	0.48	N/A
[80]	EOS M280	N_2	190	787	110	40	54.9	**AB**	661±24	1255±3	16.2±2.5		333±2HV
								H900	945±12	1417±6	15.5±1.3		375±3HV
								H1025	870±25	1358±8	13.3±1.5		399±8HV
								H1150	1005±15	1319±2	11.1±0.4		381±3HV
								CA	939±9	1188±6	9.0±1.5		330±3HV
								CA-H900	1352±18	1444±2	4.6±0.4		417±5HV
								CA-H1025	1121±9	1172±2	9.6±1.7		350±4HV
								CA-H1150	859±11	1017±15	16.6±1.2		317±3HV
[17]	EOS M270 DMLS	N_2	175	1050	-	40	-	**AB**	477±3	1073±5	16.88±2.82		265HV*
								H900	522±17	1068±8	22.25±1.24		265HV*
								H1025	465±7	1243±14	18.29±2.1		290HV*
								H1150	360±21	1073±10	5.48±0.5		320HV*
								H1150M	637±18	1095±23	12.25±1.32		385.5±11HV
								CA	339±10	846±57	4.4±1.04		315HV*
								CA-H900	602±11	1028±12	5.16±0.45		285HV*
								CA-H1025	575±7	1128±6	10.29±1.2		355HV*
								CA-H1150	592±18	970±14	6.47±1.1		424.5±12.1HV
								CA-H1150M	605±34	958±8	11.23±3.62		350HV*
								AB	535	1090	11.2		N/A

[29]	ProX 300	N_2	135	1200	50	40	56.25	**N= 1200°C, 4 h+Furnace cooling**	600	1140	8.3	N/A
								S= 1060°C, 1 h+Gas cooling	593	1120	13.1	N/A
								SA= S+482°C, 4 h+Air	722	1210	12.15	N/A
								NSA=N+SA	1265	1380	12.95	N/A
[18]	Self-developed SLM machine (LSNF-I)	Ar	200	167 333 500 667 833 1000 1167	90 110 130	20 30 40	-	**AB**	633.75-666.25	1103.77–1105.75	20.48– 21.28	259HV
								(1040°C, 0.5 h) + (550°C, 4 h	1027.42–1032.05	1089.14–1123.44	14.72–16.64	361HV
[49]	EOS INT M270 SLM	N_2	195	800	100	40	60.94	**AB**	570	944	50	N/A
								650°C/2h	619	915	12	N/A
								788°C/2h	857	1487	7	N/A
								788°C/2h+ 482°C/1h	1126	1457	12	N/A
[37] Manufacturer parameters	ProX 100 ™ SLM	Ar	49	350	50	30	93.3	**AB**	**V**	660	N/A	4	350HV
									V (single built)	640	N/A	4,1	332HV
									H	660	N/A	9,7	300HV
								H900	**V**	740	N/A	3,44	377HV
									H	940	N/A	7,85	414HV
[37] optimized parameters			48	300			106.7	**AB**	**V**	600	N/A	6,56	300HV
								H900		940	N/A	2,56	433HV
								AB-Ar		830	887	45.86 0.61	270HV*

[81]	EOS M290	Ar / N_2	220	755,5	100	40	72.8	**1050°C/ 0.5h+552°C/4 h-Ar**	1140		1167		25.93	0.30	330HV*
								AB-N_2	835		1169		48.42	0.66	285HV*
								1050°C/ 0.5h+552°C/4 h-N_2	1176		1170		32.7	0.39	295HV*
[19]	In-house SLM machine with an IPG YLR AC 500W SLM		240	1000	70	40	85.7	**AB**	803±49		1228±7.5		12.7±1.4		365.4±6.7HV
								SHT=788°C/ 2h+WQ	966±42		1268±2.5		8.8±0.9		420.1±6.8HV
								Direct Aging=482°C /1h	1173±89		1478±1		9.8±1.3		453.2±4.6HV
								SHT+Aging	1276±16		1381±3		13.6±0.3		488.6±5.5HV
[27]	EOS M270		200	1000	100	20	100	**AB**	N/A		N/A		N/A		30HRC
								H900							43HRC
[82]	EOS M270 L-PBF		195	750	100	20	130	**650°C/1h in argon**	**V**	576.6	1357.9		24.6		N/A
									H	527.1	1423.6		24.1		N/A
[83]	3DSystems ProX300 SLM		N/A	N/A	60	N/A	N/A	**AB**	N/A		N/A		N/A		334.5±15HV
								1038°C/4h	N/A		N/A		N/A		355.2±8HV
								1038°C/4h +482°C /1h	N/A		N/A		N/A		524.5±6HV
[32]	EOSINT M280 SLM		N/A	N/A	N/A	N/A	N/A	**AB**	N/A		N/A		N/A		275HV
								1050°C/4h+ WQ	N/A		N/A		N/A		340HV
[52]	ProXTM 100 SLM		48	300	50	30	106.67	**AB**	**V**	580	940		5.8		N/A
									H	650	1060		14.5		N/A
								HT=1040°C/ 0.5h+AC+48 2°C/1h+AC	**V**	1020	1150		2.8		N/A
									H	1250	1410		11		N/A
[43]	SLM 280 HL	Ar	275	760	120	50	60.3	**Build direction**	**XY Axes (H)**	**Z (V)**	**XY Axes (H)**	**Z (V)**	**XY Axes (H)**	**Z (V)**	
								AB	840	740	890	790	12.5	2	300HV30
								T480=480°C/ 1 h	N/A	N/A	760	555	N/A	N/A	430HV30

								T550=550°C/ 4 h	1220	N/A	1245	535	0.5	N/A	430HV30	
								T620=620°C/ 4 h	940	N/A	1020	690	14	N/A	340HV30	
								T760	600	540	840	720	17.5	7	275HV30	
								SHT+T480 (SHT=1040 °C/1.5h)	760	580	980	755	4.5	0.5	300HV30	
								H+SHT+T480 (H=1190 °C/2 h)	1280	1240	1400	1320	3	0.5	480HV30	
								Atomizing media	**G**	**W**	**G**	**W**	**G**	**W**	**G**	**W**
[46]	3D Systems ProX 200 SLM	Ar	150	1550	50	30	64	**1051°C, 1h in H_2+482°C for 1h in N_2**	1116	365	1358	510	5.1	1	45 HRC	18 HRC
								1315°C, 45 min in H_2+482°C, 1h in N_2	1186	650	1308	780	2.6	0.7	45 HRC	24 HRC
			195	1250			104	**1051°C, 1h in H_2+482°C, 1h in N_2**	1200	500	1368	990	2.6	3.3	42 HRC	24 HRC
								1315°C, 45 min in H_2+482°C, 1h in N_2	1255	1000	1300	1261	2	5.5	43 HRC	40 HRC
									YS		**UTS**		**Strain (%)**	**HV grip**	**HV gage**	
[53]	EOS INT M270	N/A	N/A	N/A	N/A	N/A	N/A	**AB**	651		1071		19	294	475	
								SR=650°C for 1h	538		1502		15	432	535	
								Powder	**A**		**A**		**A**		**HV**	
															A	**B**
[79]	SLM 280 HL "Ar" A: Martensitic microstructure B: Ferritic microstructure		Interior:200 Border: 100	Interior:820 Border:400	108	30	N/A	**AB**	533		1150		8		350± 13.2HV	303± 4.5HV
								Direct Aging **5h**	-		-		-		477± 16.8HV	434 HV
								15h							451±21	N/A
								24h							N/A	482±12

									CA-H900	1120	1300	9	N/A	N/A
									HIP (1150°C, 4h at 100 Mpa) + SA+Aging	1233	1380	7	NA	N/A
									HIP+Aging	1167	1400	8	N/A	N/A
										YS	**UTS**	**Strain (%)**	**U_{OT} (static toughness) MJ.m^{-3}**	**HV**
[59]	EOS 280	Ar	195	900	100	40	54.2	**AB**	784	922	16.7	139.88	328 HV
								1150°C/ 0.5h+482°C /1h	1130	1231	6	69.39	426 HV
								1150°C/ 1h+482°C/1h	1280	1399	10.5	140.5	466 HV
								1150°C/ 4h+482°C/1h	1309	1431	7.2	97.49	470 HV
								1150°C/ 8h+482°C/1h	1165	1293	9	111.26	438 HV
									Density	**UTS**	**Elongation**	**HRC**	
[84]	3D Systems ProX 200 (Gas atomized powder D_{50}=13 µm)	Ar	150	1550	30	30	64	**AB**	96.6±0.5	1050±50	25±0.5	28±2 HRC	
			150	1250	30	30	80	**AB**	97.4± 0.5	1090±30	22±0.5	31±1 HRC	
			195	1550	30	30	84	**AB**	97.6±0.5	1110±30	22±0.5	36±1 HRC	
			195	1250	30	30	104	**AB**	97.5±0.5	950±50	16±1	31±1 HRC	
Average values of AB 17-4PH									676±246	1033±105	16±8	308±27HV	

Not available (N/A), Air cooling (AC), Water quenching (WQ), Vertical sample orientation (V), Horizontal sample orientation (H), Longitudinal sample orientation (L), Rockwell C Hardness (HRC), Vickers Hardness (HV), Gas atomized powder (G), Water atomized powder (W).

* From plots

Table 5: Mechanical properties of 316L[86-97], 304L[98-106], 15-5PH[57, 107-113], and 420[114-120] SS produced by AM from previous studies.

Alloy	Reference No.	Processing parameters						Mechanical properties			
		P (W)	V (mm/s)	h (µm)	t (µm)	E (J/mm^3)	Orientation	YS (Mpa)	UTS (MPa)	Elongation (%)	Hardness
316L	[86]	570/750	12.5/16.67	N/A	500	N/A	L	490	685	51	N/A
							T	280	580	62	N/A
	[87]	N/A	N/A	N/A	N/A	N/A	H	500	630	39	245±21HV
							L	500	630	47	
	[88]	100	200	N/A	50	N/A	T	N/A	N/A	N/A	255±6HV1
							L	517±38	687±40	32±5	247±9HV1
		200	220				T	N/A	N/A	N/A	212±7HV1
							L	N/A	N/A	N/A	202±5HV1
		200	220				T	N/A	N/A	N/A	229±3HV1
							L	N/A	N/A	N/A	211±7HV1
	[89]	100	222-	N/A	30	N/A	-	590±17	705±15	44±8	325±15HV
	[90]	N/A	N/A	N/A	30	N/A	-	462	565	53.7	N/A
	[91]	N/A	N/A	N/A	N/A	N/A		637.9±11.3	751.6±15.9	41.2±2.7	280HV
	[92]	175	700	120	60	N/A	L (ox)	534±6	653±3	16.2±0.8	N/A
							L (oy)	528±4	659±3	16.6±0.4	N/A
							T	444±27	567±19	8±2.9	N/A
	[93]	N/A	1000	N/A	N/A	N/A	-	487±3	594±4	49±4	219±5HV
	[97]	600	6.67	N/A	N/A	N/A	-	400*	425*	13.5*	200-240 HV
		800	10	N/A	N/A	N/A	-	415*	440*	14.5*	
		1000	13.33	N/A	N/A	N/A	-	405*	455*	21.5*	
		1150	16.67	N/A	N/A	N/A	-	440*	465*	17*	
		1450	20	N/A	N/A	N/A	-	450*	510*	20*	
		1650	23.33	N/A	N/A	N/A	-	N/A	N/A	N/A	
		245	900			110.7		N/A	625	-	-

	[94]	215	800	100	30	109.2		N/A	-	55	-
		215	1000			87.4		N/A	707	30	219
	[95]	200	-	90	50	44,4	-	540.1	651.6	59.2	N/A
								543.4	654.7	53.7	N/A
		250				55,6	-	533.1	630.5	58.1	N/A
								529.1	633.7	60.3	N/A
		300				66,7	-	N/A	N/A	N/A	N/A
		350				77,8	-	N/A	N/A	N/A	N/A
		400				88,9	-	454.8	556.8	59.4	N/A
								451.4	556.6	67.8	N/A
		$E = \frac{P*time}{h*t*d}$; point distance d=60µm and Exposure time=60 **µs**									
	[96]	195	800	100	N/A	N/A	-	456	703±8	N/A	325HV
		Average values of 316L						481±55	602±73	41.96±15.1	229±6HV
304L	[98]	105	50-	50	30	N/A	-	540±15	660±20	36±12	254±7HV
	[99]	N/A	N/A	N/A	N/A	N/A	-	485.2±0.2	693.9±3.9	56.3±0.2	N/A
	[100]	200	800	80	N/A	N/A	H	510±6	699±8	72±3	237±10HV
							V	488±4	645±4	86±3	229±9HV
	[101]	140	700	60	30	133.33	V	522.725	661.003	N/A	N/A
							H	551.759	694.458	N/A	N/A
			1100			84.85	V	486.110	647.663	N/A	N/A
							H	521.727	666.693	N/A	N/A
			1500			62.22	V	428.256	511.895	N/A	N/A
							H	428.652	514.493	N/A	N/A
	[102]	200	950	70	30	100.25	-	510.71±12	624.76±14	57.89±2	N/A
	[103]	200	1000	60	30	111,11	-	N/A	N/A	N/A	69HRB
		200	800	90		92,59	-	N/A	N/A	N/A	70HRB
		200	600	120		92,59	-	N/A	N/A	N/A	71HRB
		190	800	60		131,94	-	N/A	N/A	N/A	72HRB
		190	600	90		117,28	-	N/A	N/A	N/A	75HRB
		190	1000	120		52,78	-	N/A	N/A	N/A	72.5HRB

		170	600	60		157,41	-	N/A	N/A	N/A	68HRB
		170	1000	90		62,96	-	N/A	N/A	N/A	73HRB
		170	800	120		59,03	-	N/A	N/A	N/A	71HRB
	[104]	220	1100	80	40	62.5	H	457	653	67	N/A
							V	411	612.5	71.75	N/A
	[105]	182	1000	55	30	110.30	V	410	665	55	N/A
							H	455	707	45	N/A
	[106]	140	900	50	30	103.70	-	435±5	670±10	64.5±0.8	N/A
	Average values of 304L							478±40	648±39	60±11	156±42HV
15-5PH	[107]	195	1200	100	40	40.625	V	846	N/A	N/A	N/A
							H	758	N/A	N/A	N/A
	[108]	N/A	N/A	N/A	N/A	N/A	L	N/A	1149	6.75	N/A
							T	N/A	1126	4.19	N/A
	[109]	200	N/A	N/A	40	N/A	H (X)	1015.87	1156.58	16.38	N/A
							Long	1028.23	1212.50	14.14	N/A
							T (Z)	948.20	1196.31	14.08	N/A
	[110]	N/A	N/A	N/A	N/A	N/A	-	819±13	1015±12	12.5±1	338HV
	[111]	N/A	N/A	N/A	N/A	N/A	-	1000	N/A	8.57	40HRC
	[112]	195	850	N/A	N/A	N/A	-	N/A	N/A	N/A	363.7HV
	[57]	230	886	100	20	130	-	N/A	1420*	19.2	N/A
		170	886			96	-	N/A	1430*	16.2*	N/A
		150	886			85	-	N/A	1440	14.4	N/A
		230	1250			92	-	N/A	1400*	10.2*	N/A
		230	1400			82	-	N/A	1220*	3.3	N/A
	[113]	N/A	N/A	N/A	N/A	N/A	V	N/A	N/A	N/A	377±1HV
							H	N/A	N/A	N/A	381±2HV
	Average values of 15-5PH							916±93	1275±118	12±4	370±15 HV
420	[114]	195	700	100	20	N/A	-	600±5	1670±54	3.5±0.3	650±15HV
	[115]	120	-	80	20	N/A	-	N/A	N/A	N/A	46.6HRC
		130				N/A	-	N/A	N/A	N/A	47.9HRC

	140				N/A	-	N/A	N/A	N/A	48HRC
	150				N/A	-	N/A	N/A	N/A	50.7HRC
[116]	90	600	120	20	63	-	700±15	1050±25	2.5±0.2	55±1HRC
[117]	370	1200	75	N/A	N/A	-	919-996	1427-1697	2.6-9.7	688HV
[118]	258.7	1066.	100	30	N/A	-	N/A	N/A	N/A	33±1.2HRC
[119]	140	800	120	30	48.61	-	N/A	N/A	N/A	653.4HV
	170	800			59.03	-	N/A	N/A	N/A	655HV*
	200	800			69.44	-	N/A	N/A	N/A	670HV*
	230	800			79.86	-	N/A	N/A	N/A	687.3HV
	260	800			90.28	-	N/A	N/A	N/A	685HV*
[120]	400	1000	80	50	100	T	711.5± 23.9	1287.1± 87.8	1.6±0.2	63.5±3.9 HRC
						L	389.5±7.6	724.6± 31.3	0.9±0.1	65.0±4.1 HRC
Average values of 420							742±108	1392±224	3±1.5	632±90 HV

* From plots

CHAPITRE 2
INFLUENCE DU PROCESSUS DE FUSION SÉLECTIVE AU LASER ET DES PARAMÈTRES DU TRAITEMENT THERMIQUE SUR LES PROPRIETES MECANIQUES DE L'ACIER INOXYDABLE 17-4 À DURCISSEMENT PAR PRÉCIPITATION

Cet article a été soumis dans The International Journal of Advanced Manufacturing Technology portant le numéro de référence JAMT-D-24-00953

2.1 RESUME EN FRANÇAIS DU DEUXIEME ARTICLE

L'acier inoxydable durcissable par précipitation (PH), 17-4PH, est largement utilisé dans les industries aérospatiales, automobile et maritime. Dans le cadre de ce travail, des échantillons d'acier 17-4PH ont été fabriqués par la technique de fusion sélective par laser (SLM), en utilisant divers paramètres de processus (puissance du laser (P) et vitesse de balayage (V)) et de traitement thermique (temps de vieillissement (A) et température de vieillissement (T)). Des études de caractérisation ont été réalisées à l'aide de la microscopie électronique à balayage, d'essais de traction et de mesures de microdureté. De plus, un modèle statistique a été établi en utilisant l'analyse de variance (ANOVA) pour déterminer les effets des paramètres de processus et de traitement thermique sur le comportement mécanique (limite d'élasticité, résistance à la traction, allongement à la rupture et la dureté) et identifier les paramètres significatifs. Les résultats montrent que l'augmentation de la puissance du laser et la réduction de la température de vieillissement entraînent une augmentation de la limite d'élasticité, la résistance à la traction et la dureté. En revanche, une température de vieillissement plus élevée a pour effet d'augmenter l'allongement à la rupture. Un modèle de prédiction a été développé pour prédire la limite d'élasticité, la résistance à la traction, l'allongement à la rupture et la dureté de l'acier 17-4PH fabriqué par SLM.

Mots clés : acier inoxydable 17-4PH, fusion sélective laser, propriétés mécaniques, traitement thermique, analyse de la variance.

Cet article, intitulé « *Influence of selective laser melting process and heat treatment parameters on the mechanical properties of 17-4 precipitation hardening stainless steel* », a été soumis au journal *The International Journal of Advanced Manufacturing Technology*. En tant que premier auteur, j'ai contribué à l'essentiel de la recherche, le développement de la méthode et à la réalisation des tests expérimentaux. Le deuxième auteur de cet article est Noureddine Barka. Il est à l'origine de ce projet de recherche en proposant l'approche et la méthodologie pour aborder la problématique. Il a également contribué à l'amélioration de la rédaction pour la version finale. Asim Iltaf a participé à la réalisation des tests de traction et à la visualisation de la microstructure.

2.2 INFLUENCE OF SELECTIVE LASER MELTING PROCESS AND HEAT TREATMENT PARAMETERS ON THE MECHANICAL PROPERTIES OF 17-4 PRECIPITATION HARDENING STAINLESS STEEL

Influence of selective laser melting process and heat treatment parameters on the mechanical properties of 17-4 precipitation hardening stainless steel

Anas Kerbout[1, a)], Noureddine Barka[1], Asim Iltaf[1]

[1]Department of Mathematics, Computer Science and Engineering, Université du Québec à Rimouski, QC G5L 3A1, Canada

[a)] Corresponding author. E-mail address: Anas.Kerbout@uqar.ca

2.3 ABSTRACT

17-4PH precipitation hardening (PH) stainless steel is widely used in the aerospace, automobile, and marine industries. In the present work, 17-4PH were fabricated by selective laser melting (SLM) technique, with various process (laser power and scanning speed) and heat treatment (aging time and aging temperature) parameters. Characterization studies were performed using scanning electron microscopy, tensile tests, and microhardness measurements. Additionally, a statistical model was established using analysis of variance to determine the effects of process and heat treatment parameters on the mechanical behavior (Yield strength (YS), Ultimate tensile strength (UTS), Elongation to failure, and hardness) and identify the significant parameters. The most significant effect is found for laser power, aging temperature, and aging time where increasing laser power and decreasing aging temperature and aging time led to an increased YS, UTS, and hardness. Conversely, higher aging temperature resulted in increased elongation to failure. A prediction model was developed to predict the YS, UTS, elongation to failure, and hardness of SLM 17-4PH.

Keywords: 17-4PH stainless steel, selective laser melting, mechanical properties, heat treatment, analysis of variance.

2.4 INTRODUCTION

Precipitation hardening (PH) martensitic 17-4PH stainless steel is known for its excellent combination of strength and corrosion resistance [161]. This combination of properties made it one of the most used materials for applications requiring moderate corrosion resistance and high mechanical strength. It is widely used in the aerospace, nuclear reactor components, and marine environments [26]. In these precision industries, there is growing demand for enhanced design freedom to improve performance and reduce weight of parts, which necessitates advanced manufacturing techniques. In this context, additive manufacturing (AM) technologies, particularly Selective Laser Melting (SLM), can meet the specific needs of various industries [162]. SLM is a class of powder bed fusion processes that uses a high-energy laser beam as a source of energy to melt a layer of deposited metal powder particles and fuse it onto a previously melted layer [42, 163]. Despite the advantages of SLM, such as design optimization and production of complex geometries, other obstacles limited the wide application perspectives of this technology, due to manufacturing defects and the difficulty to determine the mechanical properties of parts by using the microstructure produced, in contrast to the conventional manufacturing (CM) [164]. The CM of 17-4 PH leads to a fully martensitic structure and coarse grains [29], except for a small amount of body centered cubic (BCC) δ-ferrite. At equilibrium, precipitation hardening stainless steels undergo solid-state phase transformation in the sequence of δ-ferrite → austenite → martensite. While the AM of the alloy exhibits different microstructures, resulting in mechanical properties that are different from CM due to incomplete austenite-to-martensite transformation resulting from rapid cooling and cyclic heating/cooling [165-167].

Some previous studies have confirmed that the as-built (AB) parts manufactured using Laser powder bed fusion (L-PBF) exhibit a non-equilibrium microstructure, including martensite, retained austenite and δ-ferrite [10]. Cheruvathur et al. [168], through X-ray diffraction measurements, determined that the AB microstructure of 17-4PH consists of two phases, with an approximate relative volume fraction of 50% FCC/austenite and 50% BCC/martensite. The significant amount of retained austenite observed after printing can be

attributed to the absorption of nitrogen, an austenite stabilizer, by the powder during atomization. Additionally, it may result from segregation effects due to rapid cooling, leading to variations in chemical composition and consequently, higher retained austenite fractions in localized areas. However, heat treatment can eliminate this effect by promoting chemical homogenization [10, 168]. The effect of powder chemical composition on the microstructure was investigated by Sabooni et al. [165] and Auguste et al. [43], using two different 17–4 PH powders. Sabooni et al. [165] found that samples from the first powder (A1) exhibited a fine martensitic microstructure with approximately 1.5% of retained austenite, while the second powder (B1) resulted in a dominant ferritic structure containing large ferrite grains. Auguste et al. [43] also revealed two different microstructures, martensitic (A2) and ferritic (B2), as listed in Table 6.

Table 6: Chemical composition (wt.%) and related ratio of equivalent chromium and equivalent nickel of the 17–4 PH powders [8, 13].

Ref	Powder	C	Mn	P	S	Si	Cr	Ni	Cu	Nb	N	Cr_{eq}/Ni_{eq}	Microstructure
[165]	Powder A1	0.07	1	-	-	0.07	17.7	4.2	3.3	0.14	0.1	1.75	Martensitic with ~ 1.5% of RA
	Powder B1	0.01	0.24	-	-	0.29	15.6	4.03	3.89	0.33	0.01	2.73	Ferritic
[43]	Powder A2	0.037	0.63	0.023	0.005	0.69	16.6	4.3	3.9	0.20± 0.02	0.085	2.04	Martensitic
	Powder B2	0.021	0.57	0.011	< 0.005	0.68	15.8	4.0	3.5	0.60± 0.07	0.059	2.41	Ferritic
[169]	-	0.03		0.008	0.003		16.1	4.16	3.73	0.3	0.033	2.375	Ferritic

Some authors have highlighted the influence of the atomizing media and the fabrication atmosphere on the mechanical properties and phase constitution of the AB 17-4 PH. Irrinki et al. [170] compared the mechanical properties of L-PBF 17–4 PH using gas-atomized and water-atomized powders. Their results indicated that specimens fabricated with gas-atomized powder exhibited better density, elongation, and ultimate tensile strength at low energy densities (64 J/mm^3). However, as the powder bed energy density was increased to 104 J/mm^3, specimens produced by water-atomized powder matched the quality of those made

with gas-atomized powder [46]. Pasebani et al. [46] reported that both as-printed water-atomized and gas-atomized samples of additively manufactured 17-4 PH comprised a combination of dual austenitic phase and lath martensitic phase, whereas after heat treatment gas-atomized powder exhibited a single martensitic phase. However, Irrinki [170] reported that regardless of energy density, the gas-atomized L-PBF parts exhibited only the martensite phase, while the water-atomized L-PBF parts appeared to consist of a mixture of austenite and martensite phases. Furthermore, studies have shown that the fabrication atmosphere influences the phases of 17-4 PH microstructure. Kartikeya Sarma et al. [171] reported that the percentage of retained austenite was higher, ranging from 50-75%, in a nitrogen atmosphere compared to only 8% in an argon atmosphere. This difference is attributed to nitrogen's higher thermal conductivity, resulting in a 40% difference in phase content due to faster cooling rates. The same findings were confirmed by Rafi et al. [49]. In addition, Murr et al. [27] reported that when an argon atmosphere is used during SLM fabrication with pre-alloyed 17-4 PH stainless steel powder, the resulting products are martensitic and exhibit magnetic properties. However, if nitrogen atmosphere is used instead, the product phase corresponds to the phase of the precursor powder, whether it is austenitic or martensitic. Moreover, Nezhadfar et al. [81] reported that AB samples made under a nitrogen atmosphere have a little higher hardness, strength and ductility than those made under argon gas. This is explained by the finer microstructure that was produced as a result of the faster cooling speeds offered by the nitrogen atmosphere, resulting in slightly higher strength and ductility.

Several studies have been undertaken in 17-4 PH to obtain the optimal SLM processing parameters that result in higher mechanical properties and material density. It has been indicated that the microstructure, density, and mechanical performances are impacted by the processing parameters. Hu et al. [172] reported that an increase in scanning speed led to an increase in density, followed by a decrease. At lower scanning speed, hatch spacing had an inferior effect on density. However, as scanning speed increased, the impact of hatch spacing became more apparent. Further, increasing the layer thickness leads to an increase in both the quantity and size of pores, while decreasing the layer thickness results in an increase in density. Moreover, reducing hatch spacing and layer thickness led to an increase in

microhardness. Gu et al. [69] found that decreasing the power and scanning speed, while keeping constant energy density, resulted in a higher porosity in L-PBFed 17-4 PH. Whereas, Wang et al. [173] reported that high scanning speed and low laser power could lead to more manufacturing defects. Consequently, reducing power and increasing scanning rate reduced laser energy density, which made it difficult to melt the metal powder. In addition to laser power, scanning speed, layer thickness, and hatch spacing, other processing parameters also affect the mechanical properties of SLM 17-4 PH. For instance, Mahmoudi et al. [37] and Yadollahi et al. [163] investigated the effect of part build orientation on the mechanical properties of 17-4PH SLM parts. They found that vertically built samples exhibited a significant reduction in strength and elongation to failure compared to the horizontally built samples. This reduction was attributed to the formation of defects, predominantly located between layers and oriented perpendicular to the direction of tensile load. This perpendicular alignment facilitated void growth and shear band coalescence during tensile loading, creating a less resistant path for material deformation. Conversely, Lebrun et al. [174] confirmed the part build orientation during SLM did not significantly impact mechanical strength.

The post-heat treatment can significantly influence the microstructure and mechanical properties of the printed parts. Several studies have investigated the effect of various heat treatment procedures on the microstructure and mechanical properties of SLM-made 17-4 PH. Nezhadfar et al. [12] emphasized the importance of solution annealing (Condition A, “CA”) prior to the aging heat treatment on the microstructure. Solution annealing eliminates the segregation of elements caused by the fabrication process and creates a more homogenized microstructure, consisting of finer lath martensite. This results in an increase in tensile strength. The highest tensile strength is typically achieved after ageing at H900 condition. Similarly, Cheruvathur et al. [168] reported that homogenizing at 1150°C for 120 minutes, followed by solutionizing at 1050°C for 30 minutes can eliminate segregation and achieve a uniform microstructure with 10% of retained austenite. In this regard Lebrun et al. [175] evaluated the impact of solution annealing (1040°C for 30 min) on mechanical properties and in eliminating the metastable austenite phase. Li et al. [13] reported that the optimal combination of strength and ductility can be achieved by subjecting the material to

homogenization for one hour followed by aging. This process refines the martensite and prior austenite grains. Additionally, solution annealing at 1150°C for 1 hour followed by air cooling can completely dissolve ε-Cu particles formed during printing. The following aging treatment at 482°C for 60 minutes promotes the formation of Cu-rich clusters coherent with the matrix, leading to strengthening. They also identified the critical role of NbC, nano-oxides, and Cu-rich clusters in reinforcing the 17-4PH produced through additive manufacturing. Si-Mo Yeon et al. [29] reported that subjecting the material to a sequence of heat treatments, including normalizing at 1200°C for four hours followed by furnace cooling, solution treating at 1600°C for one hour followed by gas cooling, and aging at 482°C for four hours with subsequent air cooling, led to higher mechanical properties that met the ASTM-693 (H900) industrial standard. The normalizing treatment helped develop a fully martensitic matrix with homogeneous Cu precipitates. However, inadequate heat treatment of L-PBF products can result in the formation of a δ-ferrite phase in their microstructure. Nezhadfar et al. [176] demonstrated that the fraction of retained austenite increases with prolonged aging for 4 hours at 621°C (CA-H1150) due to the diffusion of austenite stabilizer elements (Ni, N, Cu) to the grain boundaries. However, reducing the amount of retained austenite by solution annealing can enhance the mechanical properties of the material. Since, the presence of austenite reduces the microhardness and the amount of copper precipitated due to the higher solubility and a lower diffusivity of copper in austenite [49, 167, 177].

At present, only a limited number of studies have investigated the combined effect of SLM and post-heat treatment various parameters on mechanical properties of 17-4 PH by using statistical analysis. Therefore, the objective of the present work was to find the optimum additive manufacturing and heat treatment parameters to achieve higher mechanical properties using statistical analysis of variance (ANOVA), preceded by a fractional factorial design based on the Taguchi method with four factors and three levels.

2.5 EXPERIMENTAL SECTION

2.5.1 Experimental design

Taguchi experiment table with the orthogonal array setting L_9 (3^4) was used for the experimental design to minimize the number of experiments. The factors considered were laser power (*P*), scanning speed (*V*), aging time (*A*), and aging temperature (*T*), and their corresponding levels are provided Table 7.

Table 7: Factor and level of experimental design.

Factor	Code	Unit	Level		
			1	2	3
Laser power	*P*	W	170	195	220
Scanning speed	*V*	mm/s	700	800	900
Aging time	*A*	min	60	150	240
Aging temperature	*T*	°C	480	550	620

ANOVA was used to evaluate the significance of each factor (*P*, *V*, *A*, *T*) in terms of percent contribution to mechanical performance. The results were analyzed by using Minitab software. The ANOVA results were presented as the degree of freedom, the sum of the squares, the percentage of contribution, the average square, the average mean square, the *F-value*, and the *p-value* for each parameter studied. The percentage of contribution indicates the degree of significance of each factor on the total variation in the experiment. The stepwise method was employed, excluding non-significant terms after each iteration without using a hierarchical model to minimize errors and computation time.

2.5.2 Material and sample preparation

The SLM manufacturing system was an EOS M290 machine (EOS GmbH Electro Optical Systems, Germany) equipped with a 400 W Ytterbium fiber laser. 17-4 PH gas-atomized powder used in this study was supplied by EOS Inc. The samples were fabricated under an Argon atmosphere, to prevent oxidation, in on-edge direction (Figure 9d) with a

constant hatch spacing (100 μm) and layer thickness (40 μm), laser power between 170 and 220 W and scanning speed varying from 700 to 900 mm/s. The Scanning Electron Microscope (SEM) image of the powder particles (Figure 9a and Figure 9b), against a carbon tape background, shows morphology mostly spherical. The chemical composition (Figure 9c) of the powder as compared to the ASTM A564/A564M is listed in Table 8.

Table 8: Chemical composition (wt.%) of 17-4 PH powder.

Composition (wt%)	C	Mn	P	S	Si	Cr	Ni	Cu	Fe
Supplied powder	-	0.06	-	0.06	0.16	17.32	3.96	3.34	bal.
ASTM A564/A564M Limits	max. 0.07	max. 1.00	0.040	0.030	max. 1.00	15.00–17.5	3.00–5.00	3.00–5.00	bal.

Samples for tensile testing was sized according to ASTM-E8 (Figure 9e), and samples for microstructure observations and hardness measurements were 15 x 15 x 20 mm cubes, as shown in Figure 9f, by using different combinations of SLM and post HT process parameters. Energy density (E) is defined as the energy input (J) per unit volume (mm^3) and is calculated using equation (2) [42]:

$$E = \frac{P}{h * V * t} \tag{2}$$

After building, the parts were heat treated before cutting from the building plate at 650° C for one hour (stress relieving) and slow cooling to convert the primary phase composition from austenite to martensite [178], and to reduce residual stresses [179] caused by the high temperature gradients that occur during SLM processing [180]. According to Nezhadfar et al. [176] and Riemer et al. [90] stress relieving does not alter the microstructure or mechanical properties of the L-PBF 17-4 PH. Consequently, a solution annealing was performed at 1040 °C for 30 min followed by air cooling. Then, aging was performed according to the parameters listed in Table 9.

2.5.3 Tensile tests

Tensile tests were performed using 810 MTS (Material Test System) universal testing machine with 100 kN capacity at room temperature with a crosshead speed of 0.4 mm/min. The loading direction of each sample was vertical to the build direction (Figure 9d). To ensure reproducibility, the average value of three tensile tests was reported in the results.

2.5.4 Microstructural Characterization

To analyze the microstructure of the 17-4PH, samples were cross-sectioned in the middle of coupons in a rectangular shape, mounted and polished, and finally chemically etched with Fry's reagent at room temperature to reveal the microstructures. The microstructure analysis was conducted using a Hitachi TM3000 scanning electron microscope (SEM).

2.5.5 Microhardness

The microhardness was measured on XY section (Figure 9f) on polished and etched surfaces after microstructure observations. A Clemex micro-hardness tester was used to measure the Vickers (HV) and Rockwell C (HRC) micro-hardness. The load applied was 300 gf ($HV_{0.3}$) with a dwell time of 10 s for each indentation. The average hardness and standard deviation were determined from 20 points measurement made per sample. To avoid hardening effects, it was ensured that the indent marks were spaced at least four diameters apart from the previous indent [17].

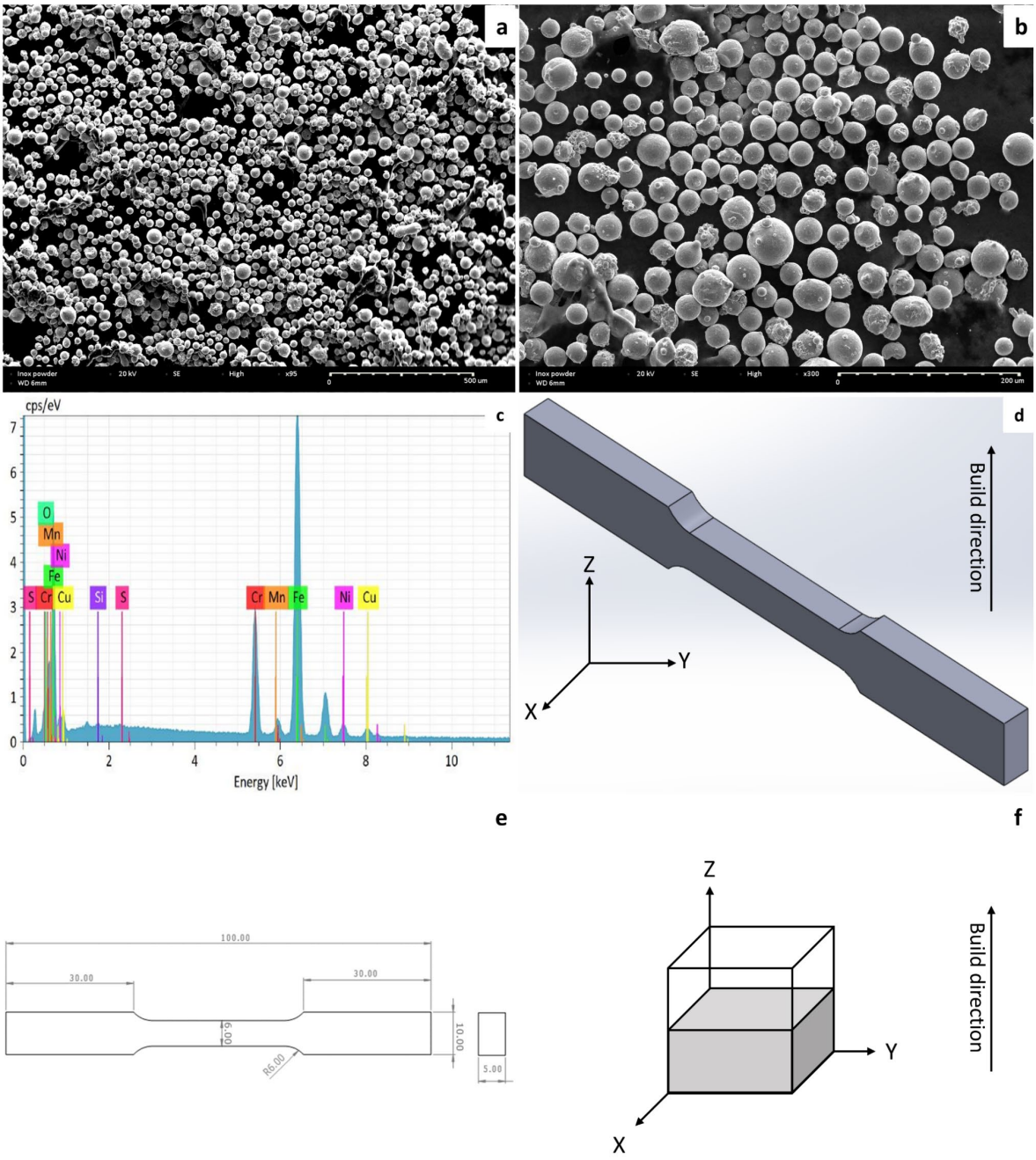

Figure 9: a) Scanning electron microscopy (SEM) image of 17-4 PH stainless steel powder at 95, b) 300 magnification scale, c) EDS analysis of 17-4 PH stainless steel powder, d) Building direction and, e) Size of tensile samples, f) The schematic of direction for microstructure analyses and microhardness measurements.

2.6 RESULTS AND DISCUSSION

2.6.1 Microstructure of the SLM printed 17-4 PH stainless steel

Additive manufacturing can introduce several factors that impact the microstructure. These factors include heating, melting, cooling and solidification, which can induce microstructural heterogeneities, anisotropy, and residual stresses. To mitigate these effects, and optimize the material properties, post heat treatments are required, especially for PH stainless steels that derive their strength from the formation of finely dispersed Cu-rich particles [10]. Figure 10 shows the representative microstructures of SLM-made 17-4PH stainless steel after different process and heat treatment parameters. After CA-H900 (480°C for 60 min) (Figure 10a), the microstructure was fully martensitic with Cu-rich precipitates in the martensitic matrix [181]. The martensitic laths become finer as the aging time increases (Figure 10c, Figure 10e, Figure 10g). The dissolution of martensitic laths can be attributed to the continuous rejection of carbon from the martensitic matrix [182]. Ghasemian Malakshah et al. [183] reported that the difference between copper precipitates formed during the different heat treatments is their size and relative coherency to the matrix. They found that samples aged at lower time and temperature (464 °C for 129 min) exhibited smaller precipitates with higher coherency with the matrix in comparison with samples aged at higher time and temperature (620 °C for 240 min), which could be attributed to increase in diffusion range of atoms. A martensite block structure with a fraction of austenite can be noticed in samples 3, 4, and 8 (Figure 10c, Figure 10d, Figure 10h) subjected to high aging temperature (620 °C). Similar observations were noted by Nezhadfar et al. [12] which attributed the formation of austenite phase and its stabilization along the lath martensite boundaries to the diffusion of austenite stabilizer elements, such as Cu, Ni, Mn, and N, during the aging at 662 °C for 240 min. Liu et al. [184] reported that materials aged at temperatures between 450°C and 510 °C reached their maximum strength and hardness due to the formation of coherent copper rich precipitates. Overaging, at temperatures above 580 °C, led to the formation of

reverted austenite and recrystallized ferrite. Furthermore, it can be observed that no inclusions or segregations were observed in the microstructure.

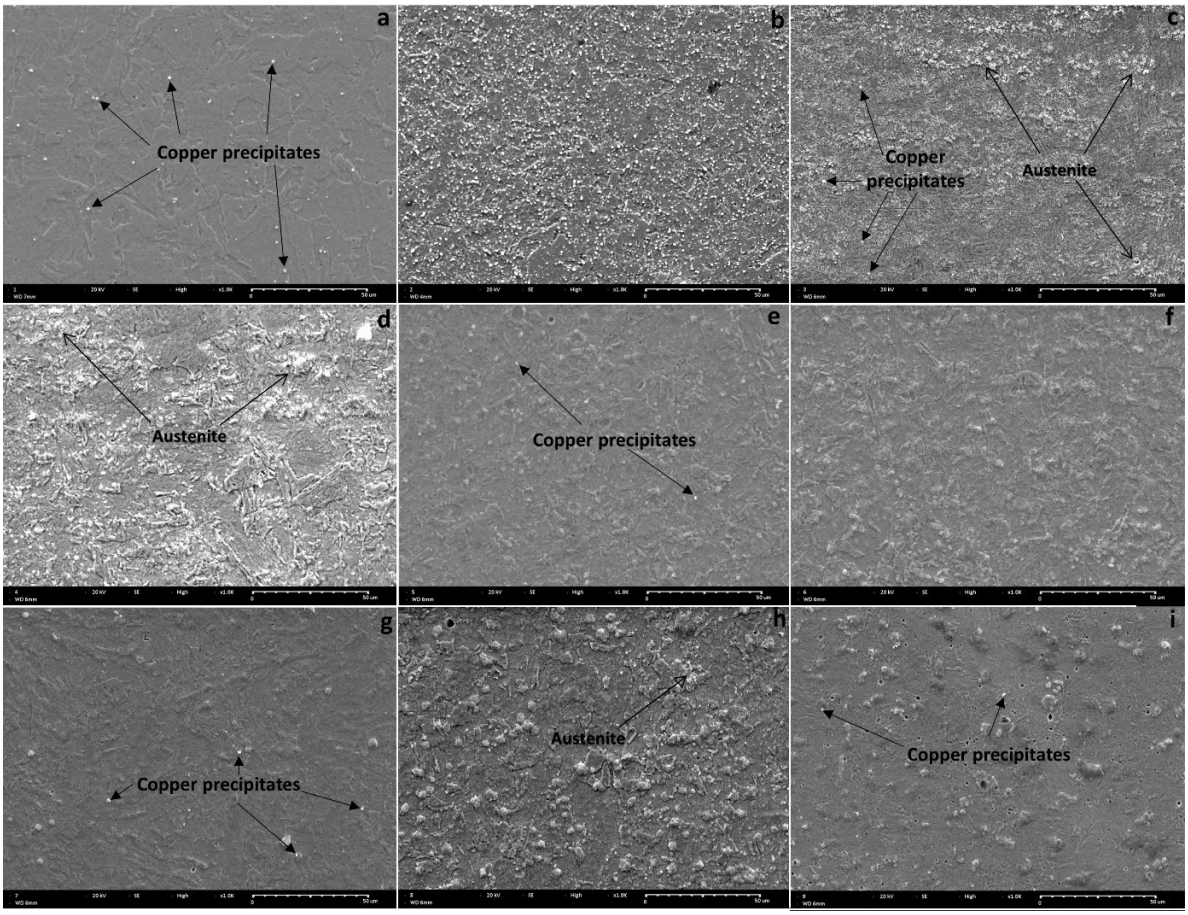

Figure 10: a-i) SEM micrographs of SLM 17-4 PH etched with Fry's reagent at different print and heat treatments parameters.

2.6.2 Mechanical performance

The stress-strain curves and the bar charts of the yield strength (YS), ultimate tensile strength (UTS), Elongation to failure, and Hardness of the SLM 17-4PH samples under different SLM and heat treatment parameters are presented in Figure 11, and the corresponding data is listed in Table 9. As depicted in Figure 11a, Figure 11b, and Figure 11c, the samples heat treated at 480 °C had the highest UTS, followed by those aged at 550 °C and 620 °C. Conversely for elongation to failure, samples heat treated at 620 °C had the

highest elongation for failure, followed by those aged at 550 °C and 480 °C. The highest value of hardness is observed in test number **7** corresponding to laser power of 220 W, scanning speed of 700 mm/s, aging temperature of 550 °C and aging time of 240 min.

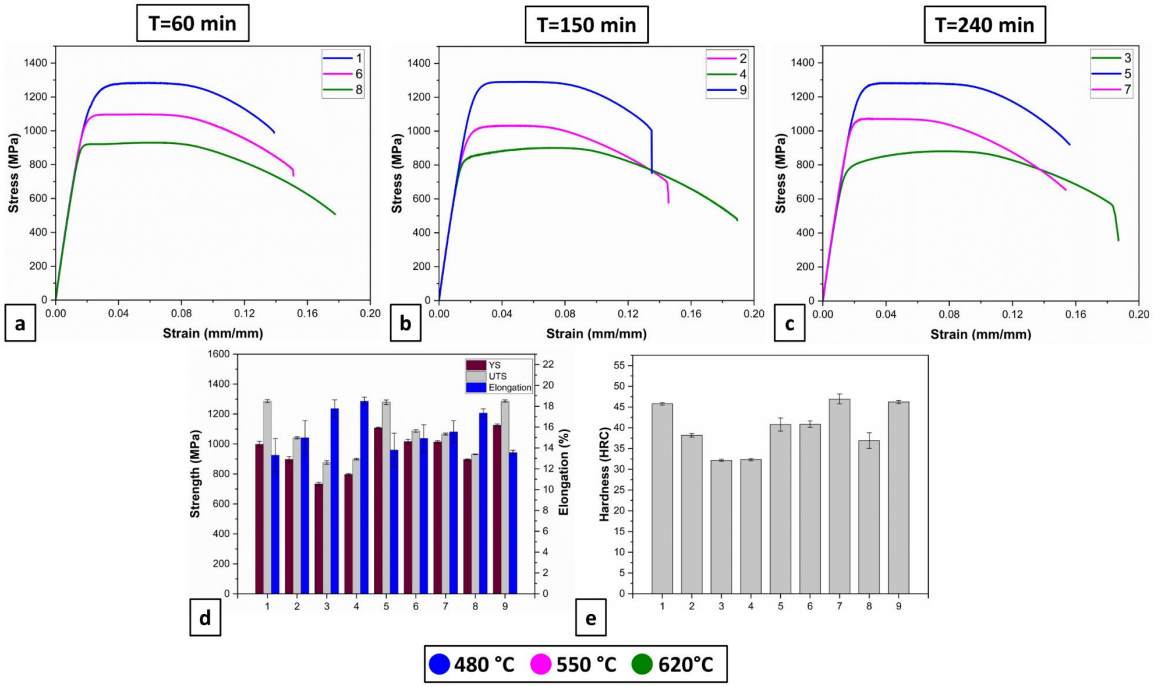

Figure 11: (a, b, c) Stress-strain curves, (d) The UTS, YS and elongation to failure, and (e) hardness of 17-4 PH stainless steel samples.

Table 9: Experimental design and results.

Sample Number	Factors					Responses			
	P **(W)**	***V*** **(mm. s^{-1})**	***A*** **(min)**	***T*** **(°C)**	***E*** **(J.mm^{-3})**	***YS*** **(Mpa)**	***UTS*** **(Mpa)**	***Elongation*** **(%)**	***Hardness*** **(HRC)**
1	170	700	60	480	60.714	998.54±19.50	1286.15± 9.45	13.31±1.6	45.77±0.32
2	170	800	150	550	53.125	897.73±18.3	1041.49±6.87	14.98±1.63	38.22±0.43
3	170	900	240	620	47.222	733.96±9.26	877.3±12.12	17.78±0.83	32.17±0.26
4	195	700	150	620	69.643	796.95±5.73	898.86±5.58	18.49±0.39	32.32±0.25
5	195	800	240	480	60.938	1108.3±3.76	1278.7±15.1	13.8±1.61	40.8±1.57
6	195	900	60	550	54.167	1017.39±14.2	1087.29±9.28	14.92±1.3	40.87±0.77
7	220	700	240	550	78.571	1013.97±8.38	1066.45±6.58	15.55±1.06	46.94±1.19
8	220	800	60	620	68.750	897.69±3.48	931.69±1.44	17.35±0.4	36.92±1.9
9	220	900	150	480	61.111	1125.15±8.98	1287.05±6.99	13.56±0.22	46.23±0.38

The tensile results indicate that an increase in laser power and decrease in aging temperature results in an increase in YS. For instance, samples with laser power exceeding 195 W and aging temperature below 550 °C exhibit a YS exceeding 1000 MPa. The UTS decreased with decreasing aging temperature. Samples No 1, 5, and 9 present higher UTS than other samples, which can be attributed to the presence of austenite in the microstructure. Austenite can attenuate the precipitation hardening effect, due to the solubility of copper (a key element for precipitate formation) in austenite [175]. Generally, the aging heat treatment process involves the precipitation of coherent Cu-rich clusters with a BCC structure at temperatures between 480 and 620 °C, resulting in a wide range of mechanical properties [17]. Bhambroo et al. [185] reported that the aging treatment for 17-4PH leads to various microstructural changes, including carbide formation, copper precipitates and the formation of reverted austenite. Reverted austenite starts forming at temperatures above 550 °C and continues to grow with longer aging times. Maximum strength is typically achieved after aging at 580 °C for 15 minutes, which can be attributed to the formation of coherent fine copper precipitates. Yeon et al. [29] reported that age hardening increases YS by precipitation of Cu particles and hindering dislocation movement through the Orowan mechanism. Additionally, the elongation to failure increased as the aging time increased, and samples

heat treated at 620 °C exhibited a ductile fracture mechanism. The maximum elongation to failure observed was 18.487%. Aging at a higher temperature of 620 °C led to a decrease in mechanical strength and an increase in elongation, which can be attributed to the presence of reverted austenite and larger precipitate size [183]. Eskandari et al. [17] confirmed that overaging led to an increase in ductility and a decrease in hardness by transforming coherent BCC copper precipitates into non-coherent FCC copper precipitates.

Some studies reported that the hardness value of samples produced through SLM is significantly higher compared to wrought samples. This was confirmed by authors [111, 186, 187] and attributed to the high cooling rate associated with the SLM process, which leads to the formation of a finer grain microstructure. This finer grain structure is responsible for the observed hardening, as it aligns with the Hall-Petch effect, which states that hardness tends to increase as the grain size decreases. Furthermore, the presence of a higher density of dislocations near the grain boundaries in finer grain structures contributes to higher hardness values compared to coarser grain structures resulting from plastic deformation [188]. The average hardness values of the 9 samples for the different parameters are given in the bar chart in Figure 11e. The hardness values for samples produced under highest P, lowest V, A, and T are significantly higher than other samples. The highest value of hardness is observed in test number 7 corresponding to laser power of 220 W, scanning speed of 700 mm/s, (highest energy density 78.57 $J.mm^{-3}$), aging temperature of 550 °C and aging time of 240 min. This result is in accordance with a study published by Pasebani et al. [46] that found that the hardness of 17-4PH L-PBF parts increases with higher energy density. The increase in hardness in 17-4 PH stainless steel is primarily attributed to the formation of coherent Cu-rich precipitates (Figure 12) during the aging treatment [189, 190]. As reported in the study conducted by Garcia-Cabezon, the Cu-rich precipitates that form during the aging process play a significant role in the hardening of the alloy [124]. These precipitates effectively impede the movement of dislocations through the Orowan mechanism [191] and create a semi-coherent interface, contributing to the increase in hardness. It is important to note that the volume percentage and size of the Cu significantly influence the hardness change [10]. The presence of martensite could be one of the factors that increase hardness additionally to

the grain size, volume fraction of austenite (retained or reversed), thermal treatment response, and work-hardenability [17].

Some samples (number 3, 4, and 8) exhibited a decrease in hardness after aging at 620 °C, which aligns with findings reported by Mirzadeh and Najafizadeh [192]. Their study revealed that aging at higher temperatures above 595°C can result in the material becoming softer in comparison to its solution annealed condition due to the coarsening of Cu-rich precipitates, the formation of reverted austenite, and the recovery of dislocations [165]. Additionally, these samples also exhibited the highest elongation to failure values. This increase in ductility can be attributed to a higher presence of retained austenite compared to martensite. Yadollahi et al. [163] emphasized that higher levels of retained austenite in 17–4 PH samples tend to reduce hardness and tensile strength while increasing ductility, elongation to failure, and strain hardening due to the transformation-induced plasticity (TRIP) effect [10].

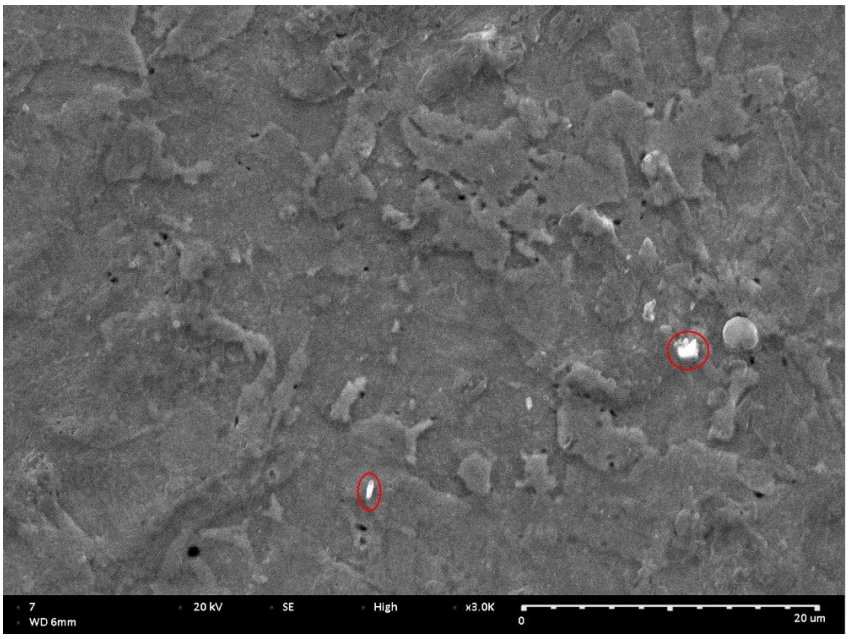

Figure 12: SEM image showing copper precipitates in sample No 7.

2.6.3 Analysis of variance (ANOVA)

To examine the impact of process parameters on the mechanical properties of SLM 17-4PH, a systematic analysis was conducted using statistical tools following collecting experimental data. ANOVA was used to investigate the effects of model input parameters (*P*, *V*, *A*, and *T*) on output responses (*YS*, *UTS*, Elongation to failure, and hardness). This analysis involved quantifying the effects of these parameters on the outcomes through hypothesis testing using the stepwise method. The goal was to determine whether the observed variations were primarily influenced by a single parameter, multiple parameters, or a combination of them. The initial model included independent variables (*P, V*, *T*, *A*), quadratic variables (P^2, V^2, T^2, A^2), and two-way interactions ($P \times V$, $P \times T$, $P \times A$, $V \times T$, $V \times A$, $T \times A$). ANOVA table contains degrees of freedom, sum of the squares, percentage of contribution, average square, average mean square, *F-value*, and *p-value* for each parameter studied. The results of the ANOVA analysis of *YS*, *UTS*, Elongation to failure, and hardness are presented in Table 10, respectively. A *p-value* below 0.05 indicates a significant effect on the response. The *YS* is primarily influenced by aging temperature with a 75.69%

contribution followed by laser power with a contribution of 19.38%. The *UTS* is influenced mainly by aging temperature with a contribution of 98.12% and significant *p-value* of 0.002 < 0.05. The elongation to failure is mainly influenced by aging time with a 94.38% contribution. The hardness is mainly influenced by two factors: the aging temperature with a contribution of 64.5% and laser power with a contribution of 12.7%. The residual value squared (R^2) is used to measure the variation in the measured data relative to the predicted data. The R^2 for *YS* and *UTS* is 100%, indicating a perfect correlation between the model and the experimental data. The R^2 for elongation to failure is 98.65% and 80.25% for hardness. Standard deviation (*S*) represents the distance between experimental and fitted values. A small value for *S* signifies a strong fit.

Table 10: Contribution of parameters on YS, UTS, Elongation to failure, and Hardness.

Source	DF	Sum of Squares	Contribution (%)	Adj SS	Adj MS	*F-value*	*p-value*
YS							
P	1	27551	19.39%	1361.57	1361.57	647.75	0.025
V	1	749	0.53%	2880.90	2880.90	1370.54	0.017
A	1	549	0.39%	1844.89	1844.89	877.68	0.021
T	1	107572	75.69%	1134.44	1134.44	539.69	0.027
T*T	1	2169	1.53%	280.59	280.59	133.49	0.055
P*T	1	1759	1.24%	1759.09	1759.09	836.86	0.022
V*A	1	1765	1.24%	1765.17	1765.17	839.75	0.022
Error	1	2	0.00%	2.10	2.10	-	-
Total	8	142116	100.00%	-	-	-	-
***R²*=100%**			**Adjusted *R²*=99.99%**			***S*=1.45**	
UTS							
P	1	1073	0.48%	278.82	278.82	10885.58	0.006
V	1	0	0.00%	203.52	203.52	7945.78	0.007
A	1	1139	0.51%	573.41	573.41	22387.17	0.004
T	1	218139	98.12%	2181.66	2181.66	85176.68	0.002
T*T	1	1592	0.72%	955.46	955.46	37303.03	0.003
P*V	1	294	0.13%	256.52	256.52	10014.89	0.006
V*T	1	87	0.04%	87.07	87.07	3399.46	0.011
Error	1	0	0.00%	0.03	0.03	-	-
Total	8	222325	100.00%	-	-	-	-
***R²*=100%**			**Adjusted *R²*=100%**			***S*=0.16**	
Elongation to failure							
P	1	0.0254	0.09	0.02535	0.02535	0.19	0.693
V	1	0.1980	0.67	0.19802	0.19802	1.48	0.311
A	1	27.9504	94.38	0.01322	0.01322	0.10	0.774
T	1	0.4004	1.35	0.40042	0.40042	3.00	0.182
A*A	1	0.6385	2.16	0.63845	0.63845	4.78	0.117
Error	3	0.4009	1.35	0.40095	0.13365	-	-
Total	8	29.6136	100.00	-	-	-	-
***R²*=98.65%**			**Adjusted *R²*=96.39%**			***S*=0.37**	
Hardness							
P	1	32.341	12.70%	32.341	32.341	2.57	0.184
V	1	5.530	2.17%	5.530	5.530	0.44	0.543
A	1	2.220	0.87%	2.220	2.220	0.18	0.696
T	1	164.222	64.50%	164.222	164.222	13.06	0.022
Error	4	50.293	19.75%	50.293	12.573	-	-
Total	8	254.606	100.00%	-	-	-	-
***R²*=80.25%**			**Adjusted *R²*=60.49%**			***S*=3.55**	

To estimate the *YS*, *UTS*, elongation to failure, and hardness as a function of *P*, *V*, *A*, and *T*, and their interactions, the following regression equations (3), (4), (5), and (6) were used:

$$YS\ (MPa) = 4829 - 11.659\,P + 1.3117\,V + 5.408\,A - 12.532\,T + 0.005405\,T^2 + 0.023967\,P*T - 0.006602\,V*A \quad (3)$$

$$UTS\ (MPa) = 2072.7 + 16.478\,P + 4.9876\,V - 0.43449\,A - 13.5964\,T + 0.010926\,T^2 - 0.020259\,P*V - 0.001885\,V*T \quad (4)$$

$$Elongation\ (\%) = 33.6 + 0.00260\,P - 0.00182\,V + 0.00287\,A - 0.0960\,T + 0.000115\,T^2 \quad (5)$$

$$Hardness\ (HRC) = 71.7 + 0.0929\,P - 0.0096\,V - 0.0068\,A - 0.0747\,T \quad (6)$$

The predictive *YS*, *UTS*, elongation to failure, and hardness presented in Table 11 were calculated by the prediction models (equations (3), (4), (5), and (6)), and the correlation curves between the predictive and the experimental measured data are plotted in Figure 13. For *YS* (Figure 13a) and *UTS* (Figure 13b), the points align perfectly on a straight line, which indicates a strong correlation between the predicted and experimental results. In the case of elongation to failure (Figure 13c), the points are grouped around a straight line, suggesting a good fit between predicted and experimental values. However, the scatter plot for hardness (Figure 13d) shows a dispersion of data points around the straight line, indicating a lower correlation.

Table 11: Measured and predictive a) YS, b) UTS, c) Elongation to failure, and d) Hardness.

Sample Number	Measured *YS* (MPa)	Predictive *YS* (MPa)	Measured *UTS* (MPa)	Predictive *UTS* (MPa)	Measured Elongation (%)	Predictive Elongation (%)	Measured Hardness (HRC)	Predictive Hardness (HRC)
1	998.54	998.02	1286.15	1286.1	13.31	13.36	45.77	44.51
2	897.73	898.62	1041.49	1041.3	14.98	15	38.22	37.71
3	733.96	733.35	877.3	877.25	17.78	17.78	32.17	30.91
4	796.95	797.13	898.86	898.8	18.49	17.95	32.32	35.76
5	1108.3	1108.5	1278.7	1278.5	13.8	13.76	40.8	44.65
6	1017.39	1016.9	1087.29	1087.2	14.92	14.63	40.87	39.68
7	1013.97	1013.4	1066.45	1066.4	15.55	15.57	46.94	42.7
8	897.69	897.9	931.69	931.51	17.35	17.57	36.92	37.74
9	1125.15	1125.3	1287.05	1287	13.56	13.38	46.23	46.62

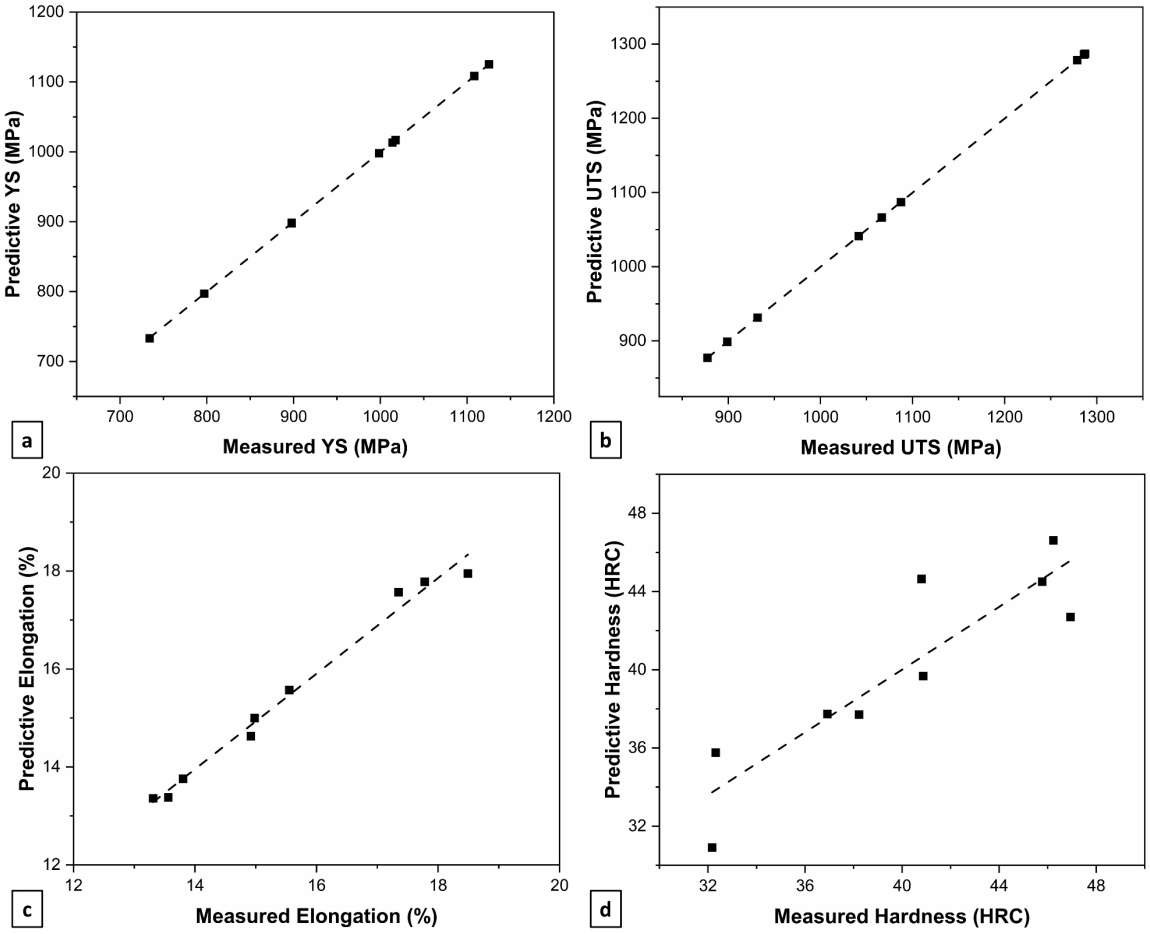

Figure 13: Correlation curves for measured and predictive a) YS, b) UTS, c) Elongation to failure, and d) Hardness.

Figure 14 shows the main effects plots for the UTS, YS, elongation to failure, and hardness. These graphs are used to interpret the effect of each parameter level on mechanical performance. It can be noticed that the increase in laser power (P) and decrease in aging temperature (T) led to an increase in YS, UTS, and hardness (Figure 14a, Figure 14b, and Figure 14d). Conversely, higher aging temperature results in increased elongation to failure. The main effects plots indicate that aging at 480 °C allowed the highest YS, UTS, and hardness values but the lowest elongation to failure.

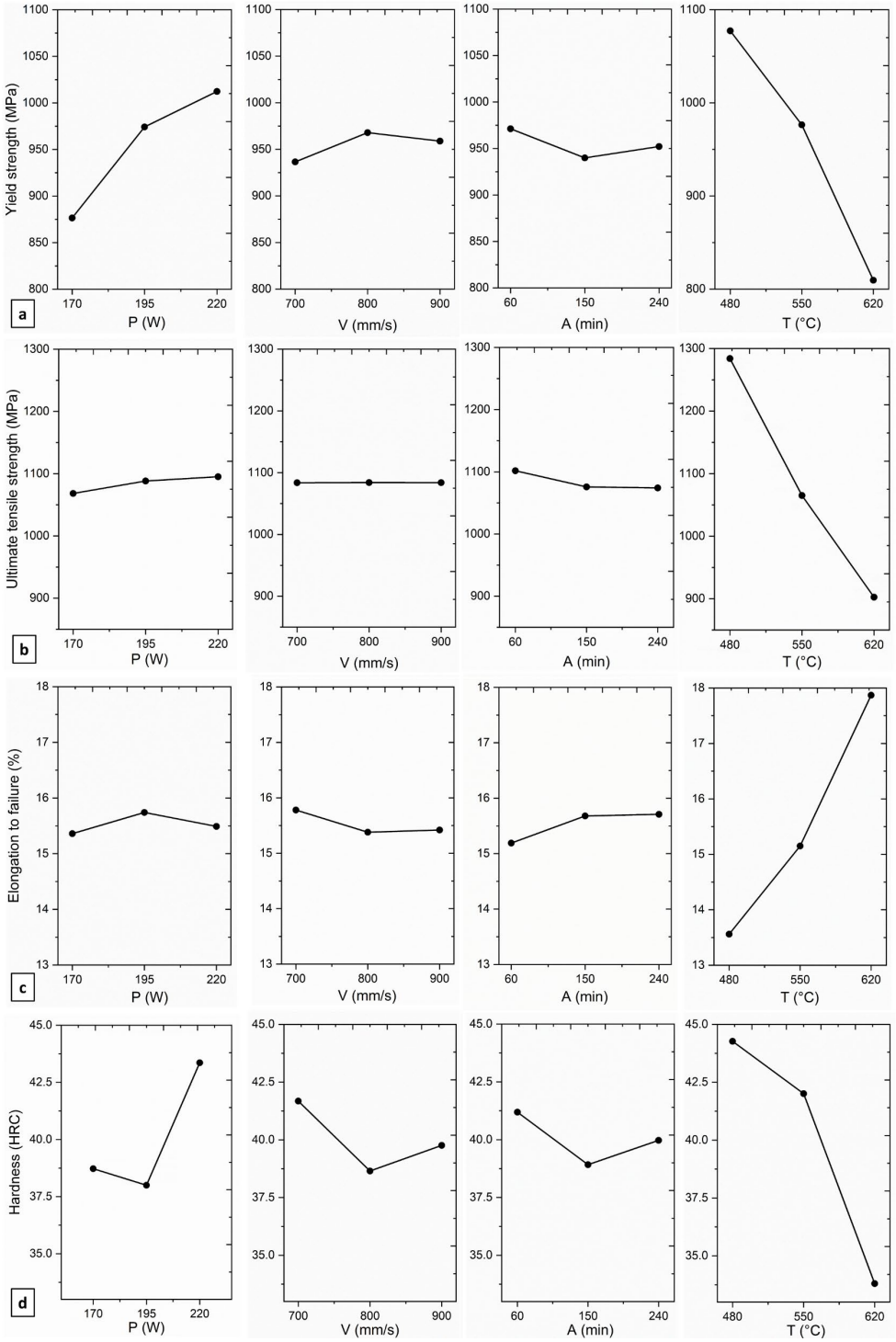

Figure 14: Main effects plot of a) Yield strength, b) Ultimate tensile strength, c) Elongation to failure, d) Hardness.

2.7 CONCLUSION

The present work concludes that the aging heat treatment process leads to different microstructures and a wide range of mechanical properties. Samples subjected to lower aging times and temperatures displayed smaller precipitates with greater coherency to the matrix, in contrast to samples aged at higher time and temperature. The experimental tests were performed using Taguchi experience planning and ANOVA. The results revealed that aging temperature primarily influences yield strength, ultimate tensile strength, and hardness, with a decrease in aging temperature resulting in higher values for these mechanical properties. Conversely, an increase in aging temperature results in an increase in elongation to failure. In particular, the best values for yield strength, ultimate tensile strength, and hardness are achieved with the following parameters: a laser power of 220 W, an aging time of 60 minutes, and an aging temperature of 480 °C. As for elongation at rupture, the optimal parameters are as follows: a laser power of 195 W, an aging time of 240 minutes, and an aging temperature of 620 °C. Regarding the scanning speed, it has been observed that it does not have a significant contribution to the results. Empirical predictive equations were performed using multiple linear regression to predict the mechanical properties of SLM-made 17-4PH. The results reveal a good correlation between the predicted and experimental results for YS, UTS, and elongation to failure.

Conflict of Interest

The authors declare that they have no conflict of interest.

Acknowledgments

The present work was funded by the support of the Natural Sciences and Engineering Research Council of Canada (NSERC) via Discovery Grant (RGPIN-2022-04796)

Data Availability

Data will be made available on request.

CHAPITRE 3
INFLUENCE DU PROCESSUS DE FUSION SÉLECTIVE AU LASER ET DES PARAMÈTRES DU TRAITEMENT THERMIQUE SUR LA RÉSISTANCE À LA CORROSION DE L'ACIER INOXYDABLE 17-4 À DURCISSEMENT PAR PRÉCIPITATION

Cet article a été soumis dans Metals and Materials International portant le numéro de référence MAMI-D-24-00233

3.1 RESUME EN FRANÇAIS DU TROISIEME ARTICLE

Dans le travail présent, la résistance à la corrosion de l'acier inoxydable martensitique 17-4PH fabriqué à l'aide de la technologie de fusion sélective par laser (SLM) a été explorée. Ce travail vise à déterminer l'effet des paramètres du processus SLM et des paramètres de traitement thermique sur la résistance à la corrosion de l'acier 17-4PH dans une solution de chlorure de sodium à 3,5%, en utilisant des techniques électrochimiques. Les résultats sont ensuite évalués à l'aide d'une analyse statistique, plus précisément de l'analyse de variance (ANOVA), afin d'identifier les paramètres significatifs et leur contribution à la densité de courant de corrosion et à la résistance du film passif. De plus, des corrélations empiriques sont utilisées pour prédire la densité de courant de corrosion et la résistance du film passif en fonction des paramètres (puissance du laser (P), vitesse de balayage (V), temps de vieillissement (A) et température de vieillissement (T)). Les résultats peuvent être utilisés pour sélectionner les paramètres optimaux de SLM et de traitement thermique afin d'améliorer les performances en termes de corrosion de l'acier 17-4PH.

Cet article, intitulé « *INFLUENCE OF SELECTIVE LASER MELTING PROCESS AND HEAT TREATMENT PARAMETERS ON THE CORROSION RESISTANCE OF 17-4 PRECIPITATION HARDENING STAINLESS STEEL* », a été soumis au journal *Metals and*

Materials International. Cet article a pu voir le jour grâce à la collaboration avec l'équipe de recherche du professeur Hendra Hermawan. Le premier auteur, Anas Kerbout, a contribué à l'essentiel des tests et travaux de rédaction sous la supervision de Ayoub Tanji, Hendra Hermawan et Noureddine Barka, qui ont contribué également à l'amélioration de la rédaction pour la version finale.

3.2 INFLUENCE OF SELECTIVE LASER MELTING PROCESS AND HEAT TREATMENT PARAMETERS ON THE CORROSION RESISTANCE OF 17-4 PRECIPITATION HARDENING STAINLESS STEEL

INFLUENCE OF SELECTIVE LASER MELTING PROCESS AND HEAT TREATMENT PARAMETERS ON THE CORROSION RESISTANCE OF 17-4 PRECIPITATION HARDENING STAINLESS STEEL

Anas Kerbout[1, *], Ayoub Tanji[2], Hendra Hermawan[2], Noureddine Barka[1]

[1]Department of Mathematics, Computer Science and Engineering, Université du Québec à Rimouski, QC G5L 3A1, Canada

[2] Department of Mining, Metallurgical and Materials Engineering, Laval University, Quebec City, QC G1V 0A6, Canada

***** Corresponding author.

E-mail address: Anas.Kerbout@uqar.ca (A.Kerbout).

3.3 ABSTRACT

Most studies on corrosion resistance of additively manufactured 17-4 PH stainless steels in comparison to their wrought counterparts revealed contradictory findings. The present work aims to determine the effect of the selective laser melting (SLM) process and heat treatment parameters on the corrosion resistance of SLM-made 17-4 PH in 3.5 wt.% NaCl solution. The employed Taguchi method and statistical analysis of variance (ANOVA)

reveal the effect of laser power, scanning speed, aging time, and aging temperature on corrosion current density and passive film resistance of the SLM-made 17-4 PH samples. The most significant effect is found for laser power and aging temperature where the decrease of laser power and the increase in aging temperature leads to a decrease in corrosion resistance as indicated by the higher corrosion current density and lower passive film resistance. This work proposes empirical predictive models to predict the electrochemical properties of SLM-made 17-4 PH.

Keywords:
17-4 PH stainless steel; selective laser melting; corrosion resistance; heat treatment; Analysis of variance.

3.4 INTRODUCTION

Precipitation hardening (PH) martensitic stainless steels like the 17-4 PH (UNS S17400, AISI 630) are known for their excellent combination of strength and corrosion resistance [161], making them one of the most used steels for applications requiring moderate corrosion resistance and high mechanical strength. 17-4 PH has been widely used in a variety of applications including biomedical implants, aerospace and oilfield components, propeller shafts, compressor impellers, and light water reactors [14, 143, 193-196]. Many of them have a complex shape ideal to be fabricated by additive manufacturing (AM), particularly the selective laser melting (SLM) process. SLM forms a complex object by adding material layer by layer as predetermined by a 3D computer-aided design file. However, the corrosion resistance of SLM-made PH stainless steels needs to be carefully assessed as it is strongly influenced by factors such as chemical composition, microstructure, and heat treatment [197].

Previous studies indicated contradictory findings on the corrosion resistance of SLM-made 17-4 PH parts when compared to non-AM parts in acidic and chloride-rich environments. Stoudt, *et al.* [198] demonstrated that AM and heat-treated 17-4 PH samples

exhibited higher pitting potentials than wrought samples in a chloride environment due to finer martensite lath structure with more homogeneously distributed niobium carbide precipitates for AM parts than those in the wrought alloy, and more stable passive film resulting from the absorbed nitrogen in the AM and heat-treated alloy. Alnajjar, *et al.* [169] reported that re-austenitized SLM-made 17-4 PH displayed superior general corrosion resistance in acidic chloride medium, attributed to reduced manganese sulfide inclusions in SLM-made sample. Schaller, *et al.* [20] found that 17-4 PH samples produced by laser powder bed fusion (LPBF) displayed a reduced passivity and higher corrosion activity as compared to wrought samples due to the presence of porosity. Sun, *et al.* [199] also confirmed that porosity reduced the pitting and repassivation potential of SLM-made 316L stainless steel in chloride environment.

Despite a surge in research activities on SLM-made 17-4 PH, most of them focused on analyzing the effect of process parameters or heat treatment on mechanical properties, corrosion resistance, density, and microstructure [29, 69, 124, 200, 201]. Only a few studies investigated a combined effect of process parameters and aging conditions on the corrosion resistance of the SLM-made 17-4 PH. For instance, Garcia-Cabezon *et al.* [14] investigated the effect of build direction and heat treatment on corrosion resistance. Therefore, this work aims to study the influence of the SLM process and heat treatment parameters on the corrosion resistance of 17-4 PH. A set of experiments was designed by using the Taguchi method and statistical analysis (ANOVA) to determine the effect of SLM and-heat treatment parameters (laser power, scanning speed, aging time, and aging temperature) on corrosion resistance (corrosion current density and passive film resistance) of 17-4 PH. Cyclic potentiodynamic polarization and electrochemical impedance experiments were performed in 3.5 wt% NaCl solution to generate corrosion data. The results of this work will advance the current understanding of corrosion of AM stainless steels by proposing multiple linear regression-based empirical predictive models to predict the electrochemical properties of SLM-made 17-4 PH.

3.5 MATERIALS AND METHODS

3.5.1 Experimental design

Taguchi experiment table (Table 12) with the orthogonal array setting L_9 (3^4) was used for the experimental design to limit the number of experiments. details the four factors: laser power (*P*), scanning speed (*V*), aging time (*A*), and aging temperature (*T*), and their levels used for the experimental works.

Table 12: Factor and level of experimental design.

Factor	Code	Unit	Level		
			1	2	3
Laser power	*P*	W	170	195	220
Scanning speed	*V*	mm/s	700	800	900
Aging time	*A*	min	60	150	240
Aging temperature	*T*	°C	480	550	620

Analysis of variance (ANOVA) was used to evaluate the significance of each factor (*P*, *V*, *A*, *T*) in terms of percent contribution to corrosion resistance. The results were analyzed by using Minitab software and presented as the degree of freedom, the sum of the squares, the percentage of contribution, the average square, the average mean square, the *F*-value, and the *p*-value for each parameter studied. The percentage of contribution indicates the degree of significance of each factor on the total variation in the experiment. The stepwise method was applied by excluding non-significant terms after each iteration without using a hierarchical model to reduce errors and computation time.

3.5.2 Sample preparation

Samples of 17-4 PH parts were fabricated as 15 x 15 x 20 mm cubes from 17-4 PH gas-atomized powders (Table 13) by using an EOS M290 SLM machine (EOS GmbH - Electro Optical Systems, Germany) equipped with a 400 W Ytterbium fiber laser at 100 µm beam diameter. The fabrication was done under Argon atmosphere with a constant hatch

spacing of 100 μm, layer thickness of 40 μm, laser power of 170 - 220 W, and scanning speed of 700 - 900 mm/s. These parameters can be combined to calculate energy density (*E*), which is defined as the energy input (*J*) per unit volume (mm^3), and calculated by using equation (7) [42]:

$$E = \frac{P}{h * v * t} \tag{7}$$

where *P* is laser power, *V* is laser scanning speed, *h* is hatch spacing, and *t* is layer thickness.

Table 13: Chemical composition (wt. %) of as received 17-4 PH powders.

C	Mn	P	S	Si	Cr	Ni	Cu	Fe
-	0.06	-	0.06	0.16	17.32	3.96	3.34	Bal.

The fabricated samples were then heat treated, before being cut from the plate, at 650° C for one hour to reduce residual stresses [179] generated due to a high temperature gradient during the SLM processing [180]. Since stress relief did not alter the microstructure or mechanical properties of LPBF-made 17-4 PH [90, 176], an annealing was performed at 1040 °C for 30 min followed by air cooling, followed by aging at various temperatures (Table 12).

3.5.3 Corrosion evaluation

The corrosion behavior of the SLM-made 17-4 PH samples was evaluated by conducting three electrochemical tests: open circuit potential (OCP), cyclic potentiodynamic polarization (CPP), and electrochemical impedance spectroscopy (EIS), using a potentiostat (CH Instruments model 760E, Austin, TX, USA). All tests were performed in 3.5 wt% NaCl solution prepared with 18.2 MΩ deionized water, maintained at room temperature, in a three-electrode cell setup with the 17-4 PH sample, saturated calomel electrode (SCE), and graphite rod as working, reference, and counter electrodes, respectively. Before each test, the sample surface was polished with SiC papers to 800 grit, then polished with 9 and 3 μm diamond suspension, and further polished with 0.05 μm colloidal silica suspensions, rinsed and cleaned with water and ethanol, and then dried immediately. The OCP tests were conducted for 1 h, subsequently followed by the AC mode EIS tests at a frequency range of 10^5 - 10^{-2}

Hz, and an AC amplitude of 10 mV from the E_{OCP}. The CPP test was then conducted, after 1 h at OCP, with a scan rate of 1 mV/s from -0.6 to 0 V/SCE. All tests were repeated three times to ensure reproducibility and reliability. Test data were collected and analyzed by using the CH Instruments and EC-Lab software. After being subjected to the electrochemical test, the corroded samples were rinsed, dried with alcohol, and observed by using optical microscopy LECO 300 to reveal the corrosion morphology.

3.6 RESULTS AND DISCUSSION

3.6.1 Surface analysis

The presence of manufacturing defects, like porosity, in SLM-made specimens can affect not only the mechanical properties but also their susceptibility to localized corrosion attack [170]. Furthermore, these defects reduce their ability to repassivate when exposed to corrosive environments [21]. Micrographs of the samples obtained before and after potentiodynamic polarization are presented in Figure 15. Optical microscopy observations showed a significant number of pits on the surface of the sample after being subjected to polarization tests, which confirmed that the passivity breakdown was associated with pitting corrosion [124]. Moreover, it can be observed that some samples exhibit pre-existing small pores before corrosion. For instance, sample 3 (Figure 15c) presents a higher level of porosity before corrosion due to the insufficient energy density (47.22 J.mm^{-3}). However, as the energy density is increased to more than 68 J.mm^{-3}, the pores are basically absent (Figure 15d, Figure 15g, and Figure 15h) in comparison to samples printed with lower energy density between 53 and 55 J.mm^{-3}, as depicted in Figure 15b and Figure 15f, where the pores are marked with yellow circles. The presence of a high porosity level leads to a decrease in corrosion resistance. Suryawanshi *et al.* [202] confirmed that a higher porosity level degrades the corrosion resistance in chloride-rich environments due to the penetration of chloride ions into pores and other defects, which destroys the passive film.

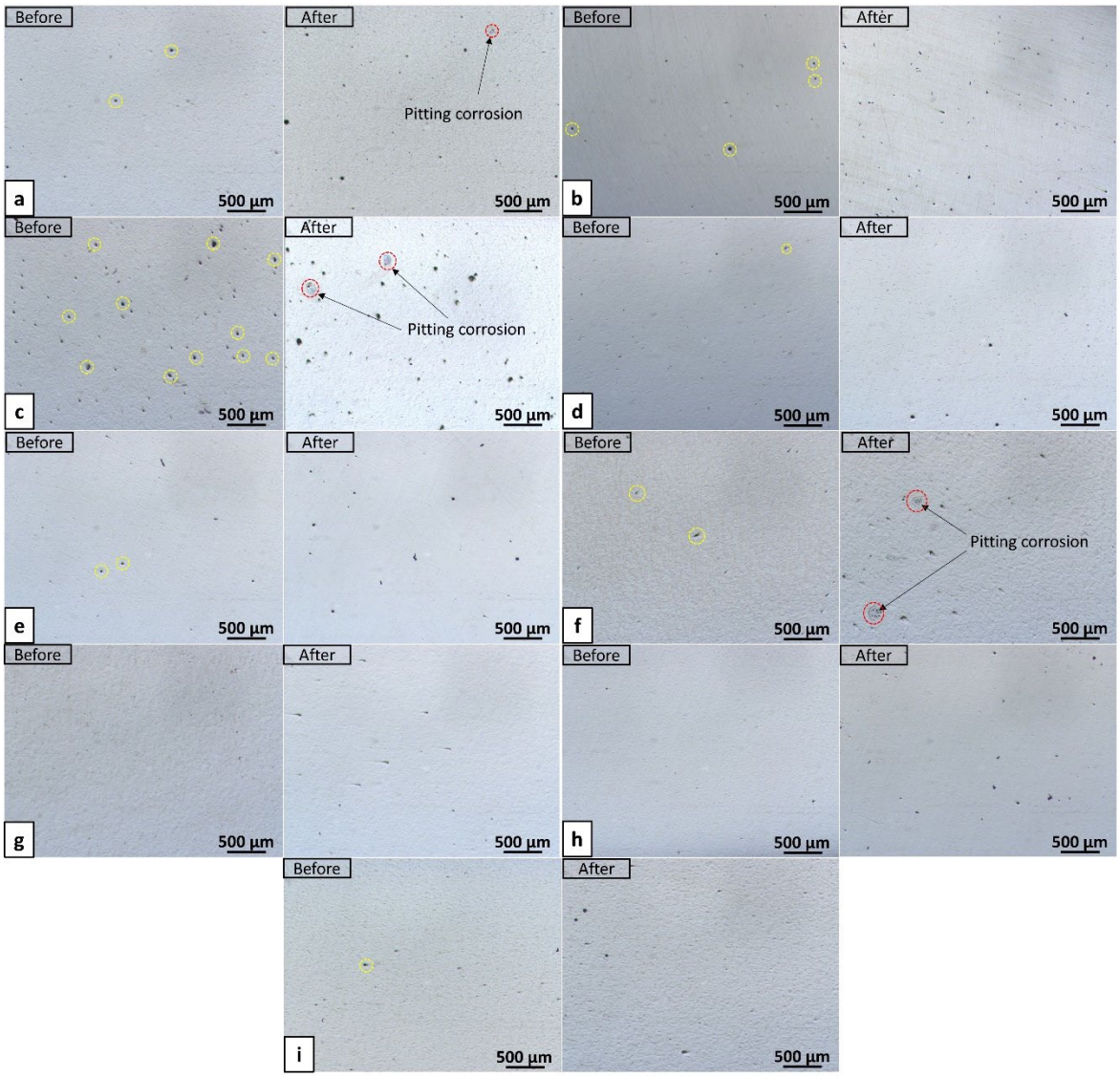

Figure 15: Optical micrographs before and after corrosion for the different process parameters of: (a-i) sample number 1 to 9, respectively.

3.6.2 Electrochemical corrosion evaluation

The corrosion behavior of SLM-made 17-4 PH samples was first evaluated by measuring the E_{OCP}. The results showed a similar sharp decrease at the beginning of the test for the different samples (Figure 16a, Figure 16b, Figure 16c) and stabilized after 1500 s of exposure, which indicates that the material exhibits active corrosion. The CPP curves (Figure 16d, Figure 16e, Figure 16f) after 1 h at OCP showed a similar shape for all the samples with

noticed passivity of sample 9 than other samples and the highest E_{corr} for samples heat treated for 60 min. The average values of E_{OCP}, E_{corr}, and i_{corr} are listed in Table 14.

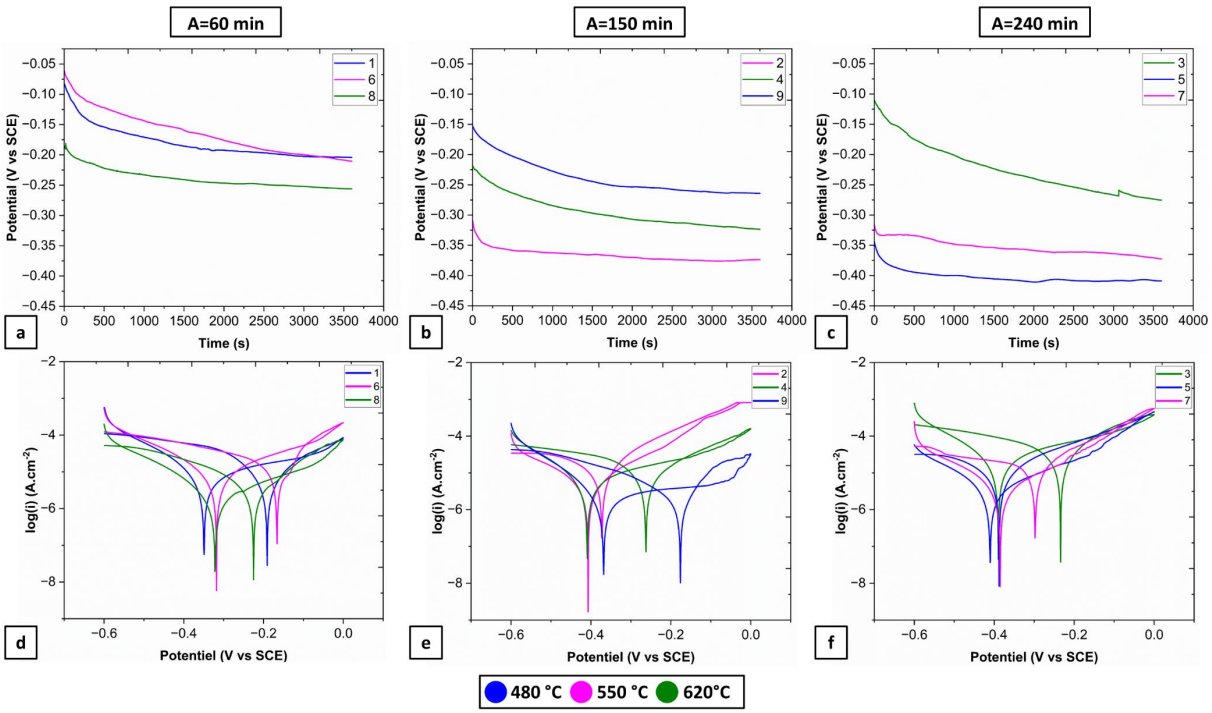

Figure 16: Results of electrochemical tests on SLM-made 17-4 PH samples: (a, b, c) OCP curves, (d, e, f) CPP curves.

Table 14: L9 orthogonal matrix and electrochemical results of SLM-made 17-4 PH samples for the different process parameters.

Sample number	Factors					Responses		
	P **(W)**	***V*** **(mm. s^{-1})**	***A*** **(min)**	***T*** **(°C)**	***E*** **($J.mm^{-3}$)**	E_{OCP} **(mV/SCE)**	E_{corr} **(mV/SCE)**	i_{corr} **(µA/cm^2)**
1	170	700	60	480	60.71	-192.77±8.54	-336.5±9.64	5.63±0.36
2	170	800	150	550	53.13	-350.80±29.6	-395.83±16.5	3.28±0.72
3	170	900	240	620	47.22	-233.57±65.05	-360.77±41.35	12.98±3.3
4	195	700	150	620	69.64	-325.10±2.78	-413.63±3.23	4.69±0.55
5	195	800	240	480	60.94	-364.93±34.67	-407.03±16.15	3.56±1.12
6	195	900	60	550	54.17	-190.83±23.02	-308.60±19.46	6.58±0.29
7	220	700	240	550	78.57	-337.57±29.01	-388.17±17.01	3.18±0.22
8	220	800	60	620	68.75	-263.17±37.13	-327.97±18.75	2.09±0.51
9	220	900	150	480	61.11	-217.63±35.07	-372.47±13.87	1.89±0.51

The EIS results are presented in Figure 17, the Nyquist plots exhibited similar capacitive arc characteristics for all samples (Figure 17a, Figure 17b, Figure 17c), which indicates the typical behavior of stainless steels. The stability of the passive film can be analyzed by the semicircle diameter, the smaller diameter represents a lower stability of the passive film and lower corrosion resistance [21]. The Bode diagram (Figure 17d, Figure 17e, Figure 17f) exhibited a resistive-capacitive behavior. The maximum value of the phase angle was below -80 degrees, correlating well with [182] and [124] suggesting the formation of a stable passive film on the sample surface and an increase in corrosion resistance.

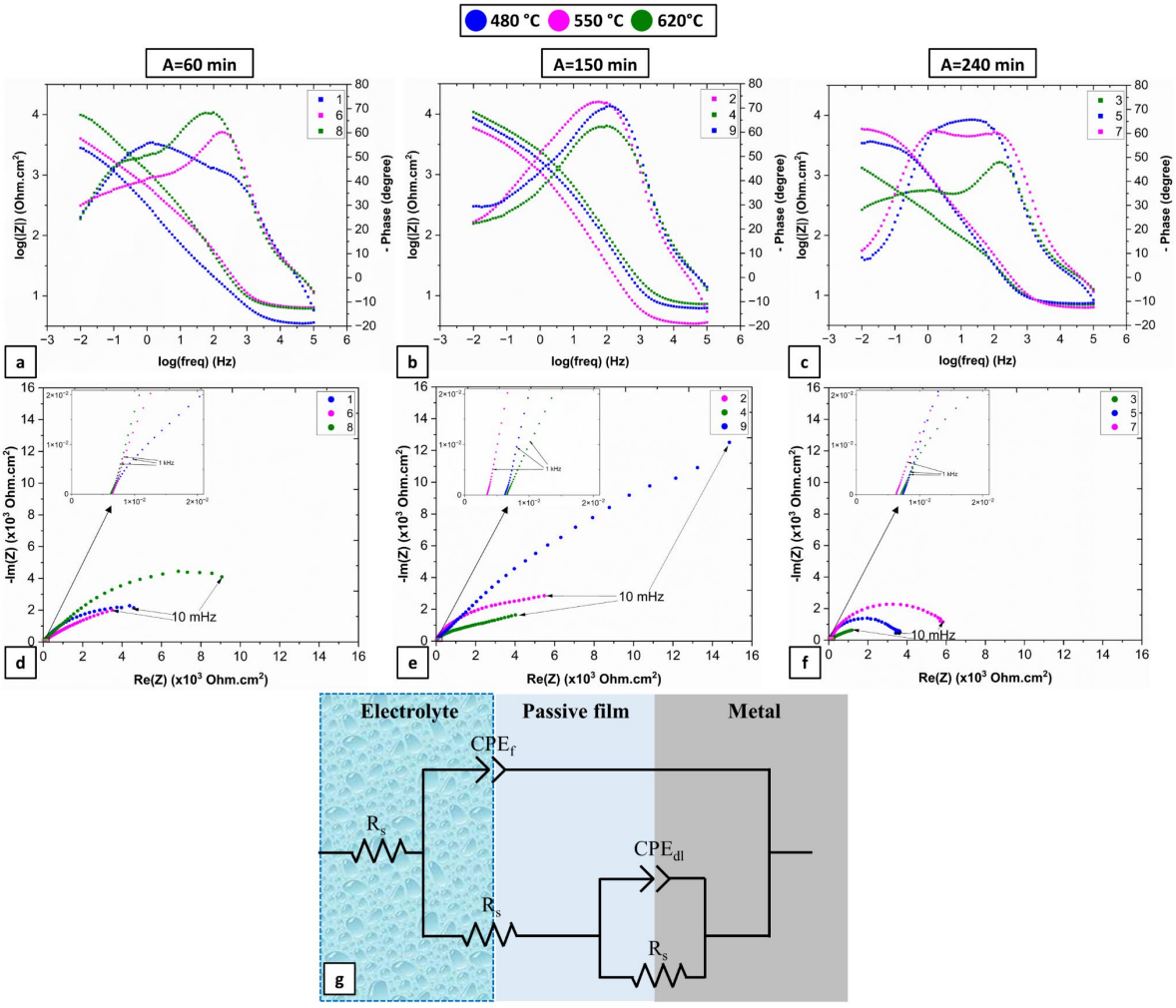

Figure 17: Results of EIS tests on SLM-made 17-4 PH samples: (a, b, c) Bode plots, (d, e, f) Nyquist plots, and (g) a proposed equivalent electrical circuit model.

An equivalent electrical circuit (EEC) model (Figure 17g) is proposed to analyze EIS plots, which presents, a solution resistance (R_s) connected in series with two constants parallel combination of the passive film resistance (R_f) // constant phase element of the passive film (CPE_f) and charge transfer resistance (R_{ct}) // constant phase element of the double layer (CPE_{dl}). The fitting parameters are listed in Table 15. The constant-phase element ($CPE\ (Q,\ n)$) was used instead of a pure capacitor to characterize the non-ideal behavior of the system. The parameter n of CPE is linked with a non-uniform current distribution related to the surface heterogeneity (roughness and defects) [203]. The impedance of CPE could be calculated as follows [204]:

$$Z_{CPE} = \frac{1}{Q(\omega i)^n} \quad (8)$$

Where Q is the CPE constant, ω is the angular frequency, i is an imaginary number ($i^2 = -1$) and n refers to an adjustable parameter with a range from -1 to 1. The CPE exhibits an inductor behavior for n = -1, a resistor for n = 0, and a pure capacitor for n = 1 [205]. Therefore, R_p, the polarization resistance (sum of R_f and R_{ct}), can be used to assess the corrosion resistance of samples [21]. It can be noticed that R_s values are very low and not affected by the parameters difference for all samples in the high-frequency region due to the highly corrosive nature of the electrolyte [124].

Table 15: Fitted electrochemical parameters from EIS data of the SLM-made 17–4 PH samples.

Sample number	Factors				Responses							
	P **(W)**	***V*** **(mm.s^{-1})**	***A*** **(min)**	***T*** **(°C)**	***Rs*** **(Ω.cm^2)**	***CPE$_f$*** **(×10^{-6} F.s$^{(n-1)}$)**	***n$_1$***	***R$_f$*** **(Ω.cm^2)**	***CPE$_{dl}$*** **(×10^{-6} F.s$^{(n-1)}$)**	***n$_2$***	***R$_{ct}$*** **(Ω.cm^2)**	***R$_p$*** **(Ω.cm^2)**
1	170	700	60	480	6.36	1000	0.683	5490	3000	0.5	4629.6	10120
2	170	800	150	550	4.35	250	0.76	2784.38	500	0.58	6771.6	9556
3	170	900	240	620	7.05	2000	0.5	1785	7500	0.87	1172.49	2957.5
4	195	700	150	620	6.57	165	0.58	3375	1000	0.67	4016.25	7391.3
5	195	800	240	480	7.44	100	0.85	676.5	110	0.33	3522.75	4199.3
6	195	900	60	550	6.46	700	0.465	9355.5	0.1	0.6	3485.79	12841
7	220	700	240	550	6.35	100	0.775	737.1	1	0.6	5807.88	6545
8	220	800	60	620	6.22	350	0.675	6075	400	0.78	9109.13	15184
9	220	900	150	480	6.23	100	0.6	8287.5	600	0.9	7588.43	15876

3.6.3 Analysis of variance (ANOVA)

The results of the ANOVA analysis of the corrosion current density and the passive film resistance are presented in Table 16 and Table 17, respectively. When the p-value is below 0.05, it involves that the associated factor has a significant effect on the response. The

factors of P, V, A, T, $P*T$, and V^2 were found to be statistically significant (p-value < 0.05) for corrosion current density. Additionally, the factors of P, V, A, T, $P*T$, $V*T$, and V^2 were found to be statistically significant for passive film resistance (p-value < 0.05). On the other hand, T^2 was found to be insignificant for corrosion current density (p-value > 0.05). The F-values are compared to values of the standard F tables for given statistical significance levels. It can be observed that the corrosion current density is influenced by P and V with a total contribution of 67.64%. On the other hand, the passive film resistance (R_f) is influenced mainly by the aging time (A), with a percentage of 65.92% and a significant p-value of 0.006 < 0.05, and the speed (V), with a percentage of 19.79%, as well as by the other parameters with a percentage of 15.85%.

To estimate the corrosion current density and the polarization resistance as a function of P, V, A, T, and their interactions, the regression equations (9) and (10) were used. The predictive values obtained were then presented in Table 18. Furthermore, the correlation curves between the predicted (i_{corr}, R_f) and the experimentally measured (i_{corr}, R_f) are plotted in Figure 18. These curves show that the points are grouped around a straight line.

$$i_{corr} = 649.4 - 1.5963\,P - 0.8000\,V + 0.03652\,A - 0.6886\,T + 0.000523\,V^2 + 0.000162\,T^2 + 0.002724\,P*T \quad (9)$$

$$R_f = -223157 + 1065.82\,P + 43.13\,V - 103.69\,A + 425.27\,T + 0.17477\,A^2 - 1.8968\,P*T - 0.07881\,V*T \quad (10)$$

The residual value squared (R^2) represents the percentage of variation in the model's predictions relative to the response variable. A higher R^2 value indicates a better fit of the model to the data. The R^2 for corrosion current density is 99.98%, and for the passive film resistance, it is 100%, indicating a high correlation between the model and the experimental data. The adjusted residual value squared (R^2_{adj}) indicates the number of independent variables used for predicting the response. The R^2_{adj} for corrosion current density is 99.82%,

suggesting that only 0.18% of the changes remain unexplained by the regression model. For the passive film resistance, it is 100%, indicating a perfect fit between the model and the data.

Table 16: Contribution of parameters on corrosion current density.

Source	DF	Sum of squares	Contribution (%)	Adj SS	Adj MS	F-value	p-value
P	1	36.1622	38.88	12.8813	12.8813	623.12	0.025
V	1	10.5338	11.32	26.5917	26.5917	1286.35	0.018
A	1	4.8961	5.26	16.2033	16.2033	783.82	0.023
T	1	12.5571	13.50	9.4704	9.4704	458.12	0.030
V*V	1	16.2260	17.44	27.3703	27.3703	1324.02	0.017
T*T	1	1.2588	1.35	1.2588	1.2588	60.89	0.081
P*T	1	11.3606	12.21	11.3606	11.3606	549.56	0.027
Error	1	0.0207	0.02	0.0207	0.0207		
Total	8	93.0150	100.00				
R^2=% 99.98				**Adjusted R^2**=% 99.82			

Table 17: Contribution of parameters on passive film resistance

Source	DF	Sum of Squares	Contribution (%)	Adj SS	Adj MS	F-value	p-value
P	1	4233970	5.21	5719420	5719420	24396.78	0.004
V	1	16091385	19.79	149817	149817	639.06	0.025
A	1	52344290	64.36	2332720	2332720	9950.46	0.006
T	1	1726994	2.12	3546847	3546847	15129.44	0.005
A*A	1	1266521	1.56	667993	667993	2849.39	0.012
P*T	1	5509363	6.77	5509363	5509363	23500.76	0.004
V*T	1	152172	0.19	152172	152172	649.10	0.025
Error	1	234	0.00	234	234		
Total	8	81324928	100.00				
R^2=% 100				**Adjusted R^2**=% 100			

Table 18: Measured and predicted corrosion current density and passive film resistance.

Sample number	Measured i_{corr} (μA/cm^2)	Predicted i_{corr} (μA/cm^2)	Measured R_f (Ω.cm^2)	Predicted R_f (Ω.cm^2)
1	5.63	5.57	5490	5501.7
2	3.28	3.2	2784.38	2786.5
3	12.98	12.87	1785	1799.3
4	4.69	4.54	3375	3388.5
5	3.56	3.37	676.5	689.13
6	6.58	6.37	9355.5	9358.4
7	3.18	3.13	737.1	739.4
8	2.09	2.02	6075	6089.3
9	1.89	1.77	8287.5	8300.8

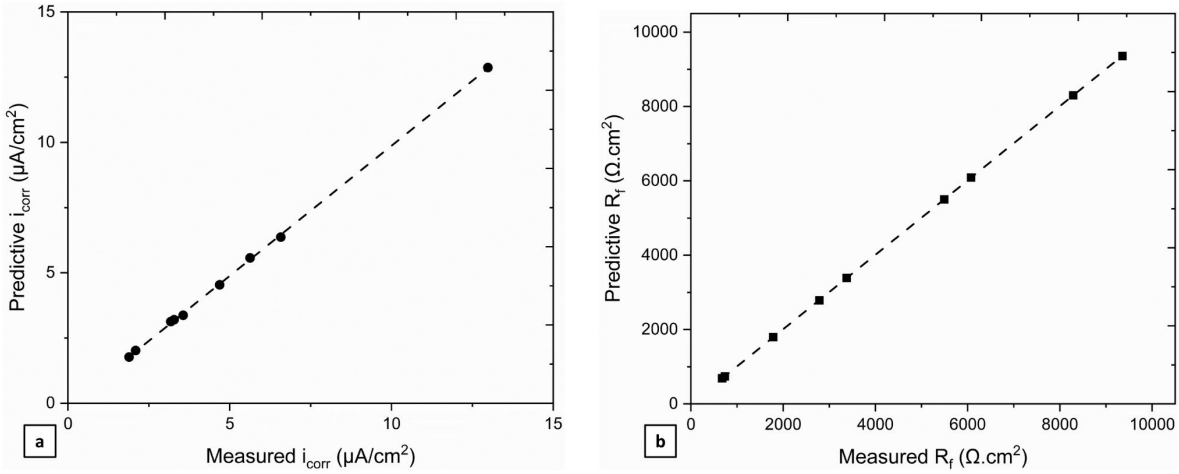

Figure 18: Correlation curves for measured and predictive a) corrosion current density and b) passive film resistance.

3.6.4 Effect of process and heat treatment parameters

Figure 19a and Figure 19b show the main effect plots of i_{corr} and R_f. These graphs are used to interpret the effect of each parameter level on corrosion resistance.

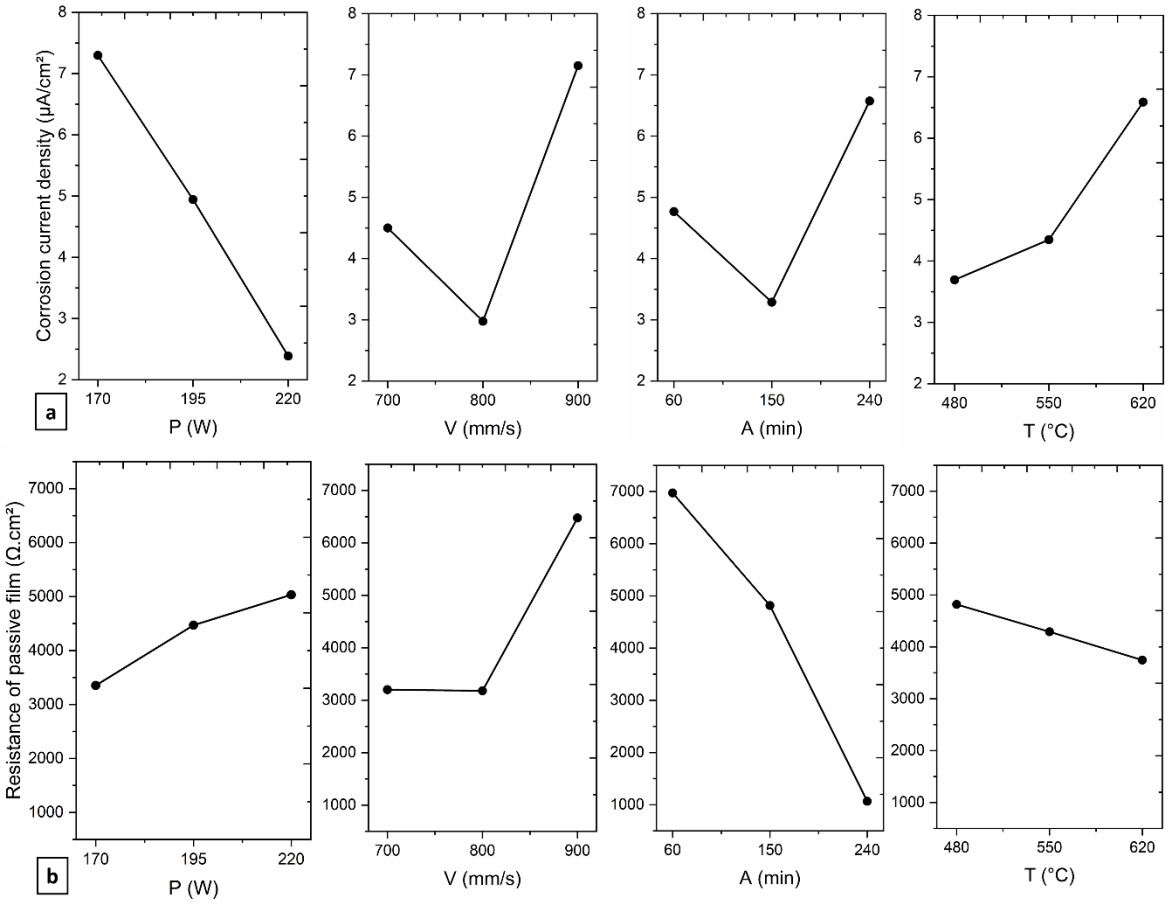

Figure 19: Correlation curves for measured and predictive a) corrosion current density and b) passive film resistance.

It can be observed that increasing laser power results in a decrease in i_{corr} and an increase in R_f, which is beneficial for corrosion resistance. Irrinki *et al.* [170] have also confirmed that increasing the energy density by increasing laser power from 150 W to 195 W improves the material density and corrosion resistance of SLM-made 17-4 PH when exposed to a 0.5 M NaCl environment. Wang *et al.* [206] reported that increasing the energy density, by increasing laser power to 230 W and decreasing scanning speed to 886 mm.s^{-1}, results in better corrosion resistance of SLM-made 15-5PH SS in a 0.1 M NaCl solution

In addition, increasing aging temperature results in an increase in i_{corr} and a decrease in R_f, which is detrimental to corrosion resistance. Sarkar *et al.* [111] reported that the SLM-made 15-5 PH SS samples heat treated at 482°C for 60 min corroded the least, while the SLM-made specimens corroded the most among all. Moreover, increasing the aging temperature and time led to an increase in the corrosion rate. This increase is attributed to the formation of a higher quantity of $Cr_{23}C_6$ precipitates. Furthermore, Tavakoli Shoushtari [207] who investigated the corrosion behavior of 17-4 PH in 3.5% NaCl by studying the pitting potential, found that raising the aging temperature to 620 °C decreases the pitting potential. This can be explained by differences in the volume fraction of ferrite, morphology, and distribution of copper-rich precipitates, and the amount of reverted austenite. Similarly, Szewczyk-Nykiel and Kazior [208] confirmed that the highest corrosion resistance in dilute sulfuric acid solution (0.5 M H_2SO_4) is exhibited by 17-4 PH after aging at 480 °C. Pan *et al.* [21] reported that aging at 482 °C for 60 min improved corrosion resistance and led to the formation of a more protective passive film in a chloride environment (3.5 wt% NaCl) due to various factors, such as the refinement of the microstructure, the formation of reverted austenite, the elimination of δ-ferrite, and the precipitation of Cu-rich particles at the grain boundaries. The same conclusion was reached by Ping *et al.* [209], where they found that 17-4 PH SS aged at low temperature around 460 °C presented the best erosion-corrosion resistance in dilute sulphuric acid slurry due to the ε-rich fine precipitation.

It can be noticed that raising the aging time to 150 min leads to a reduction in i_{corr}, suggesting an improvement in corrosion resistance. Conversely, elevating the aging time to 240 min results in an increase of i_{corr}, signifying a reduction in corrosion resistance. This was confirmed by Ghasemian Malakshah *et al.* [183], who reported that overaging of 17-4 PH SS at 620 °C for 240 min leads to the formation of a significant amount of returned austenite and amplification of the galvanic effect between the two adjacent phases (austenite and martensite). This behavior enhances susceptibility to general corrosion compared to samples aged at 464 °C for 129 min.

The high corrosion resistance of samples heat treated at 480 °C can be attributed to the precipitation of Cu-rich precipitates. Copper is commonly used as an alloying element to

enhance the uniform corrosion resistance of stainless steels. It is enriched at the surface during the anodic dissolution of the alloy, leading to a reduction in its corrosion rate [210]. Some studies reported that Cu had a positive impact on the pitting corrosion resistance of stainless steels. Lin *et al.* [211] confirmed that Cu increased the pitting protection potential in a 3.5 wt.% NaCl solution. The same conclusion was reached by SU *et al.* [212], they confirmed that the addition of Cu increased the corrosion resistance and suppressed the nucleation and propagation of pitting. In a similar study by Pan *et al.* [21], it was reported that the precipitation of Cu-rich particles contributed to an improvement in the pitting corrosion resistance of the heat-treated 17-4 PH samples. Luo *et al.* [182] emphasized that the pitting corrosion increased with increasing aging time and became more severe after 240 min of aging. They also observed that Cu within the passive film disappeared after this period, which they attributed to the precipitation of Cu-rich nanoparticles in the matrix.

3.7 CONCLUSION

By employing the Taguchi method and statistical analysis (ANOVA), this study reveals the effect of SLM and heat treatment parameters (laser power, scanning speed, aging time, aging temperature) on corrosion resistance (corrosion current density, passive film resistance) of 17-4 PH in 3.5 wt% NaCl solution. Notably, optimal corrosion resistance is achieved under the following conditions: a laser power of 220 W, a scanning speed ranging between 800 and 900 mm/s, an aging time between 60 and 150 minutes, and an aging temperature of 480°C. The most significant effect is found for laser power and aging temperature where the decrease of laser power and the increase in aging temperature leads to a decrease in corrosion resistance, as indicated by the higher corrosion current density and lower passive film resistance. However, a decrease in laser power leads to lower energy density, resulting in microstructural defects, while an increase in aging temperature leads to the coarsening of copper precipitates, which degrades corrosion resistance. By using a multiple linear regression, empirical predictive models were proposed to predict the

electrochemical properties of SLM-made 17-4 PH. The results demonstrate that the models closely approximate the experimental values, achieving correlations close to 100%.

Declaration of competing interest

The authors declare that they have no known competing financial interests or personal relationships that could have appeared to influence the work reported in this paper.

Acknowledgments

The authors acknowledge the Natural Sciences and Engineering Research Council of Canada (NSERC) for their support via Discovery Grants: RGPIN-2022-04796 (N.B.) and RGPIN-2023-03884 (H.H.).

Data Availability

Data will be made available on request.

CONCLUSION GÉNÉRALE

La fabrication additive, notamment la fusion sélective au laser, représente une avancée significative dans le domaine industriel. Son application s'étend de plus en plus dans divers secteurs de haute technologie. Cependant, la technologie de fabrication additive est peu exploitée dans le domaine maritime, qui présente des conditions environnementales extrêmes favorisant la corrosion. Cette technologie présente plusieurs paramètres dont l'optimisation pourrait encore améliorer les propriétés des pièces imprimées, en plus d'intégrer des techniques de post-traitement, telles que le traitement thermique. Dans le but d'étudier les effets du processus de la fusion sélective au laser et le post-traitement thermique sur les propriétés mécaniques et électrochimiques de l'acier inoxydable 17-4PH, ce mémoire répond à trois objectifs. Le premier objectif vise à présenter en premier lieu la technologie de la fabrication additive, en mettant particulièrement l'accent sur la fusion sélective au laser, tout en abordant les limitations de cette technologie et les méthodes d'amélioration des propriétés mécaniques et électrochimiques tout en réduisant les défauts. Cet article objectif cherche aussi à identifier le matériau le plus approprié pour les applications maritimes, en se focalisant sur l'influence des paramètres de fabrication additive et de traitement thermique sur les propriétés mécanique et électrochimiques de divers types d'aciers inoxydables. Ensuite, le second objectif consiste à déterminer la combinaison optimale des paramètres de la fusion sélective au laser de l'acier inoxydable 17-4PH (la puissance du laser et la vitesse de balayage) et du post-traitement thermique (le temps de vieillissement et la température de vieillissement) qui permettent d'obtenir les meilleures propriétés mécaniques. Le dernier objectif se concentre sur l'étude des effets de ces mêmes paramètres sur les propriétés électrochimiques de l'acier inoxydable 17-4PH, dans le but d'identifier les paramètres qui donnent la meilleure résistance à la corrosion.

La première partie de l'étude se consacre à une revue de la littérature, mettant en lumière l'étude des propriétés mécanique et électrochimiques des aciers inoxydables (316L, 304, 420, 17-4 PH et 15-5 PH) fabriqués par la technologie de fabrication additive, dans le but d'identifier le matériau qui présente la combinaison optimale de propriétés mécaniques

et électrochimiques particulièrement adapté à un environnement marin. Parmi ces aciers, le 17-4PH a été sélectionné en raison de ses excellentes propriétés mécaniques et de sa résistance à la corrosion, grâce à sa teneur plus élevée en chrome, en faisant ainsi un choix privilégié pour les applications nécessitant simultanément une grande résistance mécanique et une bonne résistance à la corrosion. Dans l'environnement marin, où les matériaux sont exposés à des conditions environnementales sévères, cette combinaison de propriétés est d'une importance cruciale pour assurer la durabilité et la fiabilité des composants.

La deuxième partie consiste en l'investigation des effets des paramètres de la fusion sélective au laser (la puissance du laser et la vitesse de balayage) et du post-traitement thermique (le temps de vieillissement et la température de vieillissement) et leurs interactions sur la limite d'élasticité, la résistance ultime à la traction, l'allongement à la rupture et la dureté de l'acier inoxydable 17-4PH. Les tests expérimentaux ont été effectués en utilisant la planification d'expérience de Taguchi et l'analyse de variance (ANOVA). Les résultats ont révélé que la température de vieillissement influence principalement la limite d'élasticité, la résistance ultime à la traction et la dureté, avec une diminution de la température de vieillissement entraînant des valeurs plus élevées pour ces propriétés mécaniques. En revanche, une augmentation de la température de vieillissement entraîne une augmentation de l'allongement à la rupture. Notamment, les meilleures valeurs de limite d'élasticité, de résistance ultime à la traction et de dureté sont atteintes avec les paramètres suivants : une puissance laser de 220 W, un temps de vieillissement de 60 minutes et une température de vieillissement de 480 °C. Pour ce qui est de l'allongement à la rupture, les paramètres optimaux sont les suivants : une puissance laser de 195 W, un temps de vieillissement de 240 minutes et une température de vieillissement de 620 °C. En ce qui concerne la vitesse de balayage, il a été constaté qu'elle n'a pas une grande contribution aux résultats. Des équations prédictives empiriques ont été établies à l'aide de la régression linéaire multiple pour prédire les propriétés mécaniques de l'acier 17-4PH fabriqué par SLM. Les résultats montrent une bonne corrélation entre les résultats prévus et expérimentaux pour la limite d'élasticité, la résistance ultime à la traction et l'allongement à la rupture.

La troisième partie portait sur l'étude des effets des mêmes paramètres (puissance laser, vitesse de balayage, temps de vieillissement, température de vieillissement) utilisé dans la deuxième partie sur les propriétés électrochimiques de l'acier inoxydable 17-4PH, dans le but d'identifier les paramètres qui donnent la meilleure résistance à la corrosion, en particulier la densité de courant de corrosion et la résistance du film passif. Le design de l'expérience a été réalisée selon la méthode de Taguchi, et une série de scans potentiodynamiques a été effectuée dans une solution de NaCl à 3,5 %. La surface a été analysée à l'aide d'un microscope optique avant et après les tests de polarisation, et une analyse statistique, ANOVA, a été utilisée pour évaluer les effets des paramètres, notamment la puissance du laser, la vitesse de balayage, le temps de vieillissement, la température de vieillissement, et leurs interactions sur la densité de courant de corrosion et la résistance du film passif. Selon les résultats de l'ANOVA, la puissance du laser a l'effet le plus significatif sur la densité de courant de corrosion et le temps de vieillissement sur la résistance du film passif. L'augmentation de la température de vieillissement entraîne une diminution de la résistance à la corrosion, et l'augmentation de la puissance du laser entraîne une augmentation de la résistance à la corrosion. Notamment, une résistance à la corrosion optimale est obtenue dans les conditions suivantes : une puissance laser de 220 W, une vitesse de balayage comprise entre 800 et 900 mm/s, un temps de vieillissement de 60 à 150 minutes et une température de vieillissement de 480 °C. Des modèles prédictifs empiriques ont été établis à l'aide de la régression linéaire multiple pour prédire les propriétés électrochimiques de l'acier 17-4PH fabriqué par la fabrication additive. Les résultats montrent que les modèles s'approchent étroitement des valeurs expérimentales, atteignant des corrélations proches de 100 %.

Des études complémentaires pourraient apporter des bénéfices et compléter efficacement le travail accompli. Cette section met en lumière les perspectives à explorer dans le futur :

- Étudier les effets des paramètres de la fusion sélective au laser et du post-traitement thermique sur la résistance à la fatigue ou la ténacité, à différentes températures.

- Investiguer les structures en treillis (lattice), fabriquées avec le 17-4PH, en utilisant les paramètres optimaux trouvés dans cette étude, pour déterminer la meilleure structure qui offre un compromis entre les meilleures propriétés mécaniques, électrochimiques et les coûts de fabrication.

- Cette étude pourrait également s'ouvrir à d'autres secteurs tels que l'aéronautique ou l'aérospatiale vu la combinaison des propriétés mécaniques et électrochimiques présentées par ce matériau.

RÉFÉRENCES BIBLIOGRAPHIQUES

1. Wischeropp, T.M. and T. Wischeropp, *Advancement of selective laser melting by laser beam shaping*. 2021: Springer.
2. Sander, G., N. Birbilis, J. Tan, P. Balan, O. Gharbi, D. Feenstra, S. Thomas, R. Kelly, C. Hutchinson, and J. Scully, *Corrosion of Additively Manufactured Alloys: A Review.* CORROSION, 2018. **74**.
3. Yang, G., Y. Xie, S. Zhao, L. Qin, X. Wang, and B. Wu, *Quality Control: Internal Defects Formation Mechanism of Selective Laser Melting Based on Laser-powder-melt Pool Interaction: A Review.* Chinese Journal of Mechanical Engineering: Additive Manufacturing Frontiers, 2022. **1**(3): p. 100037.
4. Zhang, B., Y. Li, and Q. Bai, *Defect Formation Mechanisms in Selective Laser Melting: A Review.* Chinese Journal of Mechanical Engineering, 2017. **30**(3): p. 515-527.
5. Aboulkhair, N.T., M. Simonelli, L. Parry, I. Ashcroft, C. Tuck, and R. Hague, *3D printing of Aluminium alloys: Additive Manufacturing of Aluminium alloys using selective laser melting.* Progress in materials science, 2019. **106**: p. 100578.
6. Hemmasian Ettefagh, A., S. Guo, and J. Raush, *Corrosion performance of additively manufactured stainless steel parts: A review.* Additive Manufacturing, 2021. **37**.
7. Ahmed, A., A. Majeed, Z. Atta, and G. Jia *Dimensional Quality and Distortion Analysis of Thin-Walled Alloy Parts of AlSi10Mg Manufactured by Selective Laser Melting*. Journal of Manufacturing and Materials Processing, 2019. **3**, DOI: 10.3390/jmmp3020051.
8. Kempen, K., E. Yasa, L. Thijs, J.P. Kruth, and J. Van Humbeeck, *Microstructure and mechanical properties of Selective Laser Melted 18Ni-300 steel.* Physics Procedia, 2011. **12**: p. 255-263.
9. Larimian, T., M. Kannan, D. Grzesiak, B. AlMangour, and T. Borkar, *Effect of energy density and scanning strategy on densification, microstructure and mechanical properties of 316L stainless steel processed via selective laser melting.* Materials Science and Engineering: A, 2020. **770**: p. 138455.
10. Zai, L., C. Zhang, Y. Wang, W. Guo, D. Wellmann, X. Tong, and Y. Tian *Laser Powder Bed Fusion of Precipitation-Hardened Martensitic Stainless Steels: A Review*. Metals, 2020. **10**, DOI: 10.3390/met10020255.
11. Stoudt, M.R., R.E. Ricker, E.A. Lass, and L.E. Levine, *Influence of Postbuild Microstructure on the Electrochemical Behavior of Additively Manufactured 17-4 PH Stainless Steel.* JOM, 2017. **69**(3): p. 506-515.
12. Nezhadfar, P.D., R. Shrestha, N. Phan, and N. Shamsaei, *Fatigue behavior of additively manufactured 17-4 PH stainless steel: Synergistic effects of surface*

roughness and heat treatment. International Journal of Fatigue, 2019. **124**: p. 188-204.
13. Li, K., J. Zhan, T. Yang, A.C. To, S. Tan, Q. Tang, H. Cao, and L.E. Murr, *Homogenization timing effect on microstructure and precipitation strengthening of 17–4PH stainless steel fabricated by laser powder bed fusion.* Additive Manufacturing, 2022. **52**: p. 102672.
14. Garcia-Cabezon, C., C.G. Hernández, M.A. Castro-Sastre, A.I. Fernandez-Abia, M.L. Rodriguez-Mendez, and F. Martin-Pedrosa, *Heat treatments of 17-4 PH SS processed by SLM to improve its strength and biocompatibility in biomedical applications.* Journal of Materials Research and Technology, 2023. **26**: p. 3524-3543.
15. Krassenstein, B. *French Project Lab-REV to Set Sale on 6-Month-Long Expedition with a 3D Printer On-Board*. 2015 [cited 2023 30 Mars]; Available from: https://3dprint.com/55537/lab-rev-3d-print-boat/.
16. Sevenson, B. *U.S. Navy Installs 3D Printer On Their First Ship, The USS Essex*. 2014 [cited 30 Mars 2023]; Available from: https://3dprint.com/2554/uss-essex-3d-printer-navy/.
17. Eskandari, H., H.R. Lashgari, L. Ye, M. Eizadjou, and H. Wang, *Microstructural characterization and mechanical properties of additively manufactured 17–4PH stainless steel.* Materials Today Communications, 2022. **30**: p. 103075.
18. Hu, Z., H. Zhu, H. Zhang, and X. Zeng, *Experimental investigation on selective laser melting of 17-4PH stainless steel.* Optics and Laser Technology, 2017. **87**: p. 17-25.
19. Hsu, T.-H., Y.-J. Chang, C.-Y. Huang, H.-W. Yen, C.-P. Chen, K.-K. Jen, and A.-C. Yeh, *Microstructure and property of a selective laser melting process induced oxide dispersion strengthened 17-4 PH stainless steel.* Journal of Alloys and Compounds, 2019. **803**: p. 30-41.
20. Schaller, R.F., J.M. Taylor, J. Rodelas, and E.J. Schindelholz, *Corrosion Properties of Powder Bed Fusion Additively Manufactured 17-4 PH Stainless Steel.* Corrosion, 2017. **73**(7): p. 796-807.
21. Pan, L., C.T. Kwok, B. Niu, X. Huang, Y. Cao, X. Zou, and J. Yi, *Enhancement in hardness and corrosion resistance of directed energy deposited 17–4 PH martensitic stainless steel via heat treatment.* Journal of Materials Research and Technology, 2023. **23**: p. 1296-1311.
22. Olson, S., M. Jansen, D. Abbot, I. Halevy, and C. Goldblatt, *The Effect of Ocean Salinity on Climate and Its Implications for Earth's Habitability.* Geophysical Research Letters, 2022. **49**.
23. Barker, S. and A. Ridgwell, *Ocean Acidification.* Nature Education Knowledge, 2012. **3**(10): p. 21.
24. Zakowski, K., M. Narozny, M. Szocinski, and K. Darowicki, *Influence of water salinity on corrosion risk—the case of the southern Baltic Sea coast.* Environmental Monitoring and Assessment : An International Journal Devoted to Progress in the Use of Monitoring Data in Assessing Environmental Risks to Man and the Environment, 2014. **186**(8): p. 4871-4879.

25. Tavares, S.S.M., J.M. Pardal, L. Menezes, C.A.B. Menezes, and C. D'Ávila, *Failure analysis of PSV springs of 17-4PH stainless steel.* Engineering Failure Analysis, 2009. **16**(5): p. 1757-1764.
26. Schade, C., A. Zavaliangos, R.D. Doherty, A. Lawley, and E. Drexel University. College of, *Processing, microstructures and properties of a dual phase precipitation-hardening PM stainless steel*. 2010, Drexel University: Philadelphia, Pa.
27. Murr, L.E., E. Martinez, J. Hernandez, S. Collins, K.N. Amato, S.M. Gaytan, and P.W. Shindo, *Microstructures and Properties of 17-4 PH Stainless Steel Fabricated by Selective Laser Melting.* Journal of Materials Research and Technology, 2012. **1**(3): p. 167-177.
28. Makoana, N.W., I. Yadroitsava, H. Möller, and I. Yadroitsev *Characterization of 17-4PH Single Tracks Produced at Different Parametric Conditions towards Increased Productivity of LPBF Systems—The Effect of Laser Power and Spot Size Upscaling*. Metals, 2018. **8**, DOI: 10.3390/met8070475.
29. Yeon, S.-M., J. Yoon, T.B. Kim, S.H. Lee, T.-S. Jun, Y. Son, and K. Choi *Normalizing Effect of Heat Treatment Processing on 17-4 PH Stainless Steel Manufactured by Powder Bed Fusion*. Metals, 2022. **12**, DOI: 10.3390/met12050704.
30. Debnath, B., M.S. Shakur, F. Tanjum, M.A. Rahman, and Z.H. Adnan *Impact of Additive Manufacturing on the Supply Chain of Aerospace Spare Parts Industry—A Review*. Logistics, 2022. **6**, DOI: 10.3390/logistics6020028.
31. International, A., *F2792-12a: Standard Terminology for Additive Manufacturing Technologies*. 2012.
32. Akita, M., Y. Uematsu, T. Kakiuchi, M. Nakajima, and R. Kawaguchi, *Defect-dominated fatigue behavior in type 630 stainless steel fabricated by selective laser melting.* Materials Science & Engineering A, 2016. **666**: p. 19-26.
33. Szondy, D. *NASA using 3D laser printing to create complex rocket parts*. 2012 [cited 2023 30 Mars]; Available from: https://newatlas.com/3d-printing-rockets-nasa-sls/24909/.
34. Boen, B. *NASA Tests Limits of 3-D Printing with Powerful Rocket Engine Check*. 07 August 2017 [cited 2023 30 Mars]; Available from: https://www.nasa.gov/exploration/systems/sls/3d-printed-rocket-injector.html.
35. Kouprianoff, D., I. Yadroitsava, A. du Plessis, N. Luwes, and I. Yadroitsev, *Monitoring of Laser Powder Bed Fusion by Acoustic Emission: Investigation of Single Tracks and Layers.* Frontiers in Mechanical Engineering, 2021. **7**.
36. Stavropoulos, P. and P. Foteinopoulos, *Modelling of additive manufacturing processes: a review and classification.* Manufacturing Review, 2018. **5**.
37. Mahmoudi, M., A. Elwany, A. Yadollahi, S.M. Thompson, L. Bian, and N. Shamsaei, *Mechanical properties and microstructural characterization of selective laser melted 17-4 PH stainless steel.* Rapid Prototyping Journal, 2017. **23**(2): p. 280-294.
38. Tan, C., D. Wang, W. Ma, Y. Chen, S. Chen, Y. Yang, and K. Zhou, *Design and additive manufacturing of novel conformal cooling molds.* Materials & Design, 2020. **196**: p. 109147.

39. Shayfull, Z., S. Sharif, A.M. Zain, R.M. Saad, and M.A. Fairuz, *Milled Groove Square Shape Conformal Cooling Channels in Injection Molding Process.* Materials and Manufacturing Processes, 2013. **28**(8): p. 884-891.
40. Miranda, G., S. Faria, F. Bartolomeu, E. Pinto, S. Madeira, A. Mateus, P. Carreira, N. Alves, F.S. Silva, and O. Carvalho, *Predictive models for physical and mechanical properties of 316L stainless steel produced by selective laser melting.* Materials Science & Engineering A, 2016. **657**: p. 43-56.
41. Zhang, Z., *Coupled Topology Optimization and Process Simulation System for Laser Powder-bed Fusion Additive Manufacturing*. 2019, UWSpace.
42. Tan, J.H., W.L.E. Wong, and K.W. Dalgarno, *An overview of powder granulometry on feedstock and part performance in the selective laser melting process.* Additive Manufacturing, 2017. **18**: p. 228-255.
43. Auguste, P., A. Mauduit, L. Fouquet, and S. Pillot, *Study on 17-4 PH stainless steel produced by selective laser melting.* UPB Scientific Bulletin, Series B: Chemistry and Materials Science, 2018. **80**: p. 197-210.
44. Herzog, D., V. Seyda, E. Wycisk, and C. Emmelmann, *Additive manufacturing of metals.* Acta Materialia, 2016. **117**: p. 371-392.
45. Fedina, T., J. Sundqvist, J. Powell, and A.F.H. Kaplan, *A comparative study of water and gas atomized low alloy steel powders for additive manufacturing.* Additive Manufacturing, 2020. **36**.
46. Pasebani, S., M. Ghayoor, S. Badwe, H. Irrinki, and S.V. Atre, *Effects of atomizing media and post processing on mechanical properties of 17-4 PH stainless steel manufactured via selective laser melting.* Additive Manufacturing, 2018. **22**: p. 127-137.
47. Pinkerton, A.J., L. Li, and W.S. Lau, *Effects of Powder Geometry and Composition in Coaxial Laser Deposition of 316L Steel for Rapid Prototyping.* CIRP Annals - Manufacturing Technology, 2003. **52**(1): p. 181-184.
48. Bourell, D., J.P. Kruth, M. Leu, G. Levy, D. Rosen, A.M. Beese, and A. Clare, *Materials for additive manufacturing.* CIRP Annals - Manufacturing Technology, 2017. **66**(2): p. 659-681.
49. Rafi, H.K., D. Pal, N. Patil, T.L. Starr, and B.E. Stucker, *Microstructure and Mechanical Behavior of 17-4 Precipitation Hardenable Steel Processed by Selective Laser Melting.* Journal of Materials Engineering and Performance, 2014. **23**(12): p. 4421-4428.
50. Guan, K., Z. Wang, M. Gao, X. Li, and X. Zeng, *Effects of processing parameters on tensile properties of selective laser melted 304 stainless steel.* Materials and Design, 2013. **50**: p. 581-586.
51. Simonelli, M., Y.Y. Tse, and C. Tuck, *Effect of the build orientation on the mechanical properties and fracture modes of SLM Ti-6Al-4V.* Materials Science & Engineering A, 2014. **616**: p. 1-11.
52. Yadollahi, A., N. Shamsaei, S.M. Thompson, A. Elwany, and L. Bian, *Effects of building orientation and heat treatment on fatigue behavior of selective laser melted 17-4 PH stainless steel.* International Journal of Fatigue, 2017. **94**(Part 2): p. 218-235.

53. Strasser, T., *Comparison of additively manufactured and wrought 17-4 PH stainless steels in ultra low cycle fatigue*. 2020, [University of Arkansas, Fayetteville]: [Fayetteville, Arkansas].
54. Kudzal, A., B. McWilliams, C. Hofmeister, F. Kellogg, J. Yu, J. Taggart-Scarff, and J. Liang, *Effect of scan pattern on the microstructure and mechanical properties of Powder Bed Fusion additive manufactured 17-4 stainless steel.* Materials & Design, 2017. **133**: p. 205-215.
55. Rashid, R., S.H. Masood, D. Ruan, S. Palanisamy, R.A. Rahman Rashid, and M. Brandt, *Effect of scan strategy on density and metallurgical properties of 17-4PH parts printed by Selective Laser Melting (SLM).* Journal of Materials Processing Tech., 2017. **249**: p. 502-511.
56. Liu, F., X. Lin, C. Huang, M. Song, G. Yang, J. Chen, and W. Huang, *The effect of laser scanning path on microstructures and mechanical properties of laser solid formed nickel-base superalloy Inconel 718.* Journal of Alloys and Compounds, 2011. **509**(13): p. 4505-4509.
57. Wang, L., C. Dong, D. Kong, C. Man, J. Liang, C. Wang, K. Xiao, and X. Li, *Effect of Manufacturing Parameters on the Mechanical and Corrosion Behavior of Selective Laser-Melted 15-5PH Stainless Steel.* steel research international, 2020. **91**(2).
58. Adeyemi, A.A., E.T. Akinlabi, R.M. Mahamood, K.O. Sanusi, S. Pityana, and M. Tlotleng, *Influence of laser power on microstructure of laser metal deposited 17-4 ph stainless steel.* IOP Conference Series: Materials Science and Engineering, 2017. **225**(1): p. 012028.
59. Li, K., S. Sridar, S. Tan, and W. Xiong. *Effect of homogenization on precipitation behavior and strengthening of 17-4PH stainless steel fabricated using laser powder bed fusion*. 2021.
60. Stopyra, W., K. Gruber, I. Smolina, T. Kurzynowski, and B. Kuźnicka, *Laser powder bed fusion of AA7075 alloy: Influence of process parameters on porosity and hot cracking.* Additive Manufacturing, 2020. **35**.
61. Strano, G., L. Hao, R.M. Everson, and K.E. Evans, *Surface roughness analysis, modelling and prediction in selective laser melting.* Journal of Materials Processing Tech., 2013. **213**(4): p. 589-597.
62. Gibson, I., D.W. Rosen, B. Stucker, and M. Khorasani, *Additive manufacturing technologies*. 2021, Springer: Cham, Switzerland.
63. Bartlett, J.L. and X. Li, *An overview of residual stresses in metal powder bed fusion.* Additive Manufacturing, 2019. **27**: p. 131-149.
64. Hideki, K. and I. Toshi-Taka *A review of metal additive manufacturing technologies: Mechanism of defects formation and simulation of melting and solidification phenomena in laser powder bed fusion process*. Mechanical Engineering Reviews, 2020. **7**, 19-00182 DOI: 10.1299/mer.19-00182.
65. Khairallah, S.A., A.T. Anderson, A. Rubenchik, and W.E. King, *Laser powder-bed fusion additive manufacturing: Physics of complex melt flow and formation mechanisms of pores, spatter, and denudation zones.* Acta Materialia, 2016. **108**: p. 36-45.

66. Roehling, J.D., W.L. Smith, T.T. Roehling, B. Vrancken, G.M. Guss, J.T. McKeown, M.R. Hill, and M.J. Matthews, *Reducing residual stress by selective large-area diode surface heating during laser powder bed fusion additive manufacturing.* Additive Manufacturing, 2019. **28**: p. 228-235.
67. Oliveira, J.P., A.D. LaLonde, and J. Ma, *Processing parameters in laser powder bed fusion metal additive manufacturing.* Materials & Design, 2020. **193**.
68. Mumtaz, K. and N. Hopkinson, *Top surface and side roughness of Inconel 625 parts processed using selective laser melting.* Rapid Prototyping Journal, 2009. **15**(2): p. 96-103.
69. Gu, H., H.-j. Gong, D. Pal, K. Rafi, T.L. Starr, and B.E. Stucker. *Influences of Energy Density on Porosity and Microstructure of Selective Laser Melted 17-4PH Stainless Steel*. in *International Solid Freeform Fabrication Symposium*. 2013.
70. Martínez Bastús, A., *Nunerical sensitivity study of residual stress and distortion in selective laser relting of 17-4 PH Steel*. 2019, Universitat Politècnica de Catalunya.
71. Simson, T., A. Emmel, A. Dwars, and J. Böhm, *Residual stress measurements on AISI 316L samples manufactured by selective laser melting.* Additive Manufacturing, 2017. **17**: p. 183-189.
72. Mercelis, P. and J.P. Kruth, *Residual stresses in selective laser sintering and selective laser melting.* Rapid Prototyping Journal, 2006. **12**(5): p. 254-265.
73. Vrancken, B. and J. Van Humbeeck, *Study of Residual Stresses in Selective Laser Melting*, in *Studie van thermische spanningen bij het Selectief Laser Smelten*. 2016.
74. Leung, C.L.A., R. Tosi, E. Muzangaza, S. Nonni, P.J. Withers, and P.D. Lee, *Effect of preheating on the thermal, microstructural and mechanical properties of selective electron beam melted Ti-6Al-4V components.* Materials & Design, 2019. **174**: p. 107792.
75. Syed, A.K., B. Ahmad, H. Guo, T. Machry, D. Eatock, J. Meyer, M.E. Fitzpatrick, and X. Zhang, *An experimental study of residual stress and direction-dependence of fatigue crack growth behaviour in as-built and stress-relieved selective-laser-melted Ti6Al4V.* Materials Science & Engineering A, 2019. **755**: p. 246-257.
76. Davis, J.R., *Stainless steels / edited by J.R. Davis*. ASM specialty handbook. 1994, Materials Park, Ohio: ASM International.
77. Company, I.N., *The Corrosion Resistance of Nickel-containing Alloys in Sulfuric Acid and Related Compounds*. 1983: International Nickel Company, Incorporated.
78. Budinski, K.G. and M.K. Budinski, *Engineering Materials: Properties and Selection*. 2010: Prentice Hall.
79. Sabooni, S., A. Chabok, S.C. Feng, H. Blaauw, T.C. Pijper, H.J. Yang, and Y.T. Pei, *Laser powder bed fusion of 17-4 PH stainless steel: A comparative study on the effect of heat treatment on the microstructure evolution and mechanical properties.* Additive Manufacturing, 2021. **46**.
80. LeBrun, T., T. Nakamoto, K. Horikawa, and H. Kobayashi, *Effect of retained austenite on subsequent thermal processing and resultant mechanical properties of selective laser melted 17-4 PH stainless steel.* Materials and Design, 2015. **81**: p. 44-53.

81. Nezhadfar, P., M. Masoomi, S. Thompson, N. Phan, and N. Shamsaei, *Mechanical Properties of 17-4 PH Stainless Steel Additively Manufactured under Ar and N2 Shielding Gas*. 2018.
82. Alfieri, V., V. Giannella, F. Caiazzo, and R. Sepe, *Influence of position and building orientation on the static properties of LPBF specimens in 17-4 PH stainless steel.* Forces in Mechanics, 2022. **8**.
83. Sun, Y., R.J. Hebert, and M. Aindow, *Effect of heat treatments on microstructural evolution of additively manufactured and wrought 17-4PH stainless steel.* 2018. **156**: p. 429-440.
84. Irrinki, H., J.S.D. Jangam, S. Pasebani, S. Badwe, J. Stitzel, K. Kate, O. Gulsoy, and S.V. Atre, *Effects of particle characteristics on the microstructure and mechanical properties of 17-4 PH stainless steel fabricated by laser-powder bed fusion.* Powder Technology, 2018. **331**: p. 192-203.
85. Facchini, L., N. Vicente Jr, I. Lonardelli, E. Magalini, P. Robotti, and A. Molinari, *Metastable Austenite in 17–4 Precipitation-Hardening Stainless Steel Produced by Selective Laser Melting.* Advanced Engineering Materials, 2010. **12**(3): p. 184-188.
86. Yu, J., M. Rombouts, and G. Maes, *Cracking behavior and mechanical properties of austenitic stainless steel parts produced by laser metal deposition.* Materials and Design, 2013. **45**: p. 228-235.
87. Montero Sistiaga, M., S. Nardone, C. Hautfenne, and J. Van Humbeeck. *Effect of heat treatment of 316L stainless steel produced by selective laser melting (SLM)*. Solid Freeform Fabrication.
88. Kurzynowski, T., K. Gruber, W. Stopyra, B. Kuźnicka, and E. Chlebus, *Correlation between process parameters, microstructure and properties of 316 L stainless steel processed by selective laser melting.* Materials Science & Engineering A, 2018. **718**: p. 64-73.
89. Carlton, H.D., A. Haboub, G.F. Gallegos, D.Y. Parkinson, and A.A. MacDowell, *Damage evolution and failure mechanisms in additively manufactured stainless steel.* Materials Science & Engineering A, 2016. **651**: p. 406-414.
90. Riemer, A., S. Leuders, M. Thöne, H.A. Richard, T. Tröster, and T. Niendorf, *On the fatigue crack growth behavior in 316L stainless steel manufactured by selective laser melting.* Engineering Fracture Mechanics, 2014. **120**: p. 15-25.
91. Kong, D., C. Dong, X. Ni, L. Zhang, J. Yao, C. Man, X. Cheng, K. Xiao, and X. Li, *Mechanical properties and corrosion behavior of selective laser melted 316L stainless steel after different heat treatment processes.* Journal of Materials Science & Technology, 2019. **35**(7): p. 1499-1507.
92. Mertens, A., S. Reginster, H. Paydas, Q. Contrepois, J. Lecomte-Beckers, T. Dormal, and O. Lemaire, *Mechanical properties of alloy Ti-6Al-4V and of stainless steel 316L processed by selective laser melting: Influence of out-of-equilibrium microstructures.* Powder Metallurgy, 2014. **57**(3): p. 184-189.
93. Zhong, Y., L. Liu, S. Wikman, D. Cui, and Z. Shen, *Intragranular cellular segregation network structure strengthening 316L stainless steel prepared by selective laser melting.* Journal of Nuclear Materials, 2016. **470**: p. 170-178.

94. Liu, J., Y. Song, C. Chen, X. Wang, H. Li, C.a. Zhou, J. Wang, K. Guo, and J. Sun, *Effect of scanning speed on the microstructure and mechanical behavior of 316L stainless steel fabricated by selective laser melting.* Materials & Design, 2020. **186**: p. 108355.
95. Wang, G., Q. Liu, H. Rao, H. Liu, and C. Qiu, *Influence of porosity and microstructure on mechanical and corrosion properties of a selectively laser melted stainless steel.* Journal of Alloys and Compounds, 2020. **831**: p. 154815.
96. Saeidi, K., X. Gao, F. Lofaj, L. Kvetková, and Z.J. Shen, *Transformation of austenite to duplex austenite-ferrite assembly in annealed stainless steel 316L consolidated by laser melting.* Journal of Alloys and Compounds, 2015. **633**: p. 463-469.
97. Ma, M., Z. Wang, D. Wang, and X. Zeng, *Control of shape and performance for direct laser fabrication of precision large-scale metal parts with 316L Stainless Steel.* Optics & Laser Technology, 2013. **45**: p. 209-216.
98. Ghayoor, M., K. Lee, Y. He, C.-h. Chang, B.K. Paul, and S. Pasebani, *Selective laser melting of 304L stainless steel: Role of volumetric energy density on the microstructure, texture and mechanical properties.* Additive Manufacturing, 2020. **32**: p. 101011.
99. Yang, F., D. Zhu, M. Jiang, H. Liu, S. Guo, Q. Wang, H. Wang, K. Zhang, A. Huang, and J. Hou, *Effect of Heat Treatment on the Microstructure, Mechanical Properties and Corrosion Resistance of Selective Laser Melted 304L Stainless Steel.* Acta Metallurgica Sinica (English Letters), 2022. **35**(10): p. 1688-1702.
100. Hung, C.-H., A. Sutton, Y. Li, Y. Shen, H.-L. Tsai, and M.C. Leu, *Enhanced mechanical properties for 304L stainless steel parts fabricated by laser-foil-printing additive manufacturing.* Journal of Manufacturing Processes, 2019. **45**: p. 438-446.
101. Zhang, H., M. Xu, Z. Liu, C. Li, P. Kumar, Z. Liu, and Y. Zhang, *Microstructure, surface quality, residual stress, fatigue behavior and damage mechanisms of selective laser melted 304L stainless steel considering building direction.* Additive Manufacturing, 2021. **46**.
102. Zhu, H., Q. Pan, K. Zhang, C. Zhou, W. Zhang, Y. Yao, D. Ying, Y. He, J. Zheng, and L. Zhang, *The difference in fatigue crack growth induced by internal and external hydrogen in selective laser melted 304L stainless steel.* International Journal of Fatigue, 2022. **163**.
103. Ma, Y., Y. Gao, L. Zhao, H. Zhang, D. Li, L. Yang, and C. Yu *Understanding of Excellent Mechanical Performance of 304L Manufactured by Optimal Selective Laser Melting (SLM) Conditions*. Materials, 2023. **16**, DOI: 10.3390/ma16041661.
104. Hou, J., W. Chen, Z. Chen, K. Zhang, and A. Huang, *Microstructure, tensile properties and mechanical anisotropy of selective laser melted 304L stainless steel.* Journal of Materials Science & Technology, 2020. **48**: p. 63-71.
105. Zhu, Z., W. Li, Q.B. Nguyen, X. An, W. Lu, Z. Li, F.L. Ng, S.M. Ling Nai, and J. Wei, *Enhanced strength-ductility synergy and transformation-induced plasticity of the selective laser melting fabricated 304L stainless steel.* Additive Manufacturing, 2020. **35**.
106. Zhang, H., C. Li, G. Yao, Y. Shi, and Y. Zhang, *Investigation of surface quality, microstructure, deformation mechanism, and fatigue performance of additively*

manufactured 304L stainless steel using grinding. International Journal of Fatigue, 2022. **160**.
107. Chae, H., M.Y. Luo, E.W. Huang, E. Shin, C. Do, S.-K. Hong, W. Woo, and S.Y. Lee, *Unearthing principal strengthening factors tuning the additive manufactured 15-5 PH stainless steel.* Materials Characterization, 2022. **184**.
108. Tapoglou, N., J. Clulow, A. Patterson, and D. Curtis, *Characterisation of mechanical properties of 15-5PH stainless steel manufactured through direct energy deposition.* CIRP Journal of Manufacturing Science and Technology, 2022. **38**: p. 172-185.
109. Alafaghani, A.a., A. Qattawi, and M.A.G. Castañón, *Effect of manufacturing parameters on the microstructure and mechanical properties of metal laser sintering parts of precipitate hardenable metals.* The International Journal of Advanced Manufacturing Technology, 2018. **99**(9-12): p. 2491-2507.
110. Zhang, B., H. Wang, X. Ran, X. Nie, J. Wang, and B. He, *Microstructure and mechanical properties of high-efficiency laser-directed energy deposited 15-5PH stainless steel.* Materials Characterization, 2022. **190**.
111. Sarkar, S., S. Mukherjee, C.S. Kumar, and A. Kumar Nath, *Effects of heat treatment on microstructure, mechanical and corrosion properties of 15-5 PH stainless steel parts built by selective laser melting process.* Journal of Manufacturing Processes, 2020. **50**: p. 279-294.
112. Wang, L., C. Dong, C. Man, D. Kong, K. Xiao, and X. Li, *Enhancing the corrosion resistance of selective laser melted 15-5PH martensite stainless steel via heat treatment.* Corrosion Science, 2020. **166**: p. 108427.
113. Lee, J.-R., M.-S. Lee, H. Chae, S.Y. Lee, T. Na, W.-S. Kim, and T.-S. Jun, *Effects of building direction and heat treatment on the local mechanical properties of direct metal laser sintered 15-5 PH stainless steel.* Materials Characterization, 2020. **167**.
114. Saeidi, K., D.L. Zapata, F. Lofaj, L. Kvetkova, J. Olsen, Z. Shen, and F. Akhtar, *Ultra-high strength martensitic 420 stainless steel with high ductility.* Additive Manufacturing, 2019. **29**.
115. Zhao, X., Q. Wei, B. Song, Y. Liu, X. Luo, S. Wen, and Y. Shi, *Fabrication and Characterization of AISI 420 Stainless Steel Using Selective Laser Melting.* Materials and Manufacturing Processes, 2015. **30**(11): p. 1283-1289.
116. Nath, S.D., H. Irrinki, G. Gupta, M. Kearns, O. Gulsoy, and S. Atre, *Microstructure-property relationships of 420 stainless steel fabricated by laser-powder bed fusion.* Powder Technology, 2019. **343**: p. 738-746.
117. Liverani, E. and A. Fortunato, *Additive manufacturing of AISI 420 stainless steel: process validation, defect analysis and mechanical characterization in different process and post-process conditions.* The International Journal of Advanced Manufacturing Technology, 2021. **117**(3): p. 809-821.
118. Shahriari, A., M. Ghaffari, L. Khaksar, A. Nasiri, A. Hadadzadeh, B.S. Amirkhiz, and M. Mohammadi, *Corrosion resistance of 13wt.% Cr martensitic stainless steels: Additively manufactured CX versus wrought Ni-containing AISI 420.* Corrosion Science, 2021. **184**: p. 109362.

119. Zeng, G.H., T. Song, Y.H. Dai, H.P. Tang, and M. Yan, *3D printed breathable mould steel: Small micrometer-sized, interconnected pores by creatively introducing foaming agent to additive manufacturing.* Materials & Design, 2019. **169**: p. 107693.
120. Jiang, C.-M., J.-R. Ho, P.-C. Tung, and C.-K. Lin, *Tempering Effect on the Anisotropic Mechanical Properties of Selective Laser Melted 420 Stainless Steel.* Journal of Materials Engineering and Performance, 2022.
121. Yu, J., M. Rombouts, and G. Maes, *Cracking behavior and mechanical properties of austenitic stainless steel parts produced by laser metal deposition.* Materials & Design, 2013. **45**: p. 228-235.
122. Gabriel, A.F., A.I.P. Patricia, and M.P. Olawale, *Computatonal Analysis of System and Design Parameters of Electrodeposition for Marine Applications*, in *Applied Studies of Coastal and Marine Environments*, M. Maged, Editor. 2016, IntechOpen: Rijeka. p. Ch. 6.
123. Schaller, R., J. Taylor, J. Rodelas, and E. Schindelholz, *Corrosion Properties of Powder Bed Fusion Additively Manufactured 17-4 PH Stainless Steel.* CORROSION, 2017. **73**.
124. Garcia-Cabezon, C., M.A. Castro-Sastre, A.I. Fernandez-Abia, M.L. Rodriguez-Mendez, and F. Martin-Pedrosa, *Microstructure–Hardness–Corrosion Performance of 17–4 Precipitation Hardening Stainless Steels Processed by Selective Laser Melting in Comparison with Commercial Alloy.* Metals and Materials International, 2022. **28**(11): p. 2652-2667.
125. Alnajjar, M., F. Christien, V. Barnier, C. Bosch, K. Wolski, A.D. Fortes, and M. Telling, *Influence of microstructure and manganese sulfides on corrosion resistance of selective laser melted 17-4 PH stainless steel in acidic chloride medium.* Corrosion Science, 2020. **168**: p. 108585.
126. Kong, D., X. Ni, C. Dong, X. Lei, L. Zhang, C. Man, J. Yao, X. Cheng, and X. Li, *Bio-functional and anti-corrosive 3D printing 316L stainless steel fabricated by selective laser melting.* Materials & Design, 2018. **152**: p. 88-101.
127. Kale, A.B., B.-K. Kim, D.-I. Kim, E.G. Castle, M. Reece, and S.-H. Choi, *An investigation of the corrosion behavior of 316L stainless steel fabricated by SLM and SPS techniques.* Materials Characterization, 2020. **163**: p. 110204.
128. Sander, G., V. Cruz, M. Jurg, N. Birbilis, X. Gao, M. Brameld, and C. Hutchinson, *On The Corrosion and Metastable Pitting Characteristics of 316L Stainless Steel Produced by Selective Laser Melting.* Journal of The Electrochemical Society, 2017. **164**: p. C250-C257.
129. Chen, W., *Effect of the Particle Size of 316L Stainless Steel on the Corrosion Characteristics of the Steel Fabricated by Selective Laser Melting.* International Journal of Electrochemical Science, 2018. **13**: p. 10217-10232.
130. Chao, Q., V. Cruz, S. Thomas, N. Birbilis, P. Collins, A. Taylor, P.D. Hodgson, and D. Fabijanic, *On the enhanced corrosion resistance of a selective laser melted austenitic stainless steel.* Scripta Materialia, 2017. **141**: p. 94-98.
131. Harun, W.S.W., R.I.M. Asri, F.R.M. Romlay, S. Sharif, N.H.M. Jan, and F. Tsumori, *Surface characterisation and corrosion behaviour of oxide layer for SLMed-316L stainless steel.* Journal of Alloys and Compounds, 2018. **748**: p. 1044-1052.

132. Trelewicz, J.R., G.P. Halada, O.K. Donaldson, and G. Manogharan, *Microstructure and Corrosion Resistance of Laser Additively Manufactured 316L Stainless Steel.* JOM, 2016. **68**(3): p. 850-859.
133. Sun, Y., A. Moroz, and K. Alrbaey, *Sliding Wear Characteristics and Corrosion Behaviour of Selective Laser Melted 316L Stainless Steel.* Journal of Materials Engineering and Performance, 2014. **23**(2): p. 518-526.
134. Mohd Yusuf, S., M. Nie, Y. Chen, S. Yang, and N. Gao, *Microstructure and corrosion performance of 316L stainless steel fabricated by Selective Laser Melting and processed through high-pressure torsion.* Journal of Alloys and Compounds, 2018. **763**: p. 360-375.
135. Lin, K., D. Gu, L. Xi, L. Yuan, S. Niu, P. Lv, and Q. Ge, *Selective laser melting processing of 316L stainless steel: effect of microstructural differences along building direction on corrosion behavior.* The International Journal of Advanced Manufacturing Technology, 2019. **104**(5): p. 2669-2679.
136. Woźniak, A., M. Adamiak, G. Chladek, and J. Kasperski, *The Influence of the Process Parameters on the Microstructure and Properties SLM Processed 316L Stainless Steel.* Archives of Metallurgy and Materials, 2020. **65**(1): p. 73-80.
137. Schaller, R.F., A. Mishra, J.M. Rodelas, J.M. Taylor, and E.J. Schindelholz, *The Role of Microstructure and Surface Finish on the Corrosion of Selective Laser Melted 304L.* Journal of The Electrochemical Society, 2018. **165**(5): p. C234-C242.
138. Kazemipour, M., J. Lunde, S. Salahi, and A. Nasiri, *On the Microstructure and Corrosion Behavior of Wire Arc Additively Manufactured AISI 420 Stainless Steel*. 2020. p. 435-448.
139. Chen, W., L. Xu, K. Hao, Y. Zhang, L. Zhao, Y. Han, Z. Liu, and H. Cai, *Effect of heat treatment on microstructure and performances of additively manufactured 15-5PH stainless steel.* Optics & Laser Technology, 2023. **157**: p. 108711.
140. Ma, H., R. Liu, P. Ke, Y. Cui, L. Liu, and F. Wang, *Effect of hydrostatic pressure on the pitting corrosion of 17-4PH martensitic stainless steel.* Engineering Failure Analysis, 2022. **138**.
141. Smith, B. *Use of Stainless Steel in Subsea Pipelines*. 2015 [cited 2023 30 Mars]; Available from: https://www.azom.com/article.aspx?ArticleID=11959.
142. Long, J.M., Q.B. Liu, K.Y. Zhao, Q.L. Yong, and J. Su, *Effect of Cl- Content, pH Value and CO2 on Electrochemical Corrosion Features of Cr15 Super Martensitic Stainless Steel.* Advanced Materials Research, 2013. **738**: p. 92-96.
143. Fantechi, F. and M. Innocenti, *Chloride stress corrosion cracking of precipitation hardening S.S. impellers in centrifugal compressor. Laboratory investigations and corrective actions.* Engineering Failure Analysis, 2001. **8**(5): p. 477-492.
144. King, R.A., *11 - Sulfide stress cracking*, in *Trends in Oil and Gas Corrosion Research and Technologies*, A.M. El-Sherik, Editor. 2017, Woodhead Publishing: Boston. p. 271-294.
145. Lasich, M., *Adsorption of H2S from Hydrocarbon Gas Using Doped Bentonite: A Molecular Simulation Study.* ACS omega, 2020. **5**(31): p. 19877-19883.
146. NACE, *NACE MR0175/ISO 15156-1*, in *Petroleum and Natural Gas Industries: Materials for Use in H2S-Containing Environments in Oil and Gas Production—*

Annex A: Environmental cracking-resistant CRAs and other alloys. 2001: Houston, TX.
147. Jiang, T., J. Zhong, X. Zhang, W. Wang, and K. Guan, *Hydrogen embrittlement induced fracture of 17-4 PH stainless steel valve stem.* Engineering Failure Analysis, 2020. **113**.
148. Barile, C., C. Casavola, S.L. Campanelli, and G. Renna, *Analysis of corrosion on sintered stainless steel: Mechanical and physical aspects.* Engineering Failure Analysis, 2019. **95**: p. 273-282.
149. Avico, L., R. Beltrami, N. Lecis, and S.P. Trasatti *Corrosion Behavior and Surface Properties of PVD Coatings for Mold Technology Applications*. Coatings, 2019. **9**, DOI: 10.3390/coatings9010007.
150. Wu, Y., Z. Zhang, Z. Leng, J. Zhang, S. Yang, W. Shen, K. Xu, H. Zhu, and Y. Liu, *Improvement of the corrosion resistance of amorphous Ni-P coatings modified by a laser–electrodeposition hybrid process: Effect of morphology evolution on the electrochemical corrosion behavior.* Applied Surface Science, 2023. **624**: p. 157016.
151. John, M., P.R. Kalvala, M. Misra, and P.L. Menezes, *Peening Techniques for Surface Modification: Processes, Properties, and Applications.* Materials (Basel), 2021. **14**(14).
152. Cruz, V., Q. Chao, N. Birbilis, D. Fabijanic, P.D. Hodgson, and S. Thomas, *Electrochemical studies on the effect of residual stress on the corrosion of 316L manufactured by selective laser melting.* Corrosion Science, 2020. **164**: p. 108314.
153. Taghavikish, M., N.K. Dutta, and N. Roy Choudhury *Emerging Corrosion Inhibitors for Interfacial Coating*. Coatings, 2017. **7**, DOI: 10.3390/coatings7120217.
154. Stojanović, I., V. Šimunović, V. Alar, and F. Kapor *Experimental Evaluation of Polyester and Epoxy–Polyester Powder Coatings in Aggressive Media*. Coatings, 2018. **8**, DOI: 10.3390/coatings8030098.
155. Li, Y., Y. Yang, J. Nie, P. Bai, Z. Liang, S. Wei, J. Cai, and Q. Guan, *Hot corrosion behavior of a NiCoCrAlY coating fabricated by laser cladding on 17-4PH stainless steel.* Engineering Failure Analysis, 2022. **133**: p. 105962.
156. Lodhi, M.J.K., K.M. Deen, and W. Haider, *Corrosion behavior of additively manufactured 316L stainless steel in acidic media.* Materialia, 2018. **2**: p. 111-121.
157. Chen, W., L. Xu, L. Zhao, Y. Han, X. Wang, C. Hu, and H. Jing, *Application of hybrid additive manufacturing technology for performance improvement of martensitic stainless steel.* Additive Manufacturing, 2022. **51**: p. 102648.
158. Ko, G., W. Kim, K. Kwon, and T.-K. Lee *The Corrosion of Stainless Steel Made by Additive Manufacturing: A Review*. Metals, 2021. **11**, DOI: 10.3390/met11030516.
159. Zhou, C., S. Hu, Q. Shi, H. Tao, Y. Song, J. Zheng, P. Xu, and L. Zhang, *Improvement of corrosion resistance of SS316L manufactured by selective laser melting through subcritical annealing.* Corrosion Science, 2020. **164**: p. 108353.
160. Kong, D., X. Ni, C. Dong, L. Zhang, C. Man, J. Yao, K. Xiao, and X. Li, *Heat treatment effect on the microstructure and corrosion behavior of 316L stainless steel fabricated by selective laser melting for proton exchange membrane fuel cells.* Electrochimica Acta, 2018. **276**: p. 293-303.

161. Bajaj, P., A. Hariharan, A. Kini, P. Kürnsteiner, D. Raabe, and E.A. Jägle, *Steels in additive manufacturing: A review of their microstructure and properties.* Materials Science and Engineering: A, 2020. **772**: p. 138633.
162. du Plessis, A., N. Razavi, M. Benedetti, S. Murchio, M. Leary, M. Watson, D. Bhate, and F. Berto, *Properties and applications of additively manufactured metallic cellular materials: A review.* Progress in Materials Science, 2022. **125**: p. 100918.
163. Yadollahi, A., N. Shamsaei, S.M. Thompson, A. Elwany, and L. Bian, *Effects of building orientation and heat treatment on fatigue behavior of selective laser melted 17-4 PH stainless steel.* International Journal of Fatigue, 2017. **94**: p. 218-235.
164. Aripin, M.A., Z. Sajuri, N.H. Jamadon, A.H. Baghdadi, J. Syarif, I.F. Mohamed, and A.M. Aziz *Effects of Build Orientations on Microstructure Evolution, Porosity Formation, and Mechanical Performance of Selective Laser Melted 17-4 PH Stainless Steel*. Metals, 2022. **12**, DOI: 10.3390/met12111968.
165. Sabooni, S., A. Chabok, S.C. Feng, H. Blaauw, T.C. Pijper, H.J. Yang, and Y.T. Pei, *Laser powder bed fusion of 17–4 PH stainless steel: A comparative study on the effect of heat treatment on the microstructure evolution and mechanical properties.* Additive Manufacturing, 2021. **46**: p. 102176.
166. Sun, Y., R. Hebert, and M. Aindow, *Effect of Heat Treatments on Microstructural Evolution of Additively Manufactured and Wrought 17-4PH Stainless Steel.* Materials & design, 2018. **156**: p. 429–440.
167. Laleh, M., E. Sadeghi, R.I. Revilla, Q. Chao, N. Haghdadi, A.E. Hughes, W. Xu, I. De Graeve, M. Qian, I. Gibson, and M.Y. Tan, *Heat treatment for metal additive manufacturing.* Progress in Materials Science, 2023. **133**: p. 101051.
168. Cheruvathur, S., E.A. Lass, and C.E. Campbell, *Additive Manufacturing of 17-4 PH Stainless Steel: Post-processing Heat Treatment to Achieve Uniform Reproducible Microstructure.* Jom, 2015. **68**(3): p. 930-942.
169. Alnajjar, M., F. Christien, V. Barnier, C. Bosch, K. Wolski, A.D. Fortes, and M. Telling, *Influence of microstructure and manganese sulfides on corrosion resistance of selective laser melted 17-4 PH stainless steel in acidic chloride medium.* Corrosion Science, 2020. **168**.
170. Irrinki, H., T. Harper, S. Badwe, J. Stitzel, O. Gulsoy, G. Gupta, and S.V. Atre, *Effects of powder characteristics and processing conditions on the corrosion performance of 17-4 PH stainless steel fabricated by laser-powder bed fusion.* Progress in Additive Manufacturing, 2018. **3**(1-2): p. 39-49.
171. Kartikeya Sarma, I., N. Selvraj, and A. Kumar. *A Review on Microstructure and Mechanical Properties of L-PBF 17-4PH and 15-5PH SS*. in *Recent Advances in Manufacturing Processes and Systems*. 2022. Singapore: Springer Nature Singapore.
172. Hu, Z., H. Zhu, H. Zhang, and X. Zeng, *Experimental investigation on selective laser melting of 17-4PH stainless steel.* Optics & Laser Technology, 2017. **87**: p. 17-25.
173. Wang, L., C. Dong, D. Kong, C. Man, J. Liang, C. Wang, K. Xiao, and X. Li, *Effect of Manufacturing Parameters on the Mechanical and Corrosion Behavior of Selective Laser-Melted 15-5PH Stainless Steel.* steel research international, 2019. **91**(2).

174. Lebrun, T., K. Tanigaki, K. Horikawa, and H. Kobayashi, *Strain rate sensitivity and mechanical anisotropy of selective laser melted 17-4 PH stainless steel.* Mechanical Engineering Journal, 2014. **1**(5): p. SMM0049-SMM0049.
175. LeBrun, T., T. Nakamoto, K. Horikawa, and H. Kobayashi, *Effect of retained austenite on subsequent thermal processing and resultant mechanical properties of selective laser melted 17–4 PH stainless steel.* Materials & Design, 2015. **81**: p. 44-53.
176. Nezhadfar, P.D., P.R. Gradl, S. Shao, and N. Shamsaei, *Microstructure and Deformation Behavior of Additively Manufactured 17–4 Stainless Steel: Laser Powder Bed Fusion vs. Laser Powder Directed Energy Deposition.* JOM, 2022. **74**(3): p. 1136-1148.
177. Nong, X.D., X.L. Zhou, J.H. Li, Y.D. Wang, Y.F. Zhao, and M. Brochu, *Selective laser melting and heat treatment of precipitation hardening stainless steel with a refined microstructure and excellent mechanical properties.* Scripta Materialia, 2020. **178**: p. 7-12.
178. Strasser, T., *Comparison of Additively Manufactured and Wrought 17-4 PH Stainless Steels in Ultra Low Cycle Fatigue*. 2020: University of Arkansas.
179. Facchini, L., N. Vicente, I. Lonardelli, E. Magalini, R. Pierfrancesco, and A. Molinari, *Metastable Austenite in 17–4 Precipitation-Hardening Stainless Steel Produced by Selective Laser Melting.* Advanced Engineering Materials, 2010. **12**: p. 184-188.
180. Kurzynowski, T., K. Gruber, W. Stopyra, B. Kuźnicka, and E. Chlebus, *Correlation between process parameters, microstructure and properties of 316 L stainless steel processed by selective laser melting.* Materials Science and Engineering: A, 2018. **718**: p. 64-73.
181. Chung, C.-Y. and Y.-C. Tzeng, *Effects of aging treatment on the precipitation behavior of ε-Cu phase and mechanical properties of metal injection molding 17-4PH stainless steel.* Materials Letters, 2019. **237**: p. 228-231.
182. Luo, H., Q. Yu, C. Dong, G. Sha, Z. Liu, J. Liang, L. Wang, G. Han, and X. Li, *Influence of the aging time on the microstructure and electrochemical behaviour of a 15-5PH ultra-high strength stainless steel.* Corrosion Science, 2018. **139**: p. 185-196.
183. Malakshah, M.G., A. Eslami, F. Ashrafizadeh, and A. Berenjkoub, *Effect of Heat Treatment on Corrosion, Fatigue, and Corrosion Fatigue Behavior of 17-4PH Stainless Steel.* Journal of Materials Engineering and Performance, 2023. **32**(15): p. 6610-6621.
184. Liu, W., J. Ma, M.M. Atabaki, R. Pillai, B. Kumar, U. Vasudevan, H. Sreshta, and R. Kovacevic, *Hybrid Laser-arc Welding of 17-4 PH Martensitic Stainless Steel.* Lasers in Manufacturing and Materials Processing, 2015. **2**(2): p. 74-90.
185. Bhambroo, R., S. Roychowdhury, V. Kain, and V.S. Raja, *Effect of reverted austenite on mechanical properties of precipitation hardenable 17-4 stainlesssteel.* Materials Science and Engineering: A, 2013. **568**: p. 127-133.

186. Shrestha, R., N. Shamsaei, M. Seifi, and N. Phan, *An investigation into specimen property to part performance relationships for laser beam powder bed fusion additive manufacturing.* Additive Manufacturing, 2019. **29**: p. 100807.
187. Sanjeev, K., P. Nezhadfar, C. Phillips, M. Kennedy, N. Shamsaei, and R. Jackson, *Tribological behavior of 17–4 PH stainless steel fabricated by traditional manufacturing and laser-based additive manufacturing methods.* Wear, 2019. **440**: p. 203100.
188. Dieter, G.E. and D. Bacon, *Mechanical metallurgy*. Vol. 3. 1976: McGraw-hill New York.
189. Yeli, G., M.A. Auger, K. Wilford, G.D.W. Smith, P.A.J. Bagot, and M.P. Moody, *Sequential nucleation of phases in a 17-4PH steel: Microstructural characterisation and mechanical properties.* Acta Materialia, 2017. **125**: p. 38-49.
190. Barroux, A., N. Ducommun, E. Nivet, L. Laffont, and C. Blanc, *Pitting corrosion of 17-4PH stainless steel manufactured by laser beam melting.* Corrosion Science, 2020. **169**.
191. Ferguson, J.B., B.F. Schultz, D. Venugopalan, H.F. Lopez, P.K. Rohatgi, K. Cho, and C.-S. Kim, *On the superposition of strengthening mechanisms in dispersion strengthened alloys and metal-matrix nanocomposites: Considerations of stress and energy.* Metals and Materials International, 2014. **20**(2): p. 375-388.
192. Mirzadeh, H. and A. Najafizadeh, *Aging kinetics of 17-4 PH stainless steel.* Materials Chemistry and Physics, 2009. **116**(1): p. 119-124.
193. Coseglio, M.S.D.R., *Sulphide stress cracking of 17-4 PH for applications in oilfield components.* Materials Science and Technology, 2017. **33**(16): p. 1863-1878.
194. Arisoy, C.F., G. Başman, and M.K. Şeşen, *Failure of a 17-4 PH stainless steel sailboat propeller shaft.* Engineering Failure Analysis, 2003. **10**(6): p. 711-717.
195. Wang, J., H. Zou, C. Li, S.-y. Qiu, and B.-l. Shen, *The effect of microstructural evolution on hardening behavior of type 17-4PH stainless steel in long-term aging at 350 °C.* Materials Characterization, 2006. **57**(4): p. 274-280.
196. Kovacs, S.E., T. Miko, E. Troiani, D. Markatos, D. Petho, G. Gergely, L. Varga, and Z. Gacsi, *Additive Manufacturing of 17-4PH Alloy: Tailoring the Printing Orientation for Enhanced Aerospace Application Performance.* Aerospace, 2023. **10**(7): p. 619.
197. Forest, I.-S., *The corrosion resistance of nickel-containing alloys in sulfuric acid and related compounds.* INCO The International Nickel Company, 1983. **1**: p. 51-82.
198. Stoudt, M.R., R.E. Ricker, E.A. Lass, and L.E. Levine, *The Influence of Post-Build Microstructure on the Electrochemical Behavior of Additively Manufactured 17-4 PH Stainless Steel.* JOM (1989), 2017. **69**(3): p. 506-515.
199. Sun, Y., A. Moroz, and K. Alrbaey, *Sliding Wear Characteristics and Corrosion Behaviour of Selective Laser Melted 316L Stainless Steel.* Journal of Materials Engineering and Performance, 2013. **23**(2): p. 518-526.
200. Huang, L., Y. Cao, H. Zhao, Y. Li, Y. Wang, and L. Wei, *Effect of process parameters on density and mechanical behaviour of a selective laser melted 17-4PH stainless steel alloy.* Open Physics, 2022. **20**: p. 66-77.

201. Ponnusamy, P., B. Sharma, S.H. Masood, R.A. Rahman Rashid, R. Rashid, S. Palanisamy, and D. Ruan, *A study of tensile behavior of SLM processed 17-4 PH stainless steel.* Materials Today: Proceedings, 2021. **45**: p. 4531-4534.
202. Suryawanshi, J., T. Baskaran, O. Prakash, S.B. Arya, and U. Ramamurty, *On the corrosion resistance of some selective laser melted alloys.* Materialia, 2018. **3**: p. 153-161.
203. Tanji, A., X. Fan, R. Sakidja, P.K. Liaw, and H. Hermawan, *Niobium addition improves the corrosion resistance of TiHfZrNbx high-entropy alloys in Hanks' solution.* Electrochimica Acta, 2022. **424**.
204. Wang, X., H. Luo, Q. Zhao, H. Cheng, Q. Li, Z. Pan, Y. Wei, Y. Ma, and X. Li, *Investigations on the passive and pitting behaviors of 17–4 PH martensitic stainless steel containing Al2O3 inclusions in chlorine environment.* Colloids and Surfaces A: Physicochemical and Engineering Aspects, 2023. **660**.
205. Jorcin, J.-B., M.E. Orazem, N. Pébère, and B. Tribollet, *CPE analysis by local electrochemical impedance spectroscopy.* Electrochimica Acta, 2006. **51**(8-9): p. 1473-1479.
206. Wang, L., C. Dong, D. Kong, C. Man, J. Liang, C. Wang, K. Xiao, and X. Li, *Effect of Manufacturing Parameters on the Mechanical and Corrosion Behavior of Selective Laser-Melted 15-5PH Stainless Steel.* steel research international, 2020. **91**(2): p. 1900447.
207. Tavakoli Shoushtari, M., *Effect of ageing heat treatment on corrosion behaviorof 17-4 PH stainless steel in 3.5% NaCl.* International Journal of Iron & Steel Society of Iran, 2010. **7**(1): p. 33-36.
208. Szewczyk-Nykiel, A. and J. Kazior, *Effect of Aging Temperature on Corrosion Behavior of Sintered 17-4 PH Stainless Steel in Dilute Sulfuric Acid Solution.* Journal of Materials Engineering and Performance, 2017. **26**(7): p. 3450-3456.
209. Li, P., Q.-z. Cai, B.-k. Wei, and X.-z. Zhang, *Effect of Aging Temperature on Erosion-Corrosion Behavior of 17-4PH Stainless Steels in Dilute Sulphuric Acid Slurry.* Journal of Iron and Steel Research, International, 2006. **13**(5): p. 73-78.
210. Sourisseau, T., E. Chauveau, and B. Baroux, *Mechanism of copper action on pitting phenomena observed on stainless steels in chloride media.* Corrosion Science, 2005. **47**(5): p. 1097-1117.
211. Lin, H.-T., W.-T. Tsai, J.-T. Lee, and C.-S. Huang, *The electrochemical and corrosion behavior of austenitic stainless steel containing Cu.* Corrosion Science, 1992. **33**(5): p. 691-697.
212. Su, H., X.-b. Luo, C.-f. Yang, F. Chai, and H. Li, *Effects of Cu on Corrosion Resistance of Low Alloyed Steels in Acid Chloride Media.* Journal of Iron and Steel Research, International, 2014. **21**(6): p. 619-624.